TOF-SIMS in Cosmochemistry

Habilitationsschrift
zur Erlangung der *Venia Legendi*
für Planetologie
im Fachbereich Geowissenschaften
der Mathematisch-Naturwissenschaftlichen Fakultät
der Westfälischen Wilhelms-Universität Münster

vorgelegt von

Thomas Stephan
aus Herbolzheim

Dezember 1999

Abstract

Time-of-flight secondary ion mass spectrometry (TOF-SIMS) was introduced into cosmochemistry about a decade ago. Major advantages of TOF-SIMS compared to other ion microprobe techniques are (a) parallel detection of all secondary ions with one polarity in a single measurement – both polarities in subsequent analyses, (b) high lateral resolution, (c) sufficient mass resolution for separation of major mass interferences, and (d) little sample destruction. This combination makes TOF-SIMS highly suitable for the analysis especially of small samples, like interplanetary and presolar dust grains, as well as tiny inclusions within meteorites. Limitations of this technique are mainly referring to isotopic measurements and quantification. The possibility to measure molecular and atomic ion species simultaneously extends the applications of TOF-SIMS to the investigation of indigenous hydrocarbons in extraterrestrial material, which might have been essential for the formation of life. The present work gives an overview of TOF-SIMS in cosmochemistry, technical aspects as well as applications, principles of data evaluation and various results.

Table of contents

1. Introduction

The analysis of micrometer-sized samples like, *e.g.*, interplanetary dust, presolar grains, and small inclusions in meteorites has become more and more important in cosmochemistry. Recent technical developments lead towards the ultimate analytical goal, the localization and identification of every single atom and its chemical bonding state in a sample. The transmission electron microscope (TEM) with an extremely high lateral resolution allows even *seeing* individual crystallographic layers. Therefore, this technique has been established widely into cosmochemistry (*e.g.*, Tomeoka and Buseck, 1984, 1985, 1988; Bradley, 1994a). New developments in mass spectrometry like resonant ionization mass spectrometry (RIMS) enable to analyze the isotopic composition of an element that is present with just a few atoms (*e.g.*, Hurst *et al.*, 1979; Pellin *et al.*, 1987; Ma *et al.*, 1995; Nicolussi *et al.*, 1996, 1998a).

Secondary ion mass spectrometry (SIMS) has also become an increasingly important tool in geo- and cosmochemistry during the last two decades. After first developments in the 1960s, a generation of instruments with high mass resolutions like the Cameca IMS 3f and the SHRIMP (sensitive high mass resolution ion microprobe) allowed to introduce SIMS into this scientific field mainly during the 1980s. Since then, this technique has been used for trace element analysis and isotope measurements in terrestrial as well as extraterrestrial geological samples. The applications range from the analysis of rare earth elements in various samples (*e.g.*, Zinner and Crozaz, 1986; Bottazzi *et al.*, 1994; Floss and Jolliff, 1998; Fahey, 1998) to isotope measurements (Zinner, 1989) in meteorites (*e.g.*, McKeegan *et al.*, 1998; Leshin *et al.*, 1998; Chaussidon *et al.*, 1998; Eiler *et al.*, 1998), interplanetary dust (*e.g.*, McKeegan *et al.*, 1985; Zinner, 1991), presolar grains (*e.g.*, Zinner *et al.*, 1989; Zinner, 1991, 1998), and also terrestrial (*e.g.*, Froude *et al.*, 1983; Chaussidon and Libourel, 1993; Didenko and Koval, 1994; Schuhmacher *et al.*, 1994) and lunar (*e.g.*, Compston *et al.*, 1984) minerals. Technical developments of conventional SIMS instruments during the last years led to increased sensitivities at high mass resolution and high spatial resolution. This culminated in the development of the Cameca IMS 1270, optimized

for high mass resolution at high transmission (de Chambost *et al.*, 1992, 1997), and the Cameca Nanosims 50 with a lateral resolution of 50 nm (Hillion *et al.*, 1994, 1997; Stadermann *et al.*, 1999a,b).

Finally, since the early 1990s, also time-of-flight (TOF-) SIMS has been introduced to the analysis of extraterrestrial sample (Stephan *et al.*, 1991; Radicati di Brozolo *et al.*, 1991).

Common to all different SIMS techniques is that secondary ions are released from a sample surface by sputtering with a primary ion beam. In conventional ion microprobes, using mainly double-focusing magnetic mass spectrometers (DF-SIMS), different secondary ions are usually measured sequentially during continuous sputtering. Since this process is destructive, the number of analyzed secondary ion species is limited depending on the available amount of sample material or, because the analyzed material may change during sputtering, on the heterogeneity of the sample. In TOF-SIMS, the secondary ions are used more efficiently. **All** secondary ion species with one polarity, either positive or negative, are here detected quasi-simultaneously. Destruction of the sample is minimized by pulsing of the primary ion beam. The high transmission and in most cases sufficient mass resolution in combination with a high lateral resolution (~0.2 μm) makes TOF-SIMS highly suitable for the analysis of small samples.

The aim of the present work is to summarize ten years of analytical experience with TOF-SIMS in cosmochemistry. After a more general introduction into the principles of secondary ion mass spectrometry, TOF-SIMS will be explained in detail with special emphasis on applications in cosmochemistry. The principles of TOF-SIMS data acquisition are illustrated as well as evaluation procedures to achieve useful information on the elemental, isotopic, and molecular composition of the respective samples. The most intriguing results of TOF-SIMS studies in cosmochemistry are reviewed in subsequent sections of the manuscript.

2. Principles of secondary ion mass spectrometry

Secondary ion mass spectrometry in general is a technique used for surface analysis. Samples are bombarded with primary ions at typical energies of 10–30 keV. Secondary particles are released in a so-called sputtering process from surface-near layers. Besides electrons, these secondary particles are atoms and molecules, which are in part (approximately 1 %) positively or negatively charged. The secondary atomic and molecular ions are extracted with electric fields and then separated and detected in a mass analyzer (Fig. 1). Depending on the type of mass analyzer, one discerns between either conventional SIMS, with magnetic or quadrupole mass spectrometers, or TOF-SIMS, with time-of-flight mass spectrometers.

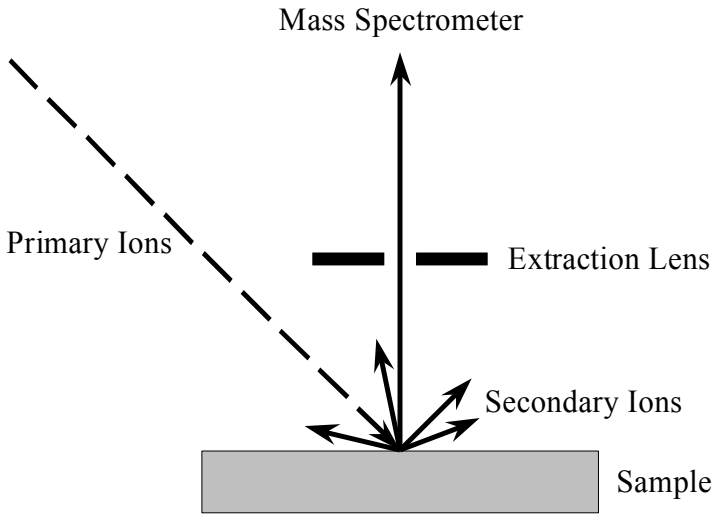

Fig. 1. The principle of secondary ion mass spectrometry: On the sample surface, an energy-rich primary ion beam generates secondary ions, which are separated and detected within a mass spectrometer.

2.1. Generation of secondary ions

2.1.1. The sputtering process

The sputtering process can be described qualitatively, at least for amorphous and polycrystalline samples, by cascades of atomic collisions (Sigmund, 1969). An impinging primary ion experiences a series of collisions in the target material (Fig. 2). Recoiling atoms with sufficient energy go through secondary collisions and create further generations of recoiling atoms. Both, primary ions and recoil atoms, have a chance to leave the target material as back-scattered ions or secondary atoms. The majority of sputtered particles result from clouds of high-order recoil atoms. They have very low energies (several electron volts) and originate from the uppermost atomic layers of the target.

The collision cascade has a characteristic dimension of 10 nm in SIMS. Crystalline targets allow typically much higher penetration depths along open crystal directions in a so-called channeling process. The collision cascade model is not applicable here, because binary collisions are relatively rare. The charging state of the sputtered particles also can not be derived from this simplified model, and multi-element targets are not considered.

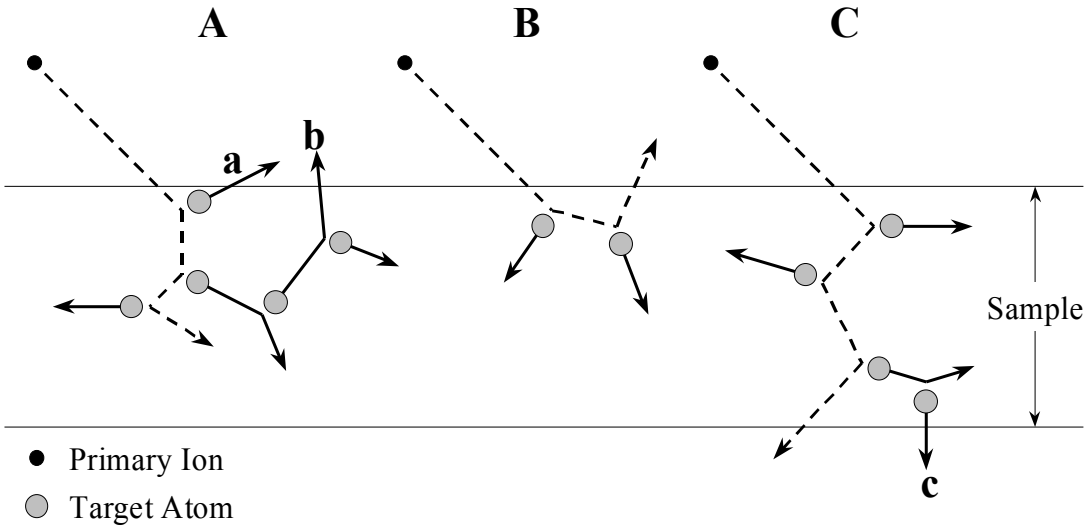

Fig. 2. Primary ions transfer energy in a collision cascade to the target atoms. Ion implantation (A) or back-scattering (B) may occur. A third alternative, for thin samples only, is forward scattering (C). Atoms from the target material can leave the sample after several collisions as secondary particles (backward sputtering: a and b; transmission sputtering: c).

2.1.2. Emission of secondary ions

The ionization energy of an element is decisive for the generation of positively charged secondary ions. Consequently, ions from alkali and alkaline-earth metals are formed most efficiently during the sputtering process. On the other hand, for negative secondary ions, the electron affinity plays the major role, and halogens have the highest ion yields. Besides this, the ionization probability depends strongly on the charging state of the respective particle within the sample, *i.e.*, its chemical environment. This characteristic, known as "matrix effect", complicates the proper quantification of SIMS results (see below).

2.1.3. Post-ionization of sputtered neutrals

About 99 % of all secondary particles escape the sample electrically neutral and are not detectable in classical SIMS. However, by subsequent ionization with electron or laser bombardment (Oechsner, 1994; Wittmaack, 1994; Kötter and Benninghoven, 1997; Arlinghaus *et al.*, 1997; Arlinghaus and Guo, 1998), the sputtered neutrals can be measured in a mass spectrometer. The mass spectrometry of secondary neutrals (SNMS) has two major advantages: (1) The ionization efficiency is increased compared to the SIMS process. (2) Matrix effects are reduced because the secondary particles are ionized **after** they have left the solid body, and when the chemical environment has lost most of its influence.

In general, multiphoton processes are necessary to exceed the first ionization potential for atoms (4–17 eV for elements aside from noble gases) and molecules. Individual photon energies of most laser systems are typically too low to ionize the atom or molecule directly. Two major techniques for post-ionization with laser light are established, resonant and non-resonant ionization.

In the non-resonant multiphoton ionization (Kampwerth *et al.*, 1990; Terhorst *et al.*, 1992, 1994; Niehuis, 1994; Schnieders *et al.*, 1996, 1998; Schnieders, 1999) an atom or molecule has to transit through a series of intermediate states to reach its ionization energy. These "virtual" states are not quantum-mechanical excitation states and have therefore very short lifetimes, of the order of 10^{-15} s. This process can be described as simultaneous absorption of several photons. Crucial for the ionization probability is the total photon flux density. Practically all atomic and molecular species are affected in this non-resonant laser ionization.

The resonant case uses quantum-mechanical transition states for ionization that are specific for an atom or a molecule (Hurst *et al.*, 1979; Pellin *et al.*, 1987; Ma *et al.*, 1995). Therefore, the photon energies of one or a few lasers have to be tuned carefully to match exactly the required excitation energies. The results are extremely high ionization yields for specific atoms or molecules. The ionization of other neutral species at the same time is effectively suppressed, if single photons cannot ionize these species and if the photon flux density does not reach values necessary for non-resonant multiphoton ionization. Because of that, isobaric interferences at same nominal masses are avoided (*e.g.*, interferences of ^{92}Mo, ^{94}Mo, and ^{96}Mo with ^{92}Zr, ^{94}Zr, and ^{96}Zr) even with a relatively low mass resolution of the spectrometer.

In cosmochemistry, resonant laser post-ionization is up to now mainly used together with laser ablation instead of primary ion bombardment. Applications have been the analysis of titanium, zirconium, and molybdenum isotopic compositions of individual presolar silicon carbide or graphite grains (Ma *et al.*, 1995; Nicolussi *et al.*, 1997a,b, 1998a,b). Microprobe two-step laser desorption/laser ionization mass spectrometry (μL^2MS) has been used for the analysis of organic molecules in various kinds of extraterrestrial material (Kovalenko *et al.*, 1991, 1992; Clemett *et al.*, 1992, 1993, 1996, 1998; Thomas *et al.*, 1995).

2.2. Separation of secondary ions

2.2.1. Conventional SIMS

In conventional SIMS instruments, secondary ions are generated continuously by use of a static primary ion beam, and the different ion species are detected sequentially, *e.g.*, in a double-focusing magnetic mass spectrometer or a quadrupole spectrometer. At a given instant, only secondary ions of a previously selected mass-to-charge ratio reach the detector. Thus, most secondary ions are not measured. Even in multi-detector instruments, only a few ion species with similar mass-to-charge ratios can be detected simultaneously. Most secondary ions are therefore lost during the analysis.

2.2.2. TOF-SIMS

Contrary to this, time-of-flight mass spectrometry allows to measure **all** secondary ions with one polarity quasi simultaneously. The sample is bombarded in TOF-SIMS with a short-time primary ion pulse with typical lengths between several hundred picoseconds

and a few nanoseconds. This is repeated every few hundred microseconds, resulting in a duty cycle of typically 10^{-5}.

All secondary ions with one polarity are accelerated in an electric field with potential U and mass separated in a field-free drift tube. Particles with different mass-to-charge ratios m/q reach the detector after the time-of-flight t:

$$m/q = \frac{2eU}{s^2}t^2 \tag{1}$$

Here, s is the effective flight path, corresponding to the length of the drift tube.

2.3. Quantification

2.3.1. Element ratios

Quantification, *i.e.*, to determine useful element ratios, is a problem in SIMS due to the above described matrix effect. Since the emission of secondary ions from multi-element samples is theoretically not well understood, only an empiric approach is possible (Meyer, 1979). Standards with a chemical composition as similar as possible to the respective sample have to be used. These standards have to have well defined element abundances. Since usually only a small volume of the standard is analyzed, this volume has to be representative for the entire standard. This leads to high demands on purity and homogeneity of the standard. Amorphous or polycrystalline standards and samples are desired, because crystalline targets lead to unwanted effects like channeling. Only relative abundances can be determined with SIMS, even if all these conditions are satisfied. The secondary ion sensitivity for each element is calculated from the standard relative to a reference element E_0, often silicon. Using these relative sensitivities, the respective element ratios E/E_0 in the analyzed sample can be calculated from the determined secondary ion intensities SI:

$$\left(\mathrm{E}/\mathrm{E}_0\right)_{\mathrm{Sample}} = \frac{\left[SI(\mathrm{E})/SI(\mathrm{E}_0)\right]_{\mathrm{Sample}}}{\left[SI(\mathrm{E})/SI(\mathrm{E}_0)\right]_{\mathrm{Standard}}}\left(\mathrm{E}/\mathrm{E}_0\right)_{\mathrm{Standard}} \tag{2}$$

The relative sensitivity

$$RS(\mathrm{E}, \mathrm{E}_0) = \frac{SI(\mathrm{E})/SI(\mathrm{E}_0)}{\mathrm{E}/\mathrm{E}_0} \tag{3}$$

depends on the respective ion species, the polarity, the sample material (matrix), as well as the analytical conditions, like primary ion type, energy, and angle of incidence, together with the detection efficiency for the secondary ion species.

2.3.2. Isotopic ratios

The matrix effect plays a much less pronounced role for isotopic ratios. Nevertheless, effects of mass fractionation occurring in the SIMS process or during subsequent mass separation and detection of the secondary ions have to be taken into account if high accuracy of isotope measurements is required (Slodzian *et al.*, 1980, 1998). Again, standards with known isotopic ratios can be used to monitor these effects.

2.4. Static and dynamic SIMS

Secondary ion mass spectrometry in general is a destructive technique. However, one often discerns between static and dynamic SIMS due to the difference in sputtering intensity. Static SIMS describes the case where the sample surface is not altered during the SIMS analysis. Dynamic SIMS, on the other hand, is much more destructive but facilitates quantification. Interaction of the primary ion beam – often O^- for positive and Cs^+ for negative secondary ions – with the sample generates more reproducible conditions in dynamic SIMS. The high abundance of oxygen facilitates the formation of positive secondary ions and the actual (pre-sputtering) oxidation state within the samples loses its influence. Cesium, the element with the lowest ionization potential, supports the generation of negative secondary ions. With this strategy, dynamic SIMS becomes much less susceptible to matrix effects than static SIMS.

Static SIMS conditions cannot be achieved strictly speaking, because primary ion bombardment even at lowest intensity alters the sample surface. However, TOF-SIMS is a good approach to static SIMS conditions especially with a less focused primary ion beam. The probability for a primary ion to hit an area on the sample already altered by sputtering can be neglected, and sputter times of several hours are necessary to consume one monolayer (Benninghoven, 1973, 1975, 1985, 1994).

2.5. Charge compensation

Since most samples of geo- or cosmochemical interest are electrical insulators, sample charging during primary ion bombardment has to be considered (Werner and Morgan, 1976; Werner and Warmoltz, 1984; Blaise, 1994). Charging affects the positioning of the primary ion beam, which is deflected by the electric surface potential, and, on the other hand, it affects the energy of the secondary ions, because they are not extracted from a well-defined electric potential.

For conventional SIMS analyses, samples are therefore often coated with 20–100 nm of carbon or gold (Zinner, 1989). The primary ion beam then sputters a small (up to 20 μm) hole into this coating, and the underlying material can be analyzed. Small samples, single grains up to 30 μm in size, can be pressed into gold foil (McKeegan *et al.*, 1985; Zinner, 1989). Although, strictly speaking, the actually investigated sample area is still insolating, charging is no longer critical in both cases. Electrons for charge compensation are picked up from the surrounding conductive neighborhood, which also takes up surplus electrons when the sample is bombarded with negative primary ions.

Surface coating has to be avoided in TOF-SIMS, because only the uppermost atomic monolayers are analyzed. Even if coating of a single spot can be removed by sputtering, larger areas would not be accessible. However, a charge compensation system has been developed especially for pulsed primary ion sources used in TOF-SIMS (Hagenhoff *et al.*, 1989). Electrons from a pulsed low-energy electron source reach the target between two primary ion shots. This process is self-regulative due to the low energy (10–20 eV) of the electrons. The secondary ion extraction field is switched off during the electron pulse. For the analysis of negative secondary ions, a slight negative retarding field at the extractor prevents the electrons from reaching the detector.

2.6. Mass interferences

A major problem in SIMS in general and TOF-SIMS in particular is the separation of mass interferences. Therefore, this subject is discussed in detail here, especially for TOF-SIMS. The ability to separate two neighboring mass peaks in mass spectrometry is described as the *mass resolution* or the *mass resolving power* ($m/\Delta m$). This mass resolution can be adjusted in DF-SIMS over a wide range at the expense of the ion transmission of

the instrument. The mass resolution in TOF-SIMS mainly depends on the accuracy of the flight time measurement as will be discussed later.

The term “required mass resolution for separation of two peaks” is used in the following for theoretical values resulting solely from the mass difference of the respective peaks. It does not include considerations on peak shape, required accuracy, or varying peak intensities, which often lead to more strict limitations for a proper peak separation. For the experimentally determined mass resolutions of an actual mass spectrometer, the width (Δm) of a mass peak has to be determined at a certain height of the peak. The *full width half maximum* (FWHM) definition is used throughout this work if not specified otherwise. The actual mass resolution for a sufficient separation of two peaks might be required at a lower peak height, depending on the relative intensities of the respective ion signals and the required accuracy. This has especially to be considered in time-of-flight mass spectrometry, where peak integrals and not peak heights are determined.

There are four major groups of mass interferences with typical characteristic features: (1) Isobaric interferences from nuclides of different elements, (2) hydrides, (3) oxides and hydroxides, (4) simple hydrocarbons. These groups are now discussed in greater detail.

2.6.1. Isobaric interferences from other nuclides

Isotopes from different elements at the same nominal mass are one group of isobaric interferences. Two stable nuclides exist for 52 isobars and even three naturally occurring nuclides can be found for five isobars. Mass resolutions between $m/\Delta m=10^4$ (^{48}Ca and ^{48}Ti) and $6\cdot10^7$ (^{187}Re and ^{187}Os) are required to separate their corresponding mass peaks from each other (Fig. 3). This is not achievable with the available TOF-SIMS instruments, as will be shown later. However, for the analysis of element abundances, these interferences have to be considered but are not crucial. They can be corrected in most cases by using other isotopes from the respective element (see below).

2.6.2. Hydrides

Due to adsorbed hydrogen atoms or hydrocarbons, hydrides are important in surface analysis and are therefore often observed, especially in TOF-SIMS mass spectra. Sometimes they can reach the same intensity as the element peak itself. Hydrides from one

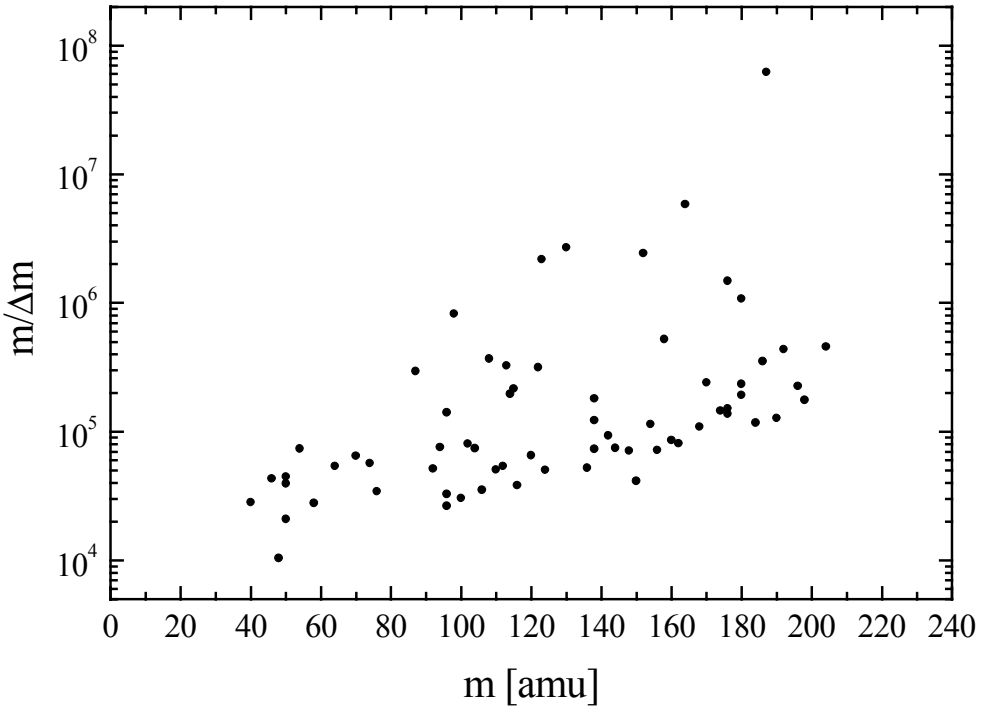

Fig. 3. Required mass resolutions for separation of isobaric interferences resulting from isotopes of other elements (resolving ^{m}A from ^{m}B).

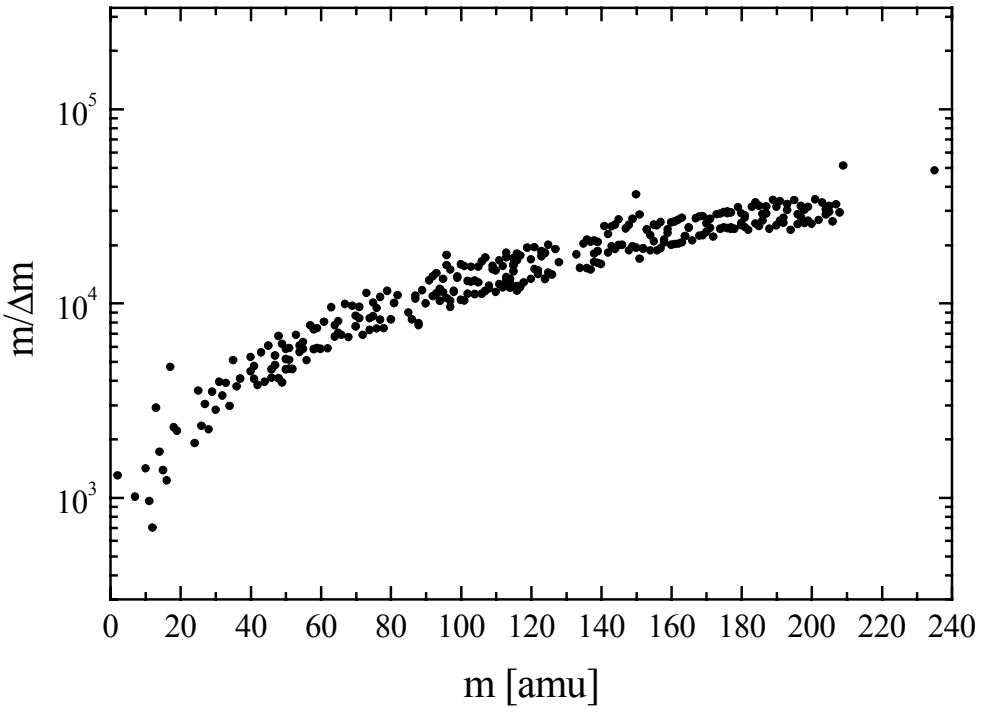

Fig. 4. Mass resolution necessary for separating hydrides ($^{m-1}$A^{1}H) from element peaks (^{m}B).

isotope may interfere with an isotope of the same or a neighboring element. The required mass resolutions are typically lower here and can be achieved in TOF-SIMS, at least for low masses, by using very short primary ion pulses. At masses above ~90 amu (amu = atomic mass unit = 1/12 of the mass of ^{12}C) the required mass resolution exceeds $m/\Delta m=10^4$ (Fig. 4), which is approximately the maximum mass resolution reachable with present TOF-SIMS instruments.

2.6.3. Oxides and hydroxides

Oxides and hydroxides account for similar problems as hydrides. Since ^{16}O (15.995 amu) almost exactly lies on the nominal mass, any nuclide and its oxide have the same deviation in mass from the nominal mass. This mass difference typically increases for low-mass nuclides with increasing mass number. Between 88 and 140 amu it is practically constant, before it decreases again for higher masses. Therefore, in the middle mass range, around 110 amu for oxides and 130 amu for hydroxides, their separation from atomic ions requires non-achievable high mass resolutions, well above $m/\Delta m=10^4$ (Fig. 5).

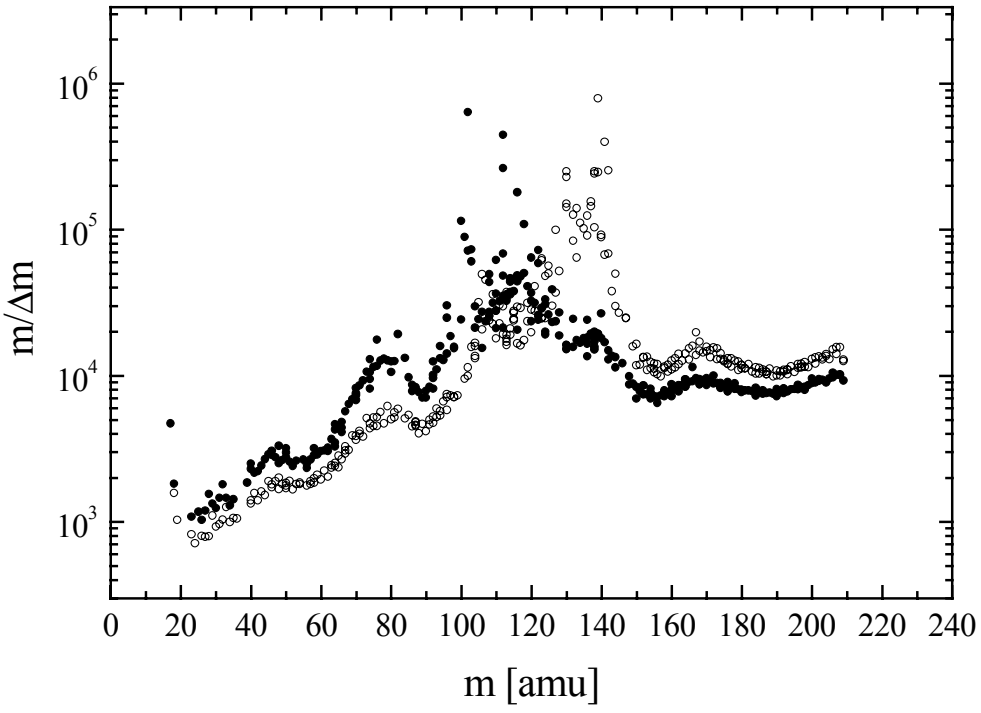

Fig. 5. Mass resolution needed for separation of oxides ($^{m-16}A^{16}O$, solid symbols) and hydroxides ($^{m-17}B^{16}O^{1}H$, open symbols) interfering with nuclides at mass *m*.

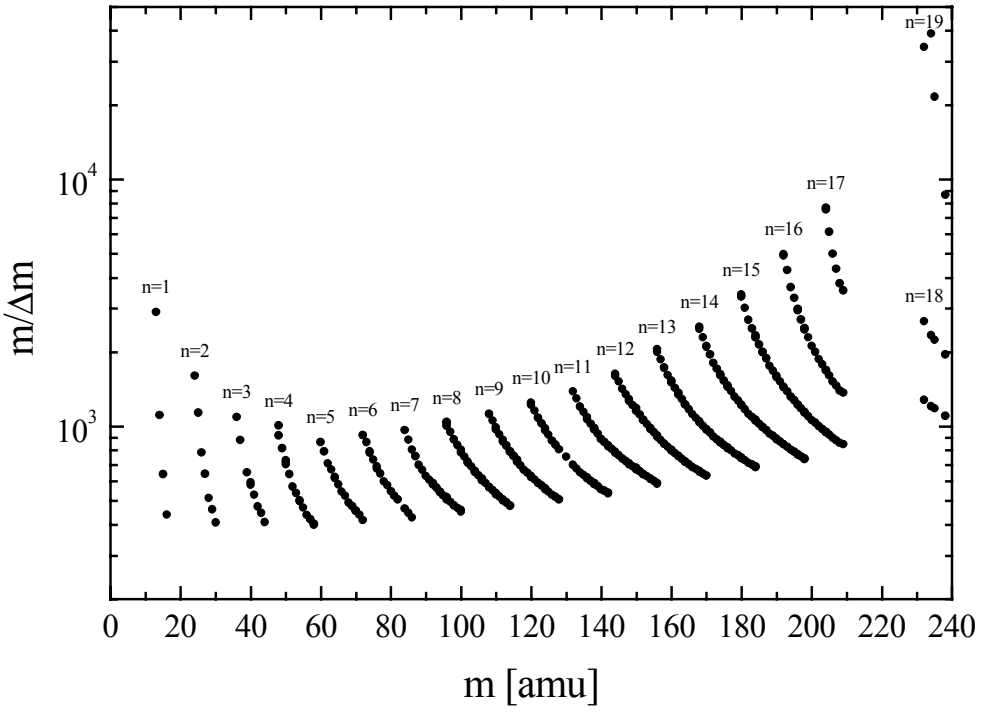

Fig. 6. Mass resolution required for separation of hydrocarbons $^{12}C_n{}^1H_{m-12n}$ from element peaks at mass m.

2.6.4. Hydrocarbons

Hydrocarbons occur almost throughout the entire mass spectrum. Nevertheless, their interferences with atomic ions are rather easy to separate, especially when several hydrogen atoms are present. Each additional H-atom shifts the peak $7.98 \cdot 10^{-3}$ amu to the right of the nominal mass (towards higher masses). Except for the light elements up to nitrogen and the very heavy elements thorium and uranium, elemental mass peaks lie left (towards lower masses) of the respective nominal mass. Up to ^{56}Fe the mass-to-nucleon ratio decreases (^{56}Fe is the nuclide with the highest binding energy). Consequently, the required mass resolution for separation of hydrocarbons has a minimum at masses around 56 amu (Fig. 6).

2.7. Mass resolution in time-of-flight mass spectrometry

In general, mass resolution in TOF mass spectrometry depends on time resolution of the flight time measurement. According to Eq. (1) follows

$$\frac{m}{\Delta m} = \frac{t}{2\,\Delta t} \tag{4}$$

This resolution depends on the resolution of the mass analyzer R_{an} (Mamyrin *et al.*, 1973), the time resolution Δt_{reg} of detector and registration electronics, and the duration Δt_p of the ionization event that in SIMS is the pulse width of the primary ion shot (Jürgens *et al.*, 1992; Jürgens, 1993):

$$\frac{m}{\Delta m} = \left(\frac{1}{R_{an}^{\ 2}} + 2 \frac{\Delta t_{reg}^{\ 2} + \Delta t_p^{\ 2}}{t^2} \right)^{-1/2} \tag{5}$$

From the linear correlation between t^2 and m (Eq. (1)) follows

$$\frac{m}{\Delta m} = \left(\frac{1}{R_{an}^{\ 2}} + \frac{\Delta t_{reg}^{\ 2} + \Delta t_p^{\ 2}}{c} \cdot \frac{1}{m} \right)^{-1/2} \tag{6}$$

where the constant c depends on instrument parameters, length of the flight path and extraction voltage.

Actual values of mass resolutions achievable in TOF-SIMS will be discussed later, when the TOF-SIMS instrument used in this study is described.

3. Time-of-flight secondary ion mass spectrometry

The following section will concentrate on practical aspects of TOF-SIMS. First, for a better understanding, the principles of conventional DF-SIMS and TOF-SIMS instruments are compared.

3.1. Secondary ion mass spectrometers

3.1.1. DF-SIMS

Double-focusing magnetic mass spectrometers in SIMS are separating secondary ions by electrostatic and magnetic sector fields (Fig. 7). In the electrostatic field, the secondary ions are dispersed according to their energy. Centrifugal and electrostatic forces are in equilibrium here:

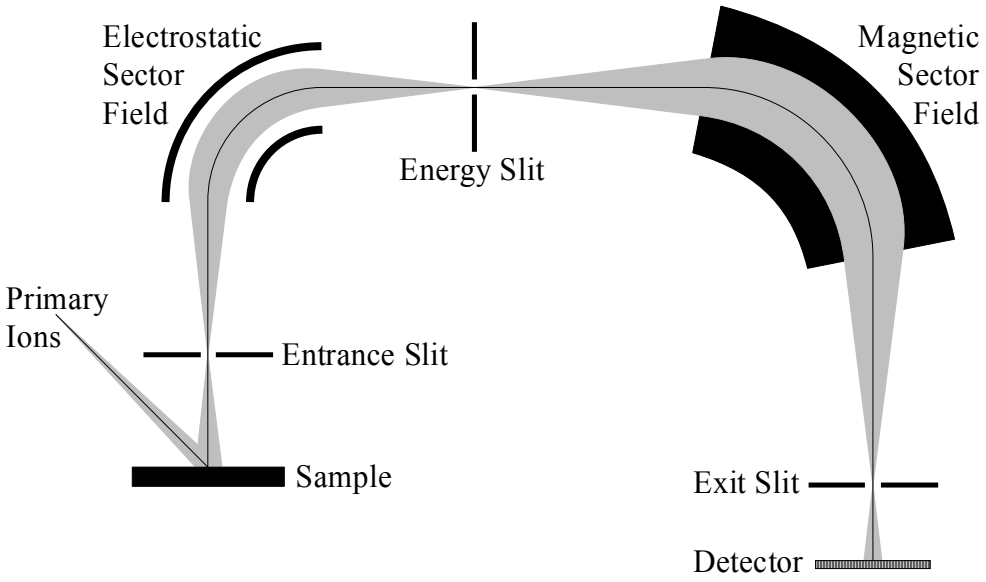

Fig. 7. Schematic view of a DF-SIMS instrument. Not shown are ion-optical elements like deflectors or electrostatic lenses.

$$\frac{mv^2}{r} = qE \tag{7}$$

The radius r depends in a given electrostatic field E on the kinetic energy ($mv^2/2$) per charge q. With the aid of the energy slit (cf. Fig. 7), selection of secondary ion energies is possible, and the system can be used as an energy filter.

In the following magnetic field B, the secondary ions are dispersed according to their mass-to-charge ratio and their energy. It can be regarded as a filter for momentum (mv). Here, centrifugal and magnetic forces are in equilibrium:

$$\frac{mv^2}{r} = qvB \tag{8}$$

The combination of electrostatic and magnetic fields allows compensation of energy dispersions from the electrostatic and magnetic analyzers. The result is separation of secondary ions according to their mass-to-charge ratio regardless of their energy, the principle of double-focusing mass spectrometry.

Nevertheless, the energy slit can be used for narrowing the energy bandwidth of the secondary ions. The width of the secondary ion energy distribution decreases with increasing complexity of the molecular ion and depends on the relative mass difference between the constituents of the molecule (Crozaz and Zinner, 1985). Consequently, energy filtering is not efficient for the removal of hydrides and most monoxides, but complex molecular mass interferences can be effectively suppressed (Crozaz and Zinner, 1985). This is done by setting the sample potential and the width of the energy slit to values that only secondary ions within a certain energy window above a specific energy reach the detector. This energy filtering technique has been successfully applied, *e.g.*, to the measurement of rare earth elements (Crozaz and Zinner, 1985; Zinner and Crozaz, 1986).

A special feature of the experimental set-up shown in Fig. 7 is that it can transport ion images, showing the lateral distribution of the respective ion species. Secondary ion images can be generated by using a defocused primary ion beam. Direct imaging through ion optical projection is often called ion microscope technique in contrast to SIMS instruments where secondary ion images are generated by scanning the primary ion beam over the sample (ion microprobe technique).

Energy filtering in DF-SIMS also reduces chromatic aberrations of secondary ion images. Analogous to light optics, the focal length of an ion-optical lens varies with the energy of the ions (equivalent to wavelength or color of light).

3.1.2. TOF-SIMS

All types of TOF-SIMS instruments are based on the same principle: The velocity of an ion with a given kinetic energy depends on its mass. One discerns between two major groups of TOF-SIMS instruments. Besides analyzers with three hemispherical electrostatic analyzers (Schueler *et al.*, 1990; Schueler, 1992), most TOF-SIMS instruments use a more simple design with an ion reflector (Mamyrin *et al.*, 1973; Niehuis *et al.*, 1987; Niehuis, 1990). Only the latter type is explained in detail here, because most analyses discussed in this study were performed with this type of instrument. However, the major difference between the two set-ups is that the triple sector spectrometer allows direct imaging through ion optical projection (ion microscope). Spatial information gets lost in the reflector instrument and the ion microprobe mode is used for imaging.

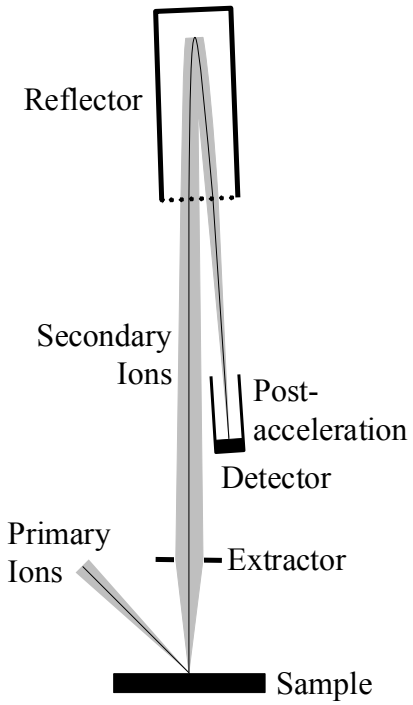

Fig. 8. Schematic view of a TOF-SIMS instrument.

A schematic view of a reflector TOF-SIMS instrument is given in Fig. 8. Secondary ions are extracted from the sample surface by acceleration in an electric field. In the subsequent drift tube, the ions are separated according to their velocity before they reach the detector. Since slightly different starting energies result in slightly different flight times, even for ions of the same species, a reflector is used for energy focusing (Mamyrin *et al.*, 1973). Ions with higher energies penetrate its electric field deeper and are therefore delayed compared to lower-energy ions. By adjusting the electric fields carefully, all secondary ions of one species can reach the detector practically simultaneously.

3.2. Description of the TOF-SIMS instrument

The Cameca/ION-TOF TOF-SIMS IV instrument used in this study is a reflector-based instrument as described in the previous section and shown in Fig. 8. The present TOF-SIMS IV instrument at the *Institut für Planetologie* in *Münster* is equipped with two primary ion sources for analysis, an electron impact ion gun mainly for argon primary ions (Niehuis *et al.*, 1987) and a gallium liquid metal ion gun (Ga-LMIS; Niehuis, 1997). In addition, the instrument has a sputter source, a combination of a cesium thermal ionization source and an electron impact source for argon or oxygen sputtering ions (Terhorst *et al.*, 1997). It can be used for cleaning of the sample surface as well as for depth profiling. All ion beams reach the sample with an angle of 45° and the secondary ions are extracted perpendicular to the sample surface with an extraction potential of 2 kV (Fig. 8). The sample is at ground potential.

After the reflection, the secondary ions are post-accelerated with energies of 8–10 keV before they reach the detector. The detector consists of a microchannel plate for ion to electron conversion, a scintillator for electron-to-photon conversion, and a photomultipier, which is placed outside the vacuum chamber. All three steps lead to an amplification of the signal, but the major advantage of this set-up is the separation of high-voltage at the detector and low-voltage of the electronics. A constant fraction discriminator converts the incoming signal to a normalized signal, which is further processed in a time-to-digital converter (TDC). The time resolution of the TDC is adjustable between 50 and 1600 ps, but it is mostly operated at 200 ps.

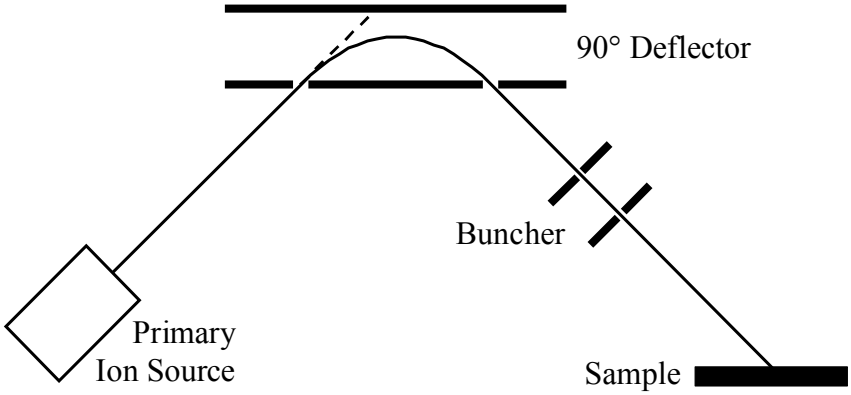

Fig. 9. Schematic view of the pulsing and bunching system of the electron impact primary ion gun. Focussing elements like lenses and deflection units for beam alignments were omitted. Primary ions, mainly Ar^+, are generated in a conventional electron impact ion source. A 90°-deflection unit is used to cut ion packages with pulse lengths of 10–15 ns out of a continuous ion beam. These pulses are compressed to pulse lengths of ~1.2 ns in a bunching system.

A second detector system is used for detection of secondary electrons. With this, a secondary electron image similar to those generated in a scanning electron microscope can be obtained by scanning the primary ion beam over the sample. A pulsed low-energy (~18 eV) electron source is used for charge compensation.

3.2.1. The argon primary ion source

A schematic view of the pulsing system of the electron impact primary ion gun is given in Fig. 9. This primary ion source is mainly used with $^{40}Ar^+$ as primary ion species. Ion pulses with typically lengths of 10–15 ns are generated from a continuous ion beam with a 90°-deflection unit. Each ion package is compressed along its flight direction to typically 1.2 ns pulse length in an electrodynamic bunching system. Ions from the rear of the package are accelerated to catch up with those from the front when they reach the target. (Niehuis *et al.*, 1987)

The argon electron impact ion source has its main advantage in producing short primary ion pulses with relatively high intensities (cf. Table 1). The major drawback of this type of ion source is the limited lateral resolution (~10 μm), due to the relatively large volume where ion formation takes place. Projection of this ionization volume onto the sample surface leads to inevitable dispersion of the ion beam. Acceleration of the ions to different energies in the bunching unit also reduces the lateral resolution. These energy variations increase chromatic aberrations of the target lens.

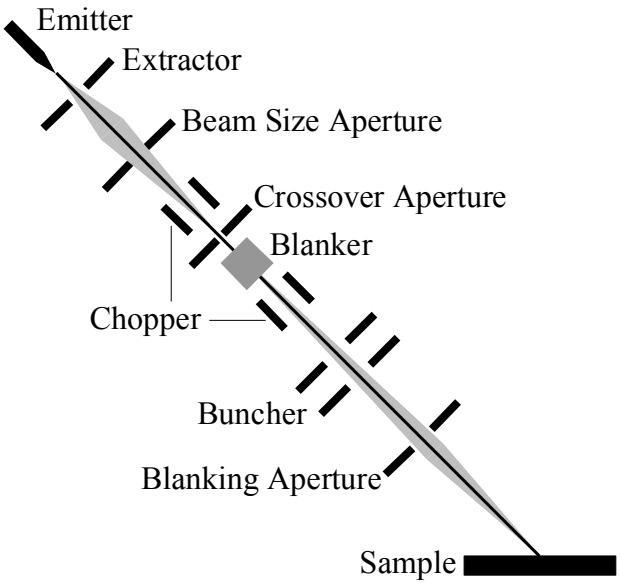

Fig. 10: Schematic view of the gallium liquid metal ion source. Focussing elements like lenses and deflection units for beam alignments were omitted. Primary ion packages with pulse lengths of ~5 ns are produced from a continuous beam with a blanking system. These packages can be chopped a second time or compressed along their flight direction in a bunching system to further reduce their pulse lengths.

3.2.2. The gallium primary ion source

The gallium primary ion source is shown in Fig. 10. A tungsten needle with a thin liquid gallium film is exposed to a high electric field. At typical extraction potentials of 5–10 keV the liquid gallium forms a so-called Taylor-cone at the tungsten tip and Ga^+ ions are emitted. These ions stem from a very small region with a typical size of 10 nm. This small spot size is responsible for the achievable high lateral resolution of the Ga-LMIS (beam diameter ~200 nm).

The Ga-LMIS can be operated in different modes, which mainly differ in length of the primary ion pulse, primary ion intensity, and achievable spatial resolution (cf. Table 1). Typical pulsing systems produce single ion packages with lengths of ~5 ns by blanking a continuous ion beam. There are two possible techniques to further reduce the pulse length. Each ion package can be chopped a second time (Fig. 11) or compressed along its flight direction in a bunching system analogous to the argon source (Niehuis *et al.*, 1987; Schwieters *et al.*, 1991, 1992).

TABLE 1. Comparison of different analytical modes for argon and gallium ion sources.

Primary ion species	Pulsing mode	Pulse width	Spatial resolution	Primary ions / cycle	Secondary ions / cycle
$^{40}Ar^+$	blanked+bunched	1.2 ns	10 µm	500	2.5
$^{69}Ga^+$	blanked	5 ns	200 nm	50	0.25
$^{69}Ga^+$	blanked+chopped	1.5 ns	200 nm	10	0.05
$^{69}Ga^+$	blanked+bunched	600 ps	5 µm	50	0.25
$^{69}Ga^+$	burst mode	n×1.5 ns	200 nm	n×10	n×0.05

A value of one secondary ion per 200 primary ions was assumed. This is only a rough estimate, based on analyses of typical glass standards. For these conditions, one sputtered particle for each primary ion can be assumed. The actual values strongly depend on sample material and surface conditions. Typical repetition rates are 5–10 kHz, leading to total count rates of several thousand secondary ions per second spread over the entire mass spectrum.

In the first case, the primary and therefore the secondary ion intensity decrease with the pulse length. Extremely short pulses result in extremely small signals, often not sufficient for trace element studies. On the other hand, the spatial resolution (beam diameter) remains unchanged in this case. Typical pulse lengths achieved with high-frequency choppers are 1.5 ns.

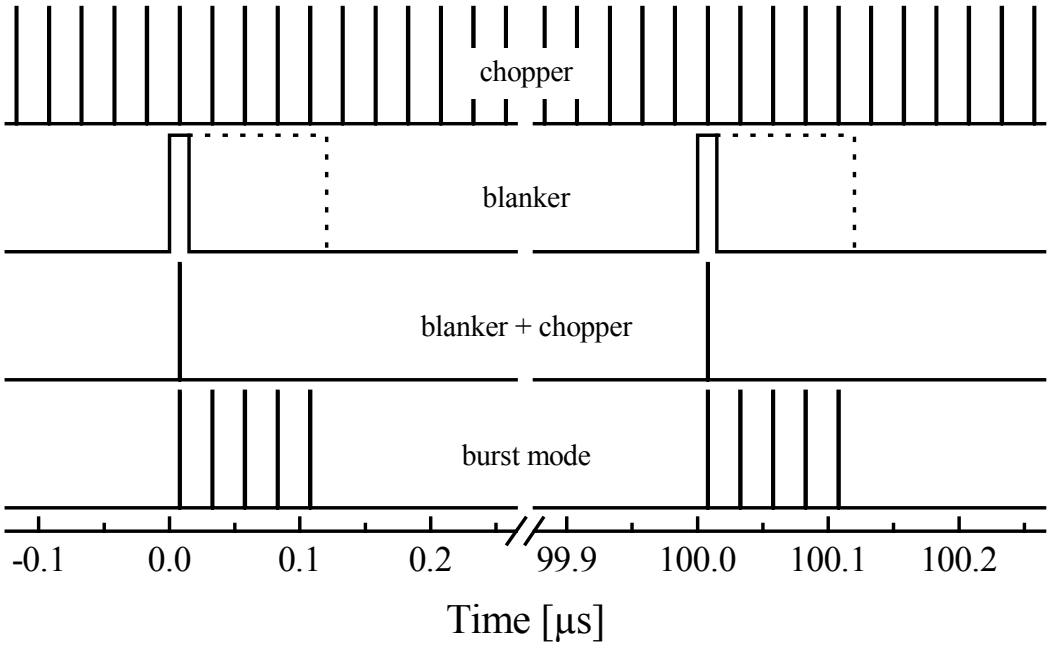

Fig. 11. Timing schemes for blanker and chopper. The blanker is used to select one or a series (burst mode, dotted line) of 1.5 ns ion pulses continuously produced by the high-frequency (40 MHz) chopper. Blanker and chopper are both pulsing units which are applied in different ways. Sometimes, these names are used in the literature the other way round.

The electrodynamic bunching system allows an axial compression of the ~5 ns ion package to ~600 ps pulse length. Since no primary ion gets lost, secondary ion intensities are usually by a factor of five higher than in the chopped mode. This is mostly sufficient for trace element studies. On the other hand, chromatic aberrations of the target lens here limit the achievable spatial resolution to ~5 µm.

3.2.3. Mass resolution – spatial resolution – signal intensity

The three parameters mass resolution, spatial resolution, and intensity of the secondary ion signals are strongly related to each other in TOF-SIMS. The mass resolution can be adjusted in DF-SIMS over a wide range by changing the widths of the different slits (Fig. 7) at the expense of the ion transmission of the instrument. This is not the case for TOF-SIMS. Here, the mass resolution depends on the duration of the primary ion pulse, the length of the flight path, the energy focusing in the reflector, the time resolution of the detection system, and, finally, on the mass itself. The dependence on time resolution of the flight time measurement has been discussed above.

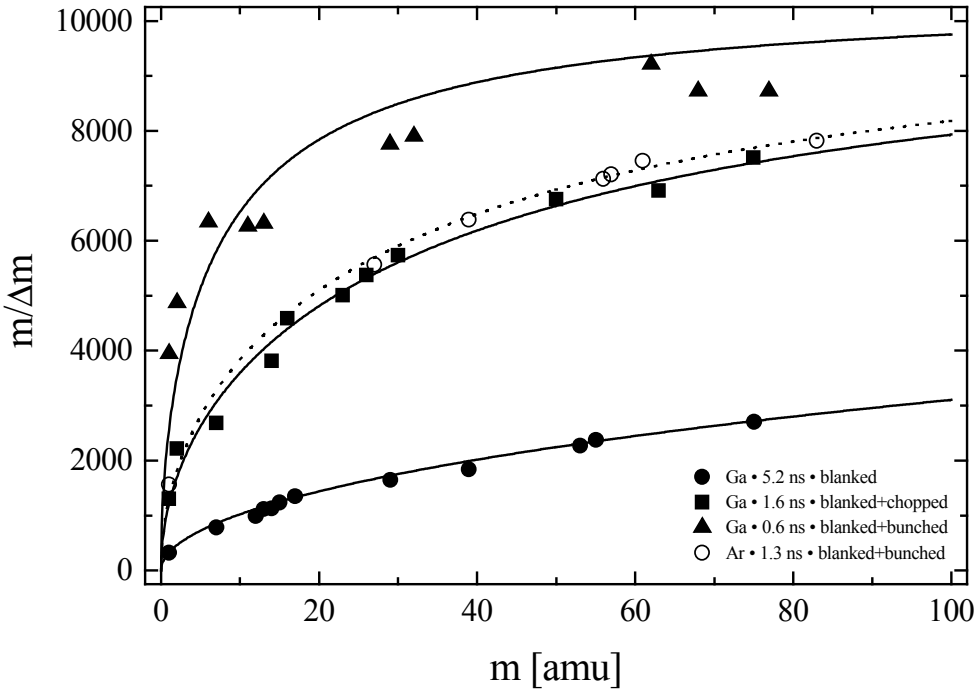

Fig. 12. Mass resolution (FWHM) depending on mass for typical measurements with gallium and argon primary ion sources. Data points show selected peaks with no apparent mass interference. The gallium ion source was operated in three different modes. The mass resolution of the analyzer is $m/\Delta m$=10500 in all cases.

The mass dependence of the mass resolution at full width half maximum (FWHM) is demonstrated in Fig. 12 for the argon primary ion source as well as for different analytical modes of the gallium source. From best fits according to Eq. (6) for the data points of undisturbed mass peaks, a resolution R_{an} for the analyzer of about 10500 has been inferred. This resolution describes the asymptotic limit at high masses, whereas the accuracy of the time measurement, mainly from Δt_p, shapes the fit curve at low masses. The time resolution of the registration system Δt_{reg} was 200 ps. Primary pulse lengths Δt_p of 1.3 ns for the argon source and 5.2, 1.6, and 0.6 ns for blanked, blanked+chopped and blanked+bunched modes of the gallium source, respectively, have been determined.

A simultaneous increase of all three parameters, mass resolution, spatial resolution, and intensity of the secondary ion signals, is restricted, because the number of charged particles within a small volume is also limited due to space charge effects. Extension of the ion package in flight direction results in low mass resolution. Extension perpendicular to the flight direction results in low spatial resolution. The different pulsing modes of the gallium source in Table 1 show the mutual influence of these parameters.

Nevertheless, if high lateral resolution **and** high mass resolution are required, the secondary ion yield can be increased by applying a series of 1.5 ns primary ion pulses, spaced 25 ns apart from each other, in every shot cycle. This so-called “burst” mode (Fig. 11) results in a series of overlapping mass spectra, which can be summed up by appropriate computer programs. For primary ion bursts of five single pulses, approximately the same intensity is reached as in the “blanked” mode (cf. Table 1). This leads to useful results for masses up to ~200 amu, where the last peak from one nominal mass begins to overlap with the first peak of the next nominal mass. By varying the number of primary ion shots within one burst, the usable mass range can be adjusted. An increasing number of ion shots within one burst leads to a decreasing upper limit for the usable mass range (*e.g.*, ~50 amu for bursts of 10 shots). Therefore, the burst mode is not applicable to the investigation of large molecules.

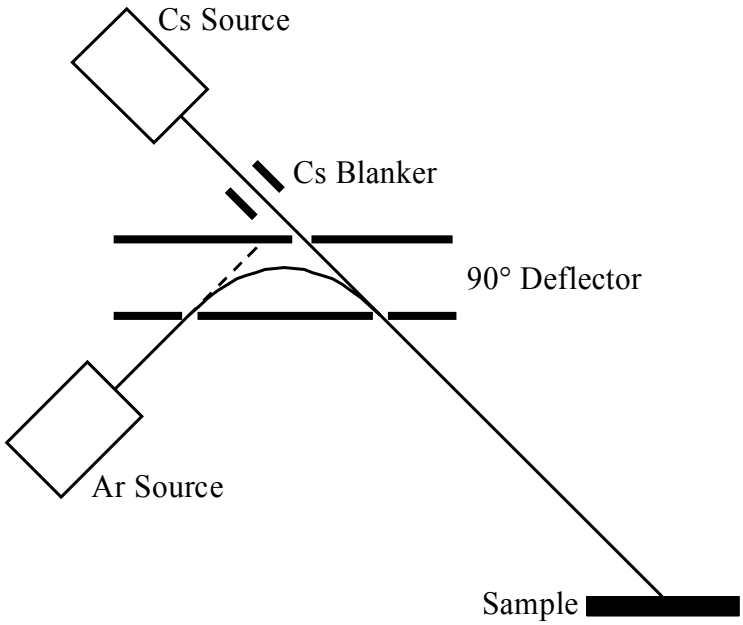

Fig. 13. Schematic view of the so-called dual beam sputter source. It is a combination of a cesium thermal ionization source and an electron impact source for argon sputtering ions. As in previous figures, focussing elements like lenses and deflection units for beam alignments were omitted.

3.2.4. Sputtering

Since TOF-SIMS analyzes the uppermost surface of a sample, contamination can be a severe problem. Therefore, the surface often has to be cleaned. To avoid adsorption of molecules present in the ambient air after the cleaning procedures, this is preferentially performed directly under ultra-high vacuum conditions in the TOF-SIMS instrument prior to the analysis. It can be done by sputtering with the primary ion gun. The TOF-SIMS IV instrument is equipped with an additional ion source exclusively for sputtering. Besides for surface cleaning, the sputter gun can also be used for depth profiling (Williams, 1998). The TOF-SIMS IV sputter source (Fig. 13) is a combination of a cesium thermal ionization source and an electron impact source for argon or oxygen sputtering ions (Terhorst *et al.*, 1997). The beam diameter is ~50 µm.

Secondary ion yields can be influenced and drastically increased by selecting specific ion species for sputtering. Bombardment with oxygen ions, *e.g.*, enhances the positive secondary ion signal (Wittmaack, 1998); cesium ions increase negative ion abundances. Although such an increase is desirable, the occurrence of molecular ions like oxides,

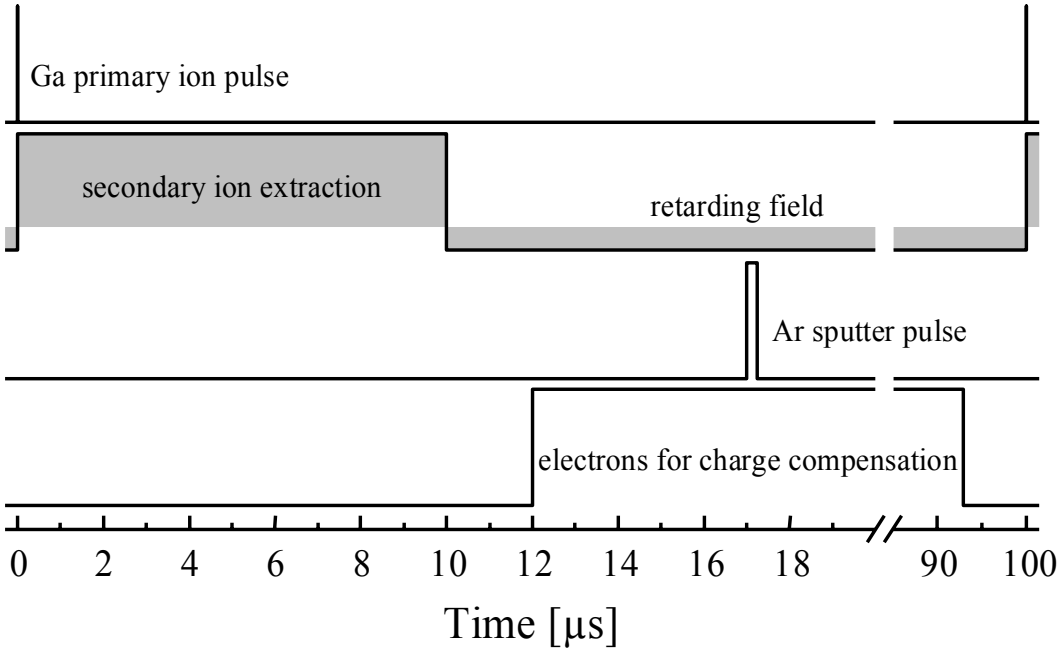

Fig. 14. Timing scheme for simultaneous use of two ion sources for insulating samples. A gallium primary ion source pulsed with 10 kHz is used for the actual TOF-SIMS analysis. Sputtering with a pulsed argon source occurs between two gallium shots. Secondary ions are only extracted directly after the gallium pulse. During the sputter pulse, a slight retarding field at the extractor prevents secondary ions from reaching the detector.

stimulated by oxygen sputter ions, may complicate the interpretation of the mass spectrum. Therefore, sputtering with inert ion species like argon is more advantageous and has been performed in this study.

After removing adsorbed hydrocarbons through sputtering, even under ultra-high vacuum conditions (~$2 \cdot 10^{-10}$ mbar), the sample surface can regain atoms and molecules like hydrogen or hydrocarbons present in the residual gas. The primary ion source is not able to prevent this adsorption sufficiently with its low duty cycle, especially when a large area is scanned with the ion beam. Therefore, an analytical mode has been developed, where the sample is analyzed with a gallium primary ion source and sputtered simultaneously with an argon sputtering source (Fig. 14). The sputter pulse is applied between two gallium pulses during charge compensation. The intensity of the sputter pulse is limited to ~100 pA at 10 kHz repetition rate (~$6 \cdot 10^4$ ions/shot) due to charging of the sample. Although the electron current for charge compensation easily exceeds 1 µA, the efficiency of charge compensation mainly depends on the number of electrons reaching the area of actual ion bombardment, ~50 µm in diameter for the sputter source. However, the sputter current of 100 pA is sufficient to suppress adsorption effectively during the analysis.

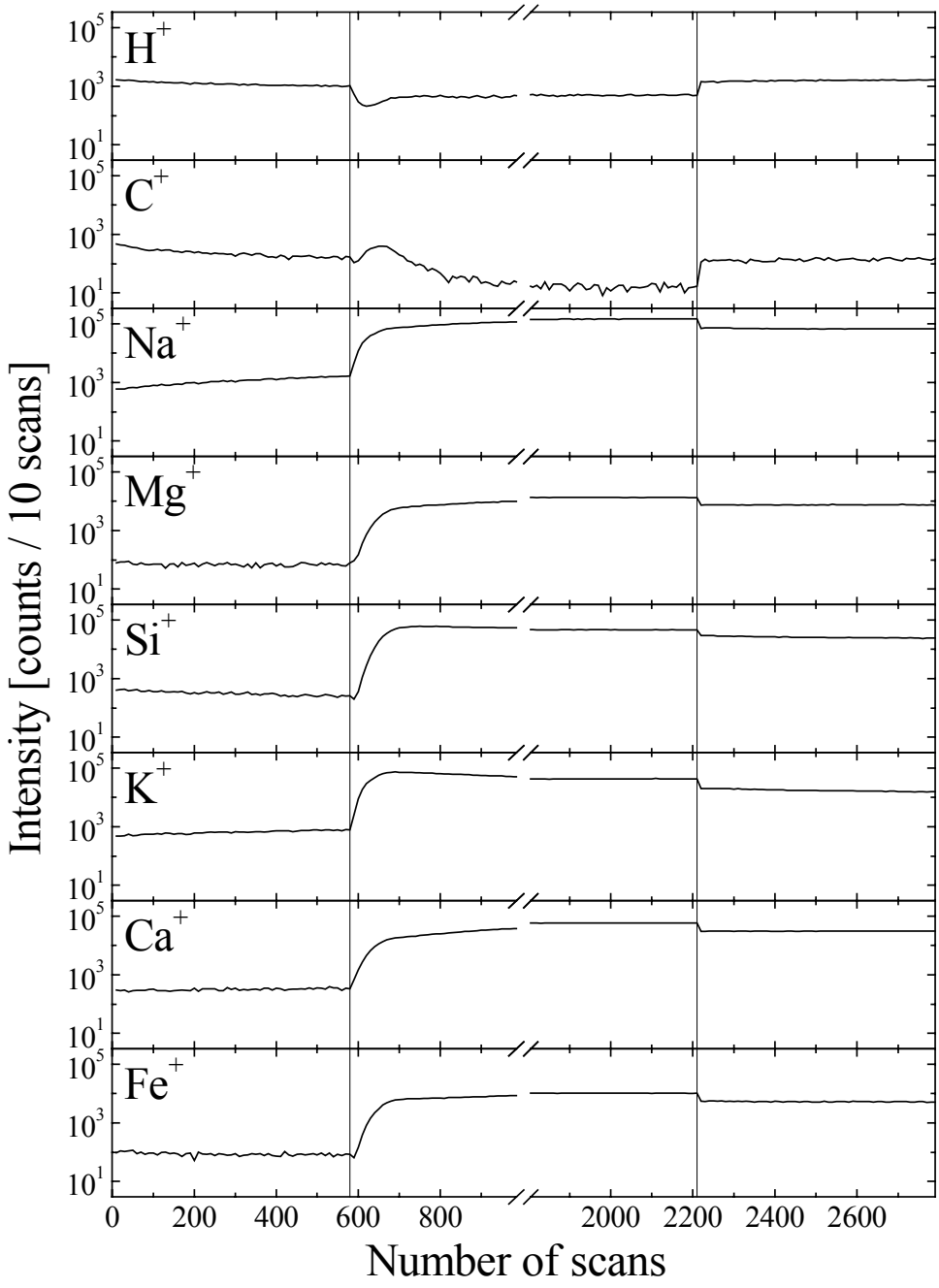

Fig. 15. Variations of secondary ion intensities caused by sputtering. A 50×50 μm^2 area of glass StHs6/80-G (cf. Appendix) was bombarded with 5 ns gallium shots. After 580 scans (256×256 pixels, one shot per pixel) the sample was simultaneously sputtered with an argon beam. This led to an increase of most secondary ion signals by factors of 50–200. Surface adsorbed hydrocarbons are suppressed efficiently. The H^+ and C^+ signals decreased by factors of 2 and 10, respectively. Stable signals were reached after 700–800 scans (~80 minutes) with simultaneous sputtering. After switching off the sputter source (after scan 2210) hydrocarbon signals increased again to values similar to those before sputtering. Signals for other elements decreased slightly, but still remained clearly above the values before sputtering.

3.3. TOF-SIMS mass spectra

TOF-SIMS mass spectra contain a wealth of information due to parallel detection of an in principle unlimited mass range. Before the rules of data evaluation are explained, examples for positive and negative secondary ion mass spectra (mass range 1–100 amu) obtained from a glass standard after extensive argon sputtering are given in Figs. 16 and 17.

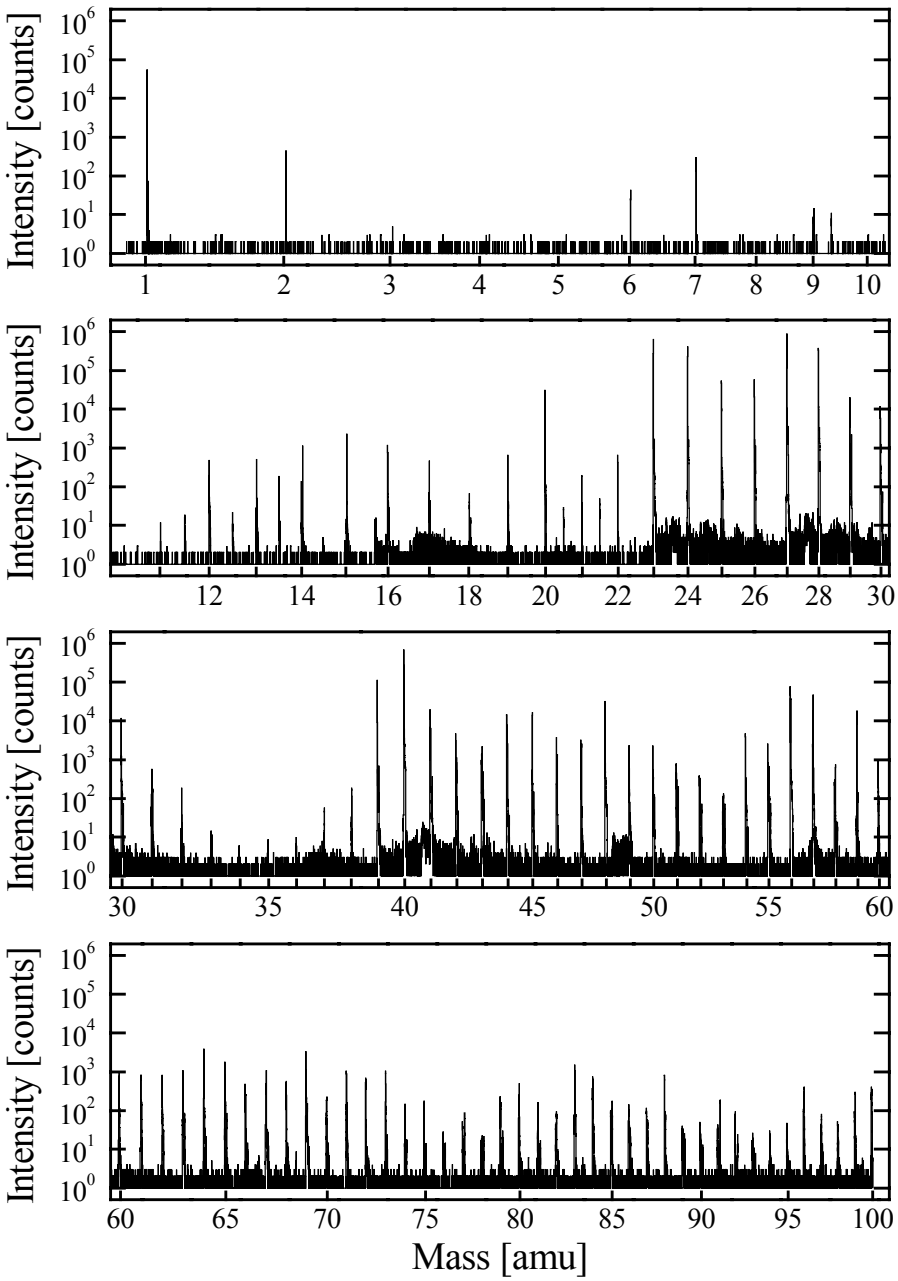

Fig. 16. Highly compressed mass spectrum of positive secondary ions obtained from glass standard KL2-G (cf. Appendix) after extensive argon sputtering. Only the mass range from 1–100 amu is shown here.

Negative ion spectra are disturbed by electrons, which partially result from charge compensation. They are also generated as secondary or tertiary electrons from interaction of primary as well as secondary ions with various surfaces within the instrument. Some of these electrons appear as distinct lines or broad peaks in the respective spectrum, but a general baseline increase is also observed throughout the entire mass range.

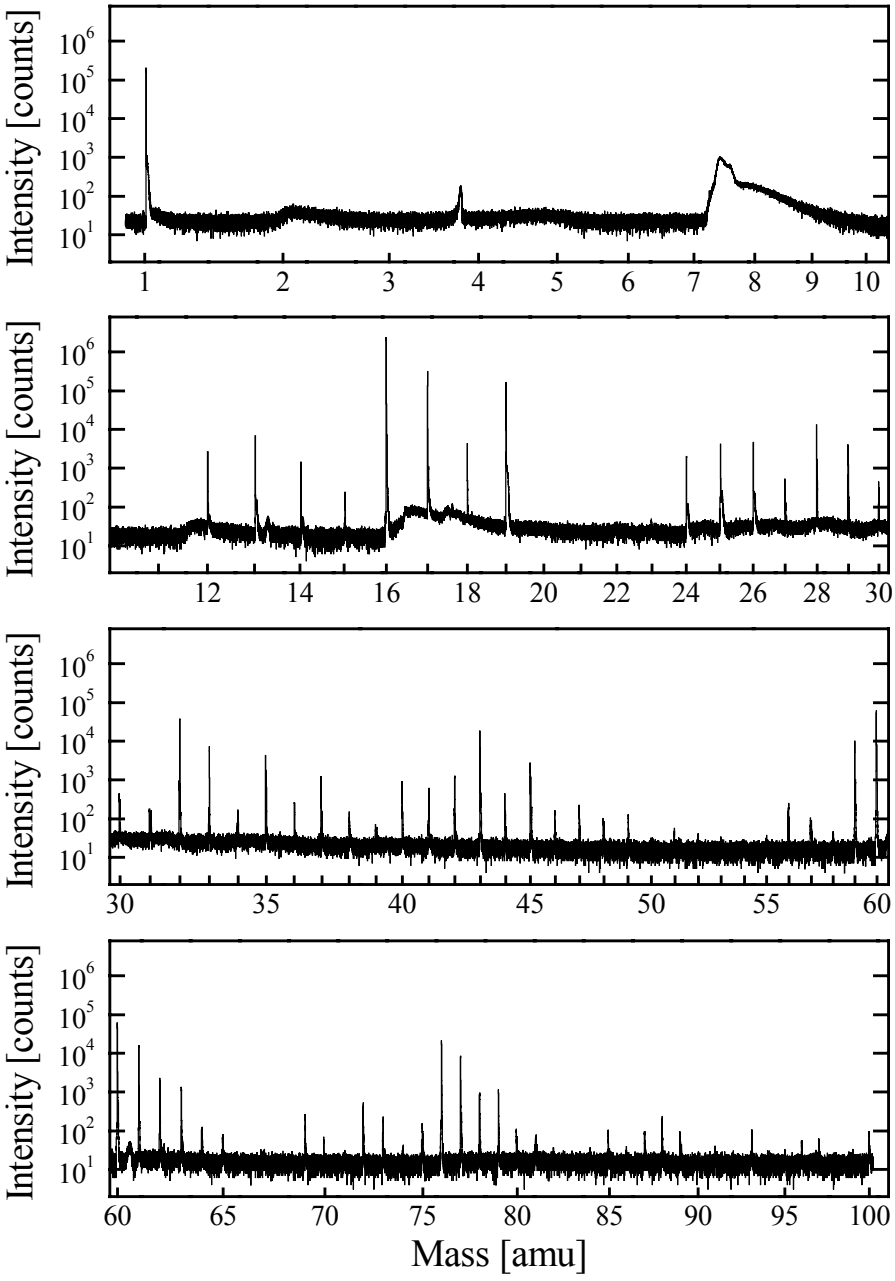

Fig. 17. Mass spectrum (1–100 amu) of negative secondary ions from glass standard KL2-G after argon sputtering. Broad peaks are caused by electrons from various origins. They are also responsible for the higher overall background in negative mass spectra compared to positive spectra (cf. Fig. 16).

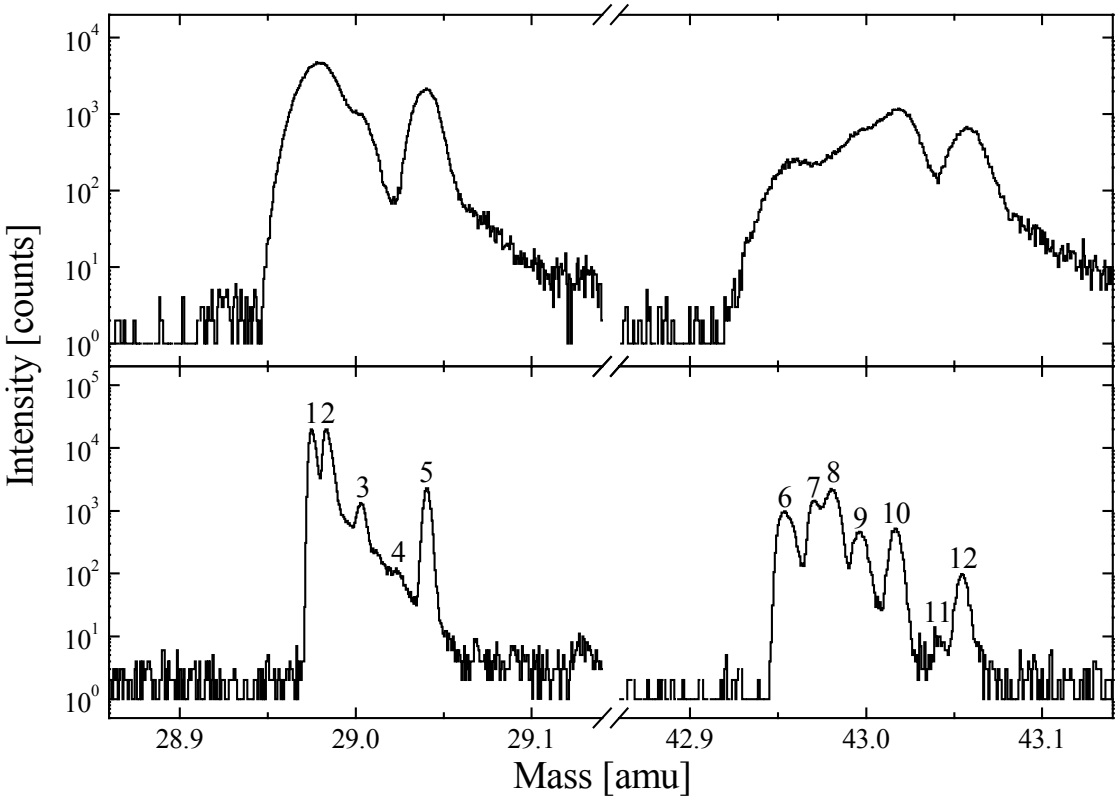

Fig. 18. Comparison between mass spectra at 29 and 43 amu at low (5 ns pulse length; top) and high (0.6 ns pulse length; bottom) mass resolution, respectively. At 29 amu the five peaks in the high-resolution spectrum can be identified as (1) $^{29}Si^+$, (2) $^{28}Si^1H^+$, (3) $^{12}C^1H^{16}O^+$, (4) $^{12}C^1H_3{}^{14}N^+$, and (5) $^{12}C_2{}^1H_5{}^+$, respectively. At 43 amu (6) $^{43}Ca^+$ with a contribution from $^{42}Ca^1H^+$, (7) $^{27}Al^{16}O^+$, (8) $^{26}Mg^{16}O^1H^+$, (9) $^{28}Si^{12}C^1H_3{}^+$ (10) $^{12}C_2{}^1H_3{}^{16}O^+$, (11) $^{12}C_2{}^1H_5{}^{14}N^+$, and (12) $^{12}C_3{}^1H_7{}^+$ emerge in the high-resolution spectrum.

The spectra in Figs. 16 and 17 are highly compressed, and peaks at identical nominal masses can not be separated in these diagrams. The actual fine structures at 29 and 43 amu, respectively, are shown in Fig. 18 for low and high-resolution mass spectra of positive secondary ions. $^{29}Si^+$ and $^{28}Si^1H^+$ can only be distinguished in the high-resolution spectrum at 29 amu. At low mass resolution, only hydrocarbon peaks can be separated. This is also obvious at nominal mass 43 amu. The unambiguous identification of every single peak is even complicated for the high-resolution spectrum. Especially for some peaks (peaks 3, 4, and 7–11 in Fig. 18) that lie between the element and the pure hydrocarbon peak, assignments made in the figure caption are equivocal.

3.4. Quantification

Quantitative evaluation of the mass spectra is one of the major objectives in TOF-SIMS analysis. From each signal in the spectrum, the abundance of the secondary ion spe-

cies and ultimately the concentration of the respective element, isotope, or molecule in the target have to be deduced. However, only elemental or isotopic *ratios* can be determined in SIMS. Absolute concentrations cannot be obtained due to insufficient knowledge of sputter volumes, absolute ion yields, transmission of the instrument, and detection efficiencies. Prerequisites to determine these ratios are, besides knowledge of the respective SIMS sensitivities, linearity of the detection and registration system, as well as control of instrumental mass fractionation effects.

3.4.1. Linearity of the detector

Linearity of the detection system over a wide dynamic range is indispensable for a quantitative evaluation of mass spectra in TOF-SIMS, where the entire spectrum is measured simultaneously. Isotopic and element ratios up to several orders of magnitude occur, and secondary ion sensitivities span a vast range. Therefore, high count rates for major peaks are often compulsory to achieve sufficient ion intensities for minor isotopes or trace elements. For single-ion-counting, the typical detection technique in TOF-SIMS, dead time effects for high-intensity mass peaks have to be considered. Since signal intensities in TOF-SIMS fluctuate on an extremely short time scale (nanoseconds), these effects become more complex than for constant or exponentially decaying signal intensities (Schiff, 1936; Esposito *et al.*, 1991). However, dead time effects have to be considered also in conventional SIMS. Especially in isotope studies, they contribute significantly to measurement uncertainties (Storms and Peterson, 1994).

The actual dead time of the TOF-SIMS IV instrument is ~40 ns, which mainly results from the exponentially decaying scintillator signal. Therefore, only one secondary ion per nominal mass can be detected for each primary ion shot. However, dead time correction of TOF-SIMS spectra may be performed using Poisson statistics. If only one mass peak is present at a given nominal mass, the dead time corrected peak integral I_{cor} becomes

$$I_{cor} = -N \ln\left(1 - \frac{I_{\exp}}{N}\right) \tag{9}$$

where I_{exp} is the measured integrated peak intensity and N the number of primary ion shots. The statistical one-sigma error of the corrected signal is

$$\Delta I_{cor} = \left(\frac{N I_{\exp}}{N - I_{\exp}} \right)^{1/2} \tag{10}$$

The correction of multiple peaks at one nominal mass becomes more complicated, but even entire mass spectra can be corrected for dead time effects by applying similar formulae. This has been demonstrated in greater detail by Stephan *et al.* (Stephan, 1992; Stephan *et al.*, 1994a). Limitations of these corrections result from two deficiencies. First, the actual dead time cannot be described by a single numerical value. A probability function has to be used instead, which is only roughly known. Second, constant peak intensities during the measurement are indispensable for an exact dead time correction. However, simplified correction techniques deliver results with sufficient precision (~10 %) for element analysis even for correction factors up to three. Restrictions are more severe for isotope studies, where higher accuracy (few per mill) is required.

3.4.2. Mass fractionation

Instrumental mass fractionation effects play a less pronounced role in TOF-SIMS. Here, general mass fractionation effects have not been observed so far. If there are any effects, they only have to be considered in isotope analysis, where high accuracy is required. But even there, statistical errors dominate at least for less abundant isotopes the analytical uncertainties. For high intensity ion signals, dead time effects often exceed mass fractionation effects. However, instrumental mass fractionation has always to be considered, before deviations from “normal” isotopic ratios can be claimed.

3.5. Element analysis

Peak assignments for quantitative analyses follow the same principles as described by Eugster *et al.* (1985). For each isotope of a given element, at most the whole intensity at the respective mass window can be assigned. This mass window is defined by the expected center of mass and the prevailing mass resolution. A value for the expected total elemental ion intensity can be calculated from each assumed isotope peak. Since mass interferences may affect one or more of these peak intensities, the minimum value deduced from the different isotopes is the upper limit for the intensity of the respective element. A proper analysis of the respective element can only be inferred, if the calculated total elemental ion intensities for major isotopes agree within statistical error limits. If this is not the case, at

least one isotope is affected by interference and the others might also be influenced by similar interferences. Consequently, one has to interpret the calculated elemental ion abundance as an upper limit. Strictly speaking, all calculated ion abundances are upper limits, if interferences cannot be unequivocally excluded.

Figures 19 and 20 comprise peak assignments and the principles of quantitative evaluation for positive and negative secondary ions, respectively. Moderate mass resolution, sufficient for a complete separation of most interfering molecules like hydrocarbons, was assumed (*e.g.*, 5 ns primary ion pulse length with the above described gallium source). In the following, the evaluation is discussed for different elements. Prerequisite for the here described principles are "normal" (=cosmic) isotopic ratios of most elements. – Throughout this study, isotopic abundances are used according to Anders and Grevesse (1989). – Cosmic isotope ratios can be assumed within statistical error limits in most cases. Nevertheless, one has to be aware of the possibility of non-solar isotopic ratios during the analysis of extraterrestrial material. Especially for the analysis of presolar grains, this has to be taken into account and will be discussed in more detail below. Some of the interferences like hydrides, considered as non-separable in the present section, can be resolved by using very short primary ion pulses or mathematical peak deconvolution techniques. The latter will be explained in an extra section. Isotopic compositions for some elements, especially the light ones, can be determined even at low mass resolution. This is discussed now, together with the principles of element analysis.

3.5.1. Hydrogen

Although hydrogen forms positive as well as negative secondary ions during the SIMS process, the negative polarity dominates. For positive secondary ions, a mass interference is observed for deuterium ($^2H^+$) from $^1H_2^+$ molecular ions. In addition, $^1H_3^+$-ions are often present in secondary ion spectra. The analysis of hydrogen with TOF-SIMS is affected by the residual gas in the vacuum apparatus, because it is typically dominated by hydrogen. Even at a pressure of several 10^{-10} mbar in the analysis chamber, hydrogen is still adsorbed onto the sample surface during primary ion bombardment and can be observed in every mass spectrum. Therefore, the analysis of indigenous hydrogen isotopic ratios was not possible so far, although H_2 forms practically no negative secondary ions and consequently $^2H^-$ is not influenced by any mass interference.

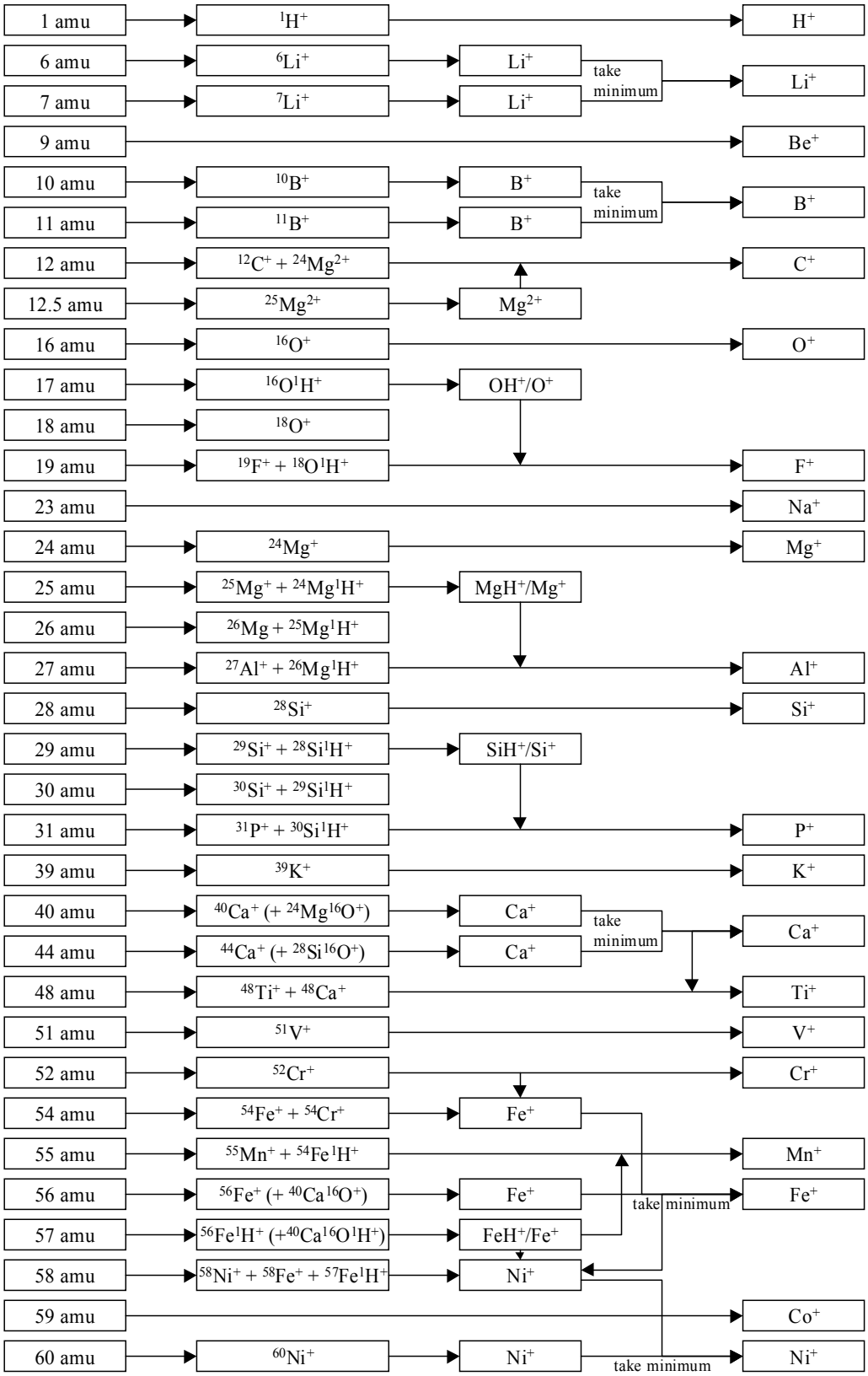

Fig. 19. Flow chart showing the principles of peak assignments and determination of positive secondary ion abundances for elements from hydrogen to nickel.

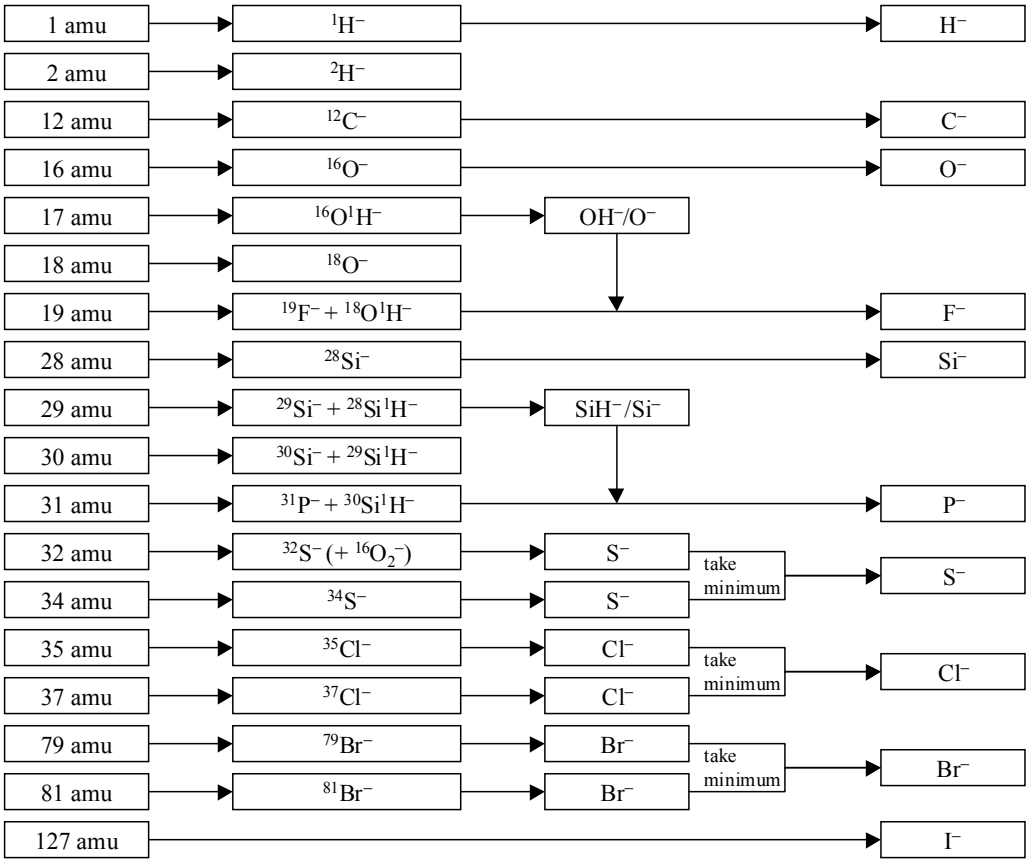

Fig. 20. Flow chart showing the principles of peak assignments and determination of negative secondary ion abundances for elements from hydrogen to iodine.

3.5.2. Lithium, beryllium, and boron

Lithium, beryllium, and boron all form positive secondary ions. Molecular interferences are almost negligible during their analysis. Like all alkali metals, lithium is not observed as hydride in the positive spectrum. It would be unequivocally identifiable as $^{7}Li^{1}H^{+}$ at nominal mass 8 amu. Any contribution of $^{6}Li^{1}H^{+}$ at mass 7 amu to the $^{7}Li^{+}$ mass peak would be easy to subtract, particularly since ^{6}Li has an isotopic abundance of only 7.5 % in "normal" lithium.

Beryllium has only one stable isotope at nominal mass 9 amu. Here no mass interference occurs except $^{27}Al^{3+}$, which can easily be separated (required mass resolution $m/\Delta m$=490). For boron, the convenient isotopic ratio of about four for $^{11}B/^{10}B$ allows a definite determination of the B^{+}-intensity. BeH^{+} in most cases plays a minor role and, if at all, only for the less abundant isotope $^{10}B^{+}$.

3.5.3. Carbon

Carbon forms positive as well as negative secondary ions during primary ion bombardment. Like observed for hydrogen, negative ions form the majority. Especially the polarity of the carbon secondary ions depends on their chemical environment. Hydrocarbons generate C^+ as well as C^- secondary ions, whereas carbonates and in particular carbides mainly form C^--ions. CH, CH_2, and CH_3 are also observed in both polarities. Consequently, separation of the $^{12}C^1H$-Signal from the ^{13}C peak is essential for the measurement of $^{12}C/^{13}C$ isotopic ratios in both polarities. A minimum in mass resolution of $m/\Delta m$=2910 is necessary for this separation. Since the intensity of the $^{12}C^1H$-ions is often comparable with the ^{12}C-signal, this mass resolution is required at ~1 % of the peak height in case of solar carbon ($^{12}C/^{13}C$=89.9).

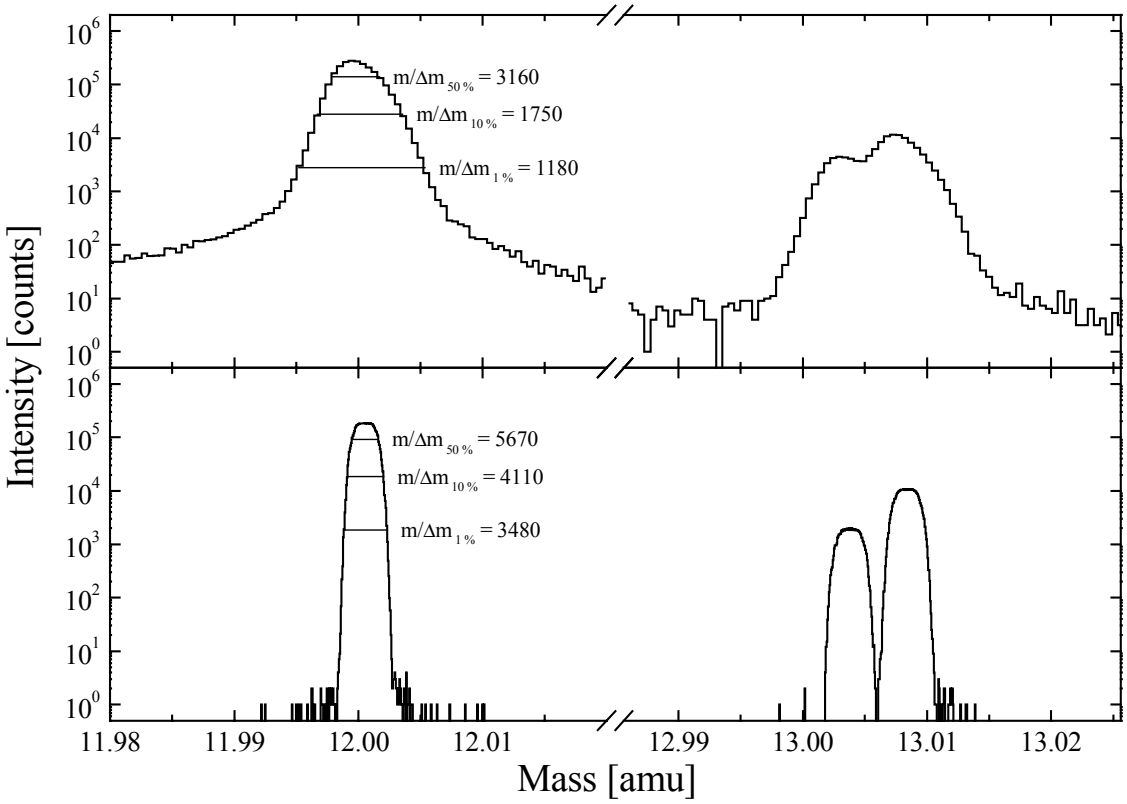

Fig. 21. Comparison between TOF-SIMS (top) and DF-SIMS (bottom, courtesy of F. J. Stadermann) spectra at masses 12 (^{12}C) and 13 amu (^{13}C and $^{12}C^1H$), respectively. With TOF-SIMS, positive secondary ions were retrieved from a Teflon sample by using an Ar^+ primary ion beam. The DF-SIMS analysis was performed on a terrestrial silicon carbide grain. TOF-SIMS analyses of silicon carbide are described in a later section. Mass resolutions ($m/\Delta m$) are given at 12 amu for full width at 50, 10, and 1 % peak height.

For a proper measurement of isotopic ratios, preferentially the amount of the hydrate CH has to be minimized. This can be done by sputtering of the sample, since hydration is often due to the residual gas in the vacuum system (see above). To separate the two peaks at 13 amu, often mathematical peak separation techniques have to be applied (cf. section on presolar grains). A comparison between TOF-SIMS and DF-SIMS spectra for masses 12 and 13 amu, respectively, is shown in Fig. 21. Although the TOF-SIMS spectrum (Fig. 21 top) was obtained under nearly optimal conditions – flat Teflon sample, only little surface adsorption of hydrocarbons (low CH-signal), and short primary ion pulses (~1.2 ns) – the two peaks at 13 amu were not separated sufficiently. In contrary to this, these two peaks are separated completely with DF-SIMS (Fig. 21 bottom).

3.5.4. Nitrogen

Nitrogen has only a small ionization yield in the SIMS process. Nevertheless, nitrogen can be measured as CN^- if carbon is present. For the measurement of $^{14}N/^{15}N$ isotopic ratios, first, the $^{12}C/^{13}C$ isotopic ratio has to be calculated. Then, the mass peaks at 26 and 27 amu are determined. The former can be identified as $^{12}C^{14}N^-$, whereas the latter is formed by $^{13}C^{14}N^-$ and $^{12}C^{15}N^-$. These two ion species cannot be separated in TOF-SIMS (required mass resolution $m/\Delta m$=4270). The $^{14}N/^{15}N$-ratio can be calculated now with the known $^{12}C/^{13}C$-ratio according to

$$^{14}\mathrm{N}/^{15}\mathrm{N} = \frac{^{12}\mathrm{C}^{14}\mathrm{N}^-}{^{12}\mathrm{C}^{15}\mathrm{N}^-} = \frac{I_{26}}{I_{27} - {}^{13}\mathrm{C}/^{12}\mathrm{C} \cdot I_{26}} \tag{11}$$

or

$$^{15}\mathrm{N}/^{14}\mathrm{N} = \frac{I_{27}}{I_{26}} - {}^{13}\mathrm{C}/^{12}\mathrm{C} \tag{12}$$

where I_x is the peak integral at x amu.

3.5.5. Oxygen

Oxygen is the classical element providing negative secondary ions in most SIMS applications. In oxidized compounds, it takes up the electrons released during the formation of positive metallic ions. Nevertheless, because of its high abundance in rocks, oxygen is

also observed as positive secondary ions, though with lower intensity. Therefore, oxygen is qualified as reference element besides silicon for the comparison of negative and positive secondary ion spectra. Because of the very low abundance of ^{17}O (CI: 0.038 %) and the high $^{16}O^{1}H^{-}$ intensity, only ^{16}O and ^{18}O can be measured satisfactorily in TOF-SIMS.

3.5.6. Fluorine, chlorine, bromine, and iodine

All halogens form preferentially negative secondary ions. Chlorine, the element with the highest electron affinity, has the maximum negative secondary ion yield. Nevertheless, especially samples with high fluorine concentrations often show signals at 19 amu also in the positive secondary ion spectrum. Fluorine and iodine are both monoisotopic elements, whereas chlorine and bromine have two stable isotopes each. Convenient isotopic ratios of about three for $^{35}Cl/^{37}Cl$ and about one for $^{79}Br/^{81}Br$, respectively, allow measuring all four nuclides. Since ^{79}Br is often disturbed by molecular interferences, ^{81}Br is the isotope of choice for a proper bromine analysis (Stephan *et al.*, 1994b).

Especially chlorine and fluorine are omnipresent in our environment. Therefore, many samples show halogen contamination on the surface, often together with the alkalis sodium and potassium. Consequently, cleanness of the sample surface is especially important for a proper halogen analysis.

3.5.7. Sodium, potassium, rubidium, and cesium

The same high demands on surface purity apply to the alkalis, especially sodium and potassium, which are often observed as surface contamination. The alkalis have the highest positive secondary ion yield, analogous to the high yield for negative ions for halogens. Hydrides and doubly charged secondary ions are not observed. The monoisotopic element sodium can unequivocally be analyzed at 23 amu, where no molecular interference appears. Potassium as $^{39}K^{+}$ can easily be separated from $C_3H_3^{+}$ at a low mass resolution ($m/\Delta m$=652). ^{40}K (0.01167 % of K) is not distinguishable from ^{40}Ca (96.941 % of Ca) due to a required mass resolution of $m/\Delta m$=28400 and its low abundance. Although the abundance of ^{41}K is higher (6.7302 %), mass 41 amu is typically dominated by $^{40}C^{1}H$ (required mass resolution $m/\Delta m$=4770). Rubidium has two primordial isotopes ^{85}Rb (72.165 %) and ^{87}Rb (27.835 %). The latter is interfering with ^{87}Sr (7.00 %, required mass resolution $m/\Delta m$=296000). Cesium is monoisotopic and can be seen at 133 amu.

3.5.8. Magnesium, calcium, strontium, and barium

The alkaline-earth metals are the group with the second highest yield for positive secondary ions. They often form hydride-ions like, *e.g.*, MgH^+, complicating isotope analyses. $^{24}Mg^1H^+$ overlaps with $^{25}Mg^+$, $^{25}Mg^1H^+$ with $^{26}Mg^+$, and finally $^{26}Mg^1H^+$ coincides with $^{27}Al^+$ (required mass resolutions $m/\Delta m$=3550, 2350, and 3040). The latter interference complicates the analysis of aluminum. However, assuming a $^{25}Mg/^{24}Mg$-ratio of 0.127, which mostly is justified for the achievable accuracy, one can calculate a possible ^{26}Mg-enrichment and also the contribution of $^{26}Mg^1H^+$ to mass 27 amu:

$$^{27}Al^+ = I_{27} - I_{24} \cdot \frac{^{26}Mg}{^{24}Mg} \cdot \frac{MgH^+}{Mg^+} \tag{13}$$

with

$$MgH^+ / Mg^+ = \frac{I_{25}}{I_{24}} - 0.127 \tag{14}$$

and

$$^{26}Mg / ^{24}Mg = \frac{I_{26}}{I_{24}} - 0.127 \cdot \frac{MgH^+}{Mg^+} \tag{15}$$

Similar to this, $^{40}Ca^1H^+$ interferes with ^{41}K like discussed above. Besides hydrides, also oxides are observed. To separate $^{24}Mg^{16}O^+$ from ^{40}Ca and $^{40}Ca^{16}O^+$ from ^{56}Fe, mass resolutions of $m/\Delta m$=2300 and 2480, respectively, are required. Hydroxides like $^{40}Ca^{16}O^1H^+$ at 57 amu also emerge in the mass spectra. ^{44}Ca, the other isotope available for quantitative calcium analysis interferes with $^{28}Si^{16}O$ ($m/\Delta m$=2690). Therefore, ^{40}Ca is more reliable for a quantitative analysis especially of silicates. ^{44}Ca can be useful only in Mg-rich, Si-poor samples like some carbonates.

Doubly charged ions like $^{24}Mg^{2+}$ or $^{40}Ca^{2+}$ are also observed for alkaline-earth metals. Since the mass scale in TOF-SIMS spectra is actually a mass-to-charge scale, they appear at 12 amu and 20 amu, respectively. Consequently, $^{24}Mg^{2+}$ interferes with $^{12}C^+$ ($m/\Delta m$=1600), but this contribution can be calculated from the $^{25}Mg^{2+}$ intensity at 12.5 amu.

Strontium is measured mainly as $^{88}Sr^+$ (82.58 %) and $^{86}Sr^+$ (9.86 %); $^{87}Sr^+$ (7.00 %) interferes with $^{87}Rb^+$ (see above). Barium is detected primarily as $^{138}Ba^+$ (71.70 %) and $^{137}Ba^+$ (11.23 %) but can also be seen as $^{136}Ba^+$ (7.854 %), $^{135}Ba^+$ (6.592 %) and $^{134}Ba^+$ (2.417 %). $^{130}Ba^+$ (0.106 %) and $^{132}Ba^+$ (0.101 %) are too rare in most spectra to be detected.

3.5.9. Aluminum

The monoisotopic element aluminum can be measured at nominal mass 27 amu considering corrections from $^{26}Mg^1H^+$ according to Eq. (13). AlO^+ at 43 amu, Al^{2+} at 13.5 amu and even Al^{3+} at 9 amu are also observed. The hydride might be present at 28 amu but is often not resolved from $^{28}Si^+$ ($m/\Delta m$=2250).

3.5.10. Silicon

Silicon has three stable isotopes, ^{28}Si (92.23 %), ^{29}Si (4.67 %), and ^{30}Si (3.10 %). Although it forms predominately positive secondary ions, also negative ions occur. For silicates it is suited as reference element besides oxygen for the comparison of negative and positive secondary ion spectra (see above). Furthermore, because of its ubiquity in rocks, it is used as normalization element for element abundances in meteorites or the solar system (Anders and Grevesse, 1989). Similar to magnesium, hydrides occur and interfere with ^{29}Si, ^{30}Si, and ^{31}P.

3.5.11. Phosphorous

The monoisotopic element phosphorous forms normally $^{31}P^-$-ions, but also positive secondary ions are observed in samples with high phosphorous concentrations like phosphates. Similar to $^{27}Al^+$ and its interference with $^{26}Mg^1H^+$, $^{31}P^+$ is influenced by $^{30}Si^1H^+$, which can be corrected analogous to Eq. (13).

3.5.12. Sulfur

Sulfur, which forms negative secondary ions, has two isotopes, ^{32}S (95.02 %) and ^{34}S (4.21 %), that are measurable in TOF-SIMS. Especially for ^{32}S, the O_2 molecule plays an annoying role in the mass spectrum, but it can be separated sufficiently at moderate mass resolution ($m/\Delta m$=1800).

3.5.13. Scandium, titanium, vanadium, and chromium

The monoisotopic element Scandium has typically very low abundances in most rocks (Sc/Si=3.42·10^{-5}, chondritic atomic abundance according to Anders and Grevesse, 1989). In addition, $^{45}Sc^{+}$ interferes with $^{28}Si^{16}O^{1}H^{+}$ and can therefore only be seen in TOF-SIMS spectra with high mass resolution.

In Ti-rich samples, all five stable isotopes (^{46}Ti: 8.0 %, ^{47}Ti: 7.3 %, ^{48}Ti: 73.8 %, ^{49}Ti: 5.5 %, and ^{50}Ti: 5.4 %) can be found as positive secondary ions. Since besides ^{48}Ca, no major interference is observed, and the share from ^{48}Ca can easily be calculated from the total calcium, ^{48}Ti is used to determine the element abundance. On the other hand, $^{48}Ti^{16}O^{+}$ interferes with $^{64}Zn^{+}$ as described below.

Because of the low abundance of ^{50}V (0.250 %) and its interference with ^{50}Ti and ^{50}Cr, vanadium can only be measured as ^{51}V. Chromium, finally, is measured as ^{52}Cr, but it also contributes significantly to the peaks at 50, 53, and 54 amu. However, $^{54}Cr^{+}$ can be neglected in most cases due to much higher contributions from $^{54}Fe^{+}$.

3.5.14. Manganese, iron, cobalt, and nickel

Iron usually dominates the positive mass spectrum at 54 and 56 amu due to its high cosmic abundance. Nevertheless, in Ca-rich, Fe-poor samples, $^{40}Ca^{16}O^{+}$ contributes significantly to the mass peak at 56 amu. Another possible interference is the $^{28}Si_2^{+}$ dimer. Whenever these peaks are not separable (required mass resolution $m/\Delta m$=2480 for $^{40}Ca^{16}O^{+}$ and 2960 for $^{28}Si_2^{+}$), the less abundant ^{54}Fe-isotope (5.8 % instead of 91.72 % for ^{56}Fe) has to be taken for calculation of the iron abundance after correction for contribution from ^{54}Cr. $^{57}Fe^{+}$ (2.2 %) is in most cases not discernable from $^{56}Fe^{1}H^{+}$ ($m/\Delta m$=7730) and often influenced by $^{40}Ca^{16}O^{1}H^{+}$ ($m/\Delta m$=1900). Especially the FeH/Fe-ratio is important to determine, since $^{54}Fe^{1}H^{+}$ is the major interference at mass 55 amu for $^{55}Mn^{+}$ ($m/\Delta m$=5850). Similarly, the analysis of cobalt, which is also monoisotopic, is complicated by $^{58}Ni^{1}H^{+}$. Nickel can be measured as $^{58}Ni^{+}$ and $^{60}Ni^{+}$, the former with interferences from $^{58}Fe^{+}$ and $^{57}Fe^{1}H^{+}$.

3.5.15. Copper and zinc

Copper and zinc have both low cosmic abundances (Cu/Si=5.22·10^{-4}, Zn/Si=1.260·10^{-3}, chondritic atomic abundances according to Anders and Grevesse, 1989)

and are therefore difficult to determine. From the easy to confirm isotopic ratio of approximately 7:3 for $^{63}Cu/^{65}Cu$, an unequivocal identification of copper is sometimes possible. Zinc, although having more stable isotopes, is harder to identify because of interferences from TiO^+.

3.5.16. Gallium

Gallium was mainly used as primary ion species for the TOF-SIMS analyses in this study. Although the ion source is equipped with "monoisotopic" ^{69}Ga, some remaining ^{71}Ga (~0.2 %) was still present, since the industrial isotope separation process is not perfect. Therefore, both isotopes cannot be used for the analysis of indigenous gallium.

3.5.17. Silver

Silver has a comparatively high ionization yield although it has a relatively high ionization energy (7.58 eV). Silver or silver oxide is often used as substrate for the analysis of organic substances since it also has a positive effect on the ionization probability of other elements and molecules (matrix effect). Both isotopes can be measured (^{107}Ag: 51.839 % and ^{109}Ag: 49.161 %) and show typically no interferences.

3.5.18. Lanthanides

Rare earth elements could be seen in the positive secondary ion spectrum. Nevertheless, an unambiguous determination of these elements is not possible so far, due to a wealth of isobaric interferences and the presence of hydrides and oxides – oxides of the low-mass lanthanides overlap with those of the high-mass ones.

3.5.19. Lead

As a surface analytical technique, TOF-SIMS often "sees" lead present in the positive secondary ion spectrum resulting from surface contamination, because this highly volatile element is omnipresent in our environment.

3.5.20. Other elements

Noble metals besides silver have typically low secondary ion yields and are therefore not suited for TOF-SIMS analysis. Noble gases normally are not ionized in the SIMS process. Other elements not mentioned specifically here are typically too rare in cosmic materials. Nevertheless, some of them can certainly be analyzed with TOF-SIMS.

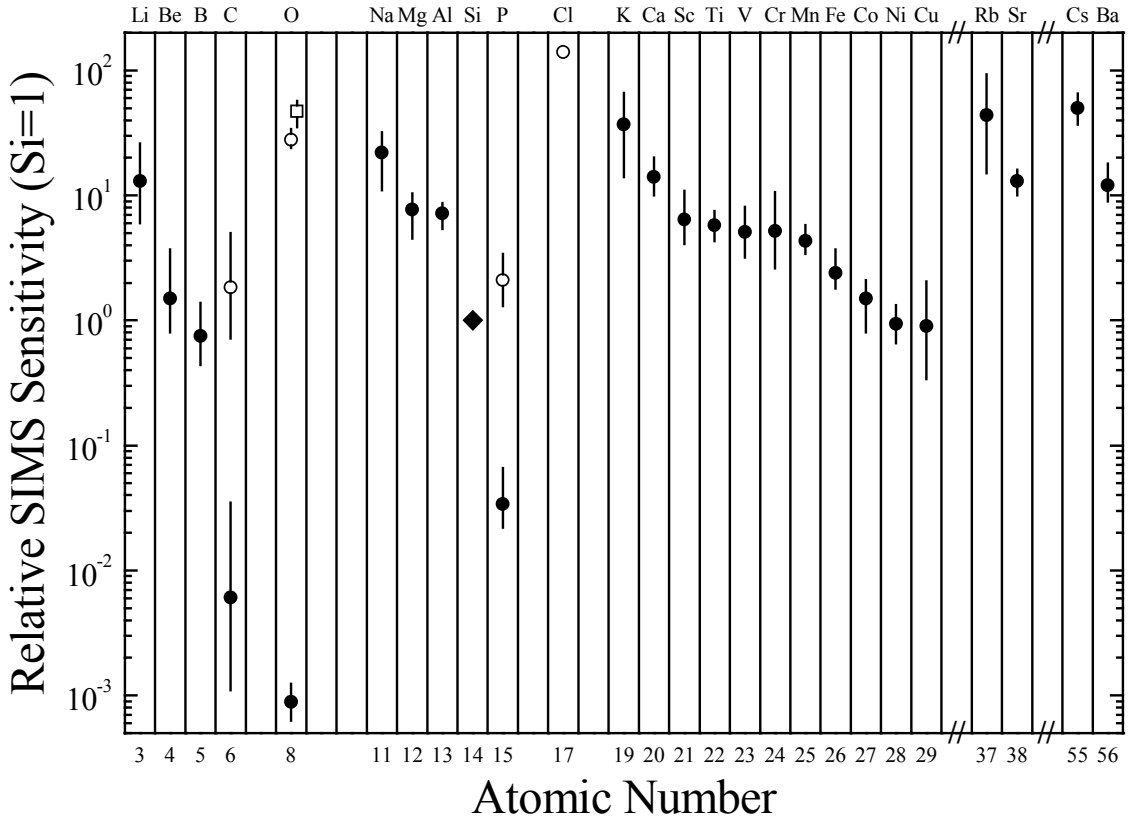

Fig. 22. Relative TOF-SIMS sensitivities for positive (solid symbols) and negative (open symbols) secondary ions relative to silicon derived from the analysis of eight glass standards with the gallium primary ion source. The sensitivities were determined from measurements with simultaneous argon sputtering and directly after sputtering. Here, only for negative oxygen ions, a significant difference between both measurements was found (the open square gives the O^--sensitivity after sputtering, the open circle during sputtering). Carbon sensitivities are determined from silicon carbide samples.

3.6. SIMS sensitivities

For a quantitative analysis with TOF-SIMS, to transform secondary ion intensities into element ratios, relative sensitivities must be determined. Therefore, carefully selected standards have to be analyzed. Since the actually investigated volume is extremely small, only a few atomic monolayers thin, sample homogeneity and purity are crucial. As described before, amorphous or polycrystalline standards are desired. However, certain materials, glass as well as some minerals, used as standards in other techniques, do not meet the requirements of TOF-SIMS concerning homogeneity on a micrometer scale. Therefore, the quality of a standard must always be monitored in the TOF-SIMS analysis.

In Fig. 22, typical TOF-SIMS sensitivities are shown for positive and negative secondary ions. These results were derived from TOF-SIMS analyses of eight glass standards

(Jochum *et al.*, 1999) with known composition. They meet the above mentioned strict requirements for standards concerning homogeneity as was shown during the TOF-SIMS analysis. The results are comparable to DF-SIMS sensitivities in the literature (*e.g.*, Meyer, 1979; Lange *et al.*, 1986).

Unfortunately, fluorine and sulfur concentrations are not known so far for these glass standards. Therefore, the data set on negative secondary ion sensitivities is quite incomplete. Previous investigations of halogens and sulfur showed that the selection of appropriate standards for these elements is rather difficult. Sensitivities here vary over more than one order of magnitude.

All glass standards were measured twice, with simultaneous argon sputtering and directly after sputtering. Sensitivities before sputtering could not be determined since no stable ion signals were reached (cf. Fig. 15). Except for O^--ions, differences between sensitivities during and after sputtering seem not to exist for most elements, although absolute secondary ion yields typically decrease after sputtering (Fig. 15). For negative oxygen ions, the sensitivity relative to silicon increases by a factor of ~1.7 after sputtering compared to the sensitivity during argon sputtering.

Detailed results from the analyses of the individual glass standards are listed in the Appendix. For chlorine, only the sensitivity obtained during sputtering from the most Cl-rich glass (ATHO-G, 400 ppm Cl) is shown in Fig. 22. All other samples showed traces of surface adsorbed chlorine. For other elements, geometric means for the sensitivity values given in the Appendix are shown in Fig. 22. Error bars mark the range of values for different measurements. Since no carbon is present in the glass standards, C-sensitivities relative to silicon were determined from the analysis of several silicon carbide grains, although it is expected that matrix effects in silicone carbide hardly resemble those in glass.

3.7. Isotope analysis

Only a few elements in typical rocks allow isotopic analysis at moderate mass resolution. For hydrogen (negative secondary ions), lithium, and boron, practically no interferences are observed in the spectrum. Starting with carbon, hydrates become a major problem, because they are not separable with moderate mass resolution. Hydrates are less important for elements with isotopes that are separated by two mass units, *e.g.*, copper or silver. Since these are typically present as trace elements in natural samples, other mass interferences like oxides often prevent proper isotopic analyses.

If isotopic analysis with high accuracy is required, short primary ion pulses are indispensable to achieve high mass resolution. Even with these, neighboring peaks are often not sufficiently separated. Therefore, only mathematical peak separation techniques provide further help. Since peak shape in TOF-SIMS is typically not Gaussian, and since it strongly depends on the respective ion species, the expected peak shape has to be known for a proper deconvolution. If an undisturbed isotope of the same element is present, its peak may be used here as an internal standard peak. This is the best available approximation under realistic conditions, since all isotopes of one element should have the same energy distribution. Peaks of other elements are not suitable, because their energy distribution might be different.

To separate, *e.g.*, the hydrate peak $^{24}Mg^{1}H^{+}$ from $^{25}Mg^{+}$, the $^{24}Mg^{+}$-peak can be used to fit the low-mass edge of the spectrum at 25 amu (Fig. 23). Here, the scaling factor for $^{24}Mg^{+}$ gives directly the $^{25}Mg/^{24}Mg$ isotopic ratio. The difference between the two spectra represents the $^{24}Mg^{1}H^{+}$-peak.

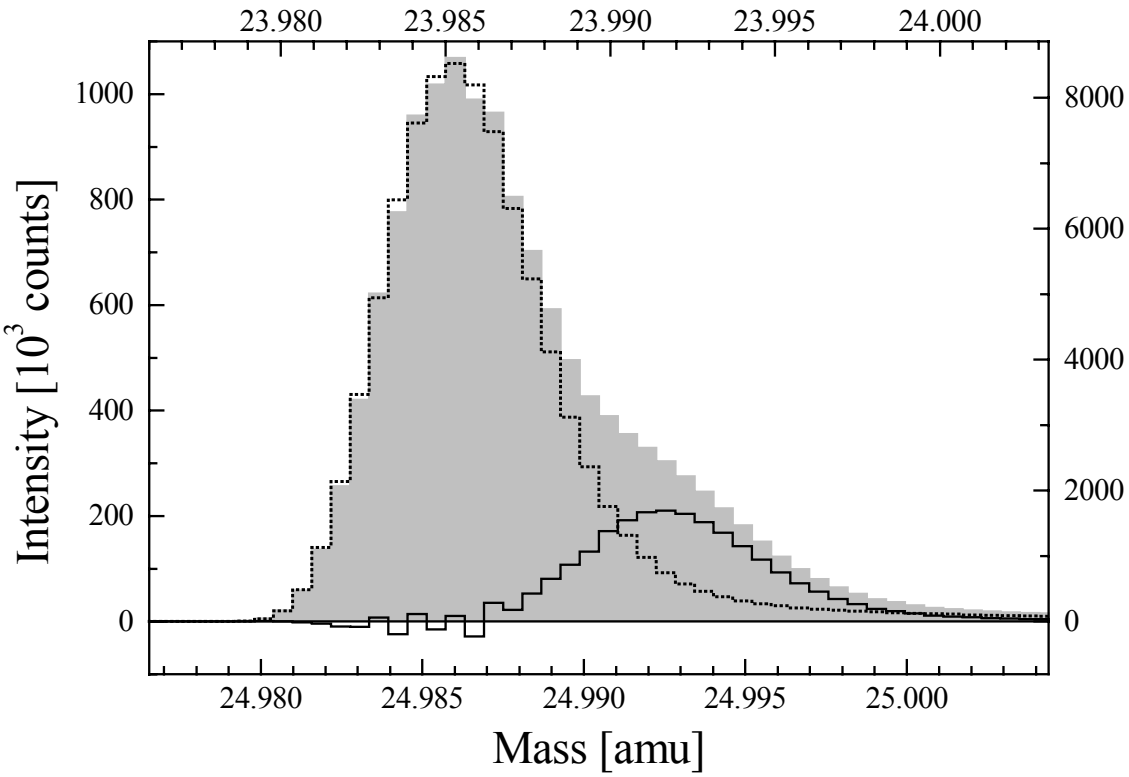

Fig. 23. Peak separation for $^{25}Mg^{+}$ and $^{24}Mg^{1}H^{+}$. The shape of the $^{24}Mg^{+}$-peak (dotted line, top x- and right y-axes) was used as model for the $^{25}Mg^{+}$-peak. As difference between the actual signal at mass 25 amu (shaded area) and the $^{24}Mg^{+}$-peak, scaled to the same height, the hydride peak (solid line) emerges. The spectrum was measured with bunched gallium primary ions (~600 ps pulse width) on glass BM90/21-G (cf. Appendix).

TABLE 2. Reproducibility of isotopic ratio TOF-SIMS measurements from the analysis of eight different glass standards.

	Isotopic ratio	δ-values [per mill]	Standard deviation [per mill]	Mean statistical error [per mill]
Positive secondary ions	$\delta(^{25}Mg/^{24}Mg)$	+5	9	2
	$\delta(^{26}Mg/^{24}Mg)$	–13	7	2
	$\delta(^{29}Si/^{28}Si)$	–23	14	4
	$\delta(^{30}Si/^{28}Si)$	–67	14	5
	$\delta(^{41}K/^{39}K)$	–42	56	7
	$\delta(^{42}Ca/^{40}Ca)$	–9	13	9
	$\delta(^{43}Ca/^{40}Ca)$	–45	41	21
	$\delta(^{44}Ca/^{40}Ca)$	–76	49	7
	$\delta(^{46}Ti/^{48}Ti)$	+97	121	27
	$\delta(^{47}Ti/^{48}Ti)$	+75	57	25
	$\delta(^{49}Ti/^{48}Ti)$	–2	91	26
	$\delta(^{53}Cr/^{52}Cr)$	–10	60	39
	$\delta(^{57}Fe/^{56}Fe)$	+1	30	14
Negative secondary ions	*$\delta(^{13}C/^{12}C)$*	*± 0*	*94*	*168*
	$\delta(^{17}O/^{16}O)$	–72	81	44
	$\delta(^{18}O/^{16}O)$	–88	36	13
	$\delta(^{29}Si/^{28}Si)$	–46	41	28
	$\delta(^{30}Si/^{28}Si)$	–71	21	33
	$\delta(^{34}S/^{32}S)$	–83	117	108
	$\delta(^{37}Cl/^{35}Cl)$	–21	37	30

Data by courtesy of T. Henkel. In the second column, the average deviation from standard isotopic ratios in per mill is given as δ-values:

$$\delta\left({}^{x}\mathrm{A}/{}^{y}\mathrm{A}\right)=1000\cdot\left(\frac{\left({}^{x}\mathrm{A}/{}^{y}\mathrm{A}\right)}{\left({}^{x}\mathrm{A}/{}^{y}\mathrm{A}\right)_{\mathrm{Std.}}}-1\right)$$

The standard deviation of this average is shown in column three, whereas column four provides the mean statistical error of individual measurements. Since carbon was only present as surface contamination on the glass standards, the deviations from cosmic ratios are not representative for samples containing carbon in the bulk.

This peak deconvolution technique has been successfully applied to various isotope systems. For the eight glass standards, already used to determine elemental sensitivities (see above), expected terrestrial values have been reproduced within deviations of a few percent for several isotopic ratios (Table 2). The accuracy achievable with this peak sepa-

ration technique strongly relies on the abundance of the respective element in the sample and therefore varies for different samples.

3.8. Organic molecules

Since the number of possible interferences for molecular ions can be very high, appropriate strategies had to be developed for their proper identification. Nevertheless, an accurate mass determination is prerequisite to discriminate most possible interferences. Fragmentation during primary ion bombardment of most organic compounds occurs, filling the respective mass spectrum with numerous peaks. Series of fragments with well-defined mass differences are striking features of organic mass spectra. They often allow the identification of organic molecules or entire molecule classes.

Quantification of these results is even more complicated than for element ratios, often limited to substances sitting on simple, well defined substrates, and requires internal standards (Hagenhoff *et al.*, 1992; Hagenhoff, 1997).

3.9. Data processing

The amount of information obtained from a TOF-SIMS analysis can be tremendous. In principle, each primary ion shot delivers a complete mass spectrum, although only a few secondary ions might be distributed over the entire mass range. Nevertheless, each secondary ion has to be registered individually to avoid loss of information. Mass spectra for a carefully selected series of primary ion shots can be obtained during subsequent data processing. Time profiles as those in Fig. 15 show the time-dependence of the respective secondary ion signals. Secondary ion images for an unlimited number of mass intervals can be obtained by scanning the primary ion beam over the sample. These images show lateral element or molecule distributions (cf. Fig. 24).

The amount of data, typically several hundred megabytes in one measurement, can be handled and processed by the present generation of personal computers. A first evaluation can be performed during the measurement, providing total mass spectra, selected ion images, or depth profiles. Nevertheless, for a detailed evaluation, all available information on every secondary ion has to be monitored.

Automated techniques are here desired for qualified data reduction and evaluation in the future to get the immense data stream under control, without losing any important information about the target.

4. Meteorites

Meteorites are the principal objects of research in cosmochemistry. They are the major source of information about our solar system, its origin and early history about 4.6 Ga ago. The investigation of small, micrometer-sized entities within meteorites has become increasingly important during the last decades. Here, TOF-SIMS was expected to be an appropriate technique due to its imaging capabilities. Elemental mapping, isotope analysis, as well as the investigation of organic matter can be performed on phases with linear dimensions even smaller than one micrometer. Several different applications of TOF-SIMS in meteorite research are presented exemplarily in the following.

4.1. Ca,Al-rich inclusions in carbonaceous chondrites

Ca,Al-rich inclusions (CAIs) are among the most primitive objects found in meteorites (MacPherson *et al.*, 1988). As high-temperature condensation products, they stem from the earliest stages of solar system formation and are therefore of special interest in cosmochemistry. After their formation, many CAIs experienced complex histories of alteration. These objects where among the first extraterrestrial samples chosen for TOF-SIMS analysis (Stephan *et al.*, 1991) to test the applicability of this technique in meteorite research. CAIs from CM, CO, and CV meteorites were investigated in a later, more extended study (Schirmeyer *et al.*, 1996a,b, 1997). Here a striking feature is the distribution of lithium, which was found enriched in Fe-rich phyllosilicates within CAIs from several different carbonaceous chondrites but not in phyllosilicates located in the surrounding matrix. Examples of ion images for several secondary ion species including $^{7}Li^{+}$ are shown in Fig. 24. They were obtained from a mineralogical thin section from a CAI within the CM chondrite Cold Bokkeveld (Fig. 25). The CAI itself can clearly be seen in the aluminum image. Although in the $^{7}Li^{+}$-image only 2790 ions were detected, a concentration of the signal within several regions of the CAI is obvious. A closer examination of the results show that lithium is especially enriched in Fe-rich phyllosilicates located between the Ca-rich pyroxene rim and the interior spinel of the CAI (Schirmeyer *et al.*, 1997). Although this hydrous phase is

similar to the surrounding water-bearing minerals in the host rock, these minerals differ by more than two orders of magnitude in their lithium contents.

From TOF-SIMS studies on various carbonaceous chondrites, it can be ruled out that lithium was already present in the proposed precursor material of these hydrous phases, most likely melilite (Schirmeyer *et al.*, 1996b, 1997). It must have been incorporated into the phyllosilicates during aqueous alteration processes.

Phyllosilicates in carbonaceous chondrites were formed by aqueous alteration in the early solar nebula and/or within meteorite parent bodies (Bischoff, 1998). Still some controversy exists about the time and environment of their formation, and, more generally, about the possibility of aqueous alteration prior to the accretion of the final parent body. While Metzler *et al.* (1992) found clear evidence for such preaccretionary processes for CM chondrites (Bischoff, 1998), solely asteroidal alteration was also proposed (Browning *et al.*, 1996; Browning and Keil, 1997; Buseck *et al.*, 1997; Zolensky, 1997).

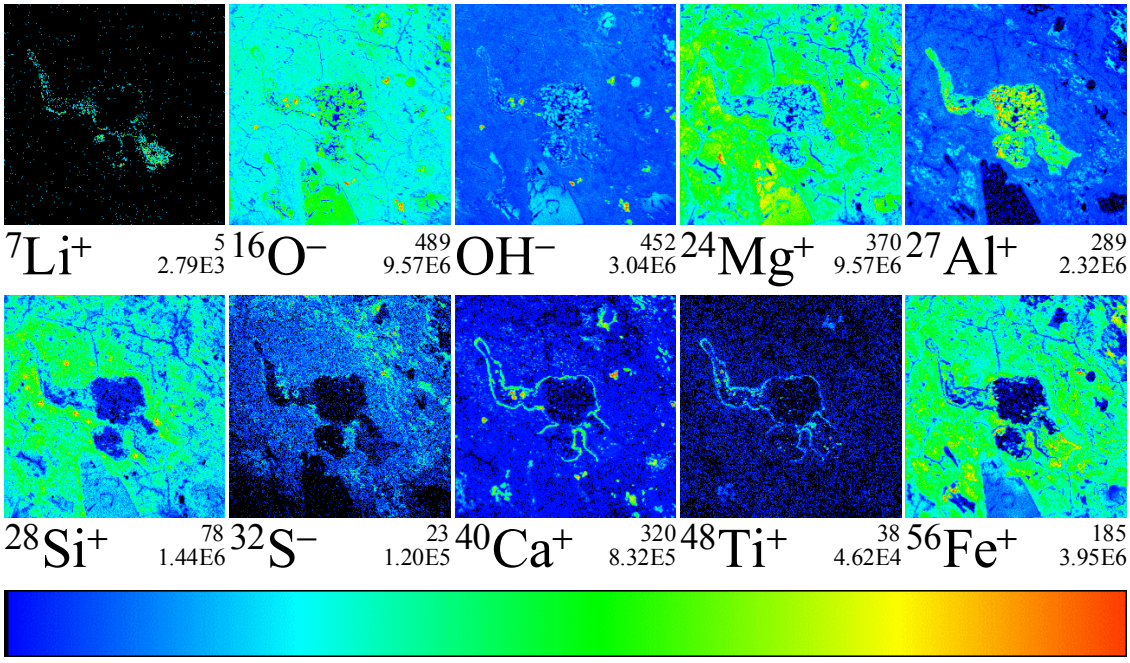

Fig. 24. Secondary ion distribution images from a CAI in Cold Bokkeveld. Field of view is 500×500 µm^2. Each image consists of 256×256 pixels. The number of primary ion shots per pixel is 1600 for positive and 1120 for negative secondary ions. Secondary ion species are given below each image (*e.g.* $^{16}O^-$). Individual secondary ion images are normalized to the number given below the image, usually the intensity in counts of the most intense pixel (489 for $^{16}O^-$), shown in red. A color bar representing the linear scale from black (equals zero) to red is displayed. The second number below each image ($9.57 \cdot 10^6$ for $^{16}O^-$) is the integrated intensity for the entire image. (Image by courtesy of D. Rost and S. Schirmeyer)

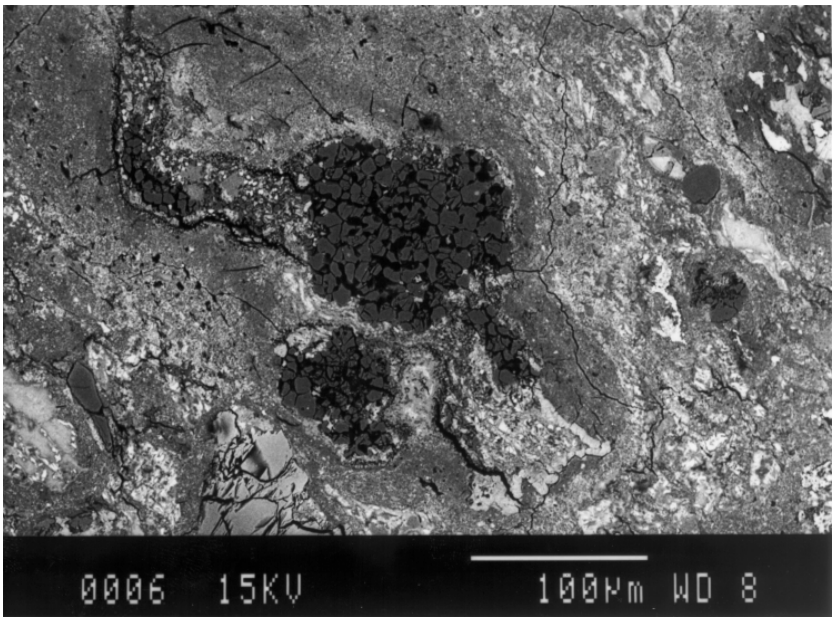

Fig. 25. SEM-BSE (scanning electron microscope, back-scattered electrons) image of the CAI shown in Fig. 24. (Image provided by S. Schirmeyer)

The TOF-SIMS observation of greatly different lithium abundances in Fe-rich phyllosilicates within CAIs and those in the adjacent matrix strongly suggest that both phases were formed in different environments. At least the phyllosilicates of the CAI must have been formed prior to the incorporation of the CAI into the meteorite parent body probably under nebular conditions (Schirmeyer *et al.*, 1997). This supports the conclusions of MacPherson and Davis (1994) who suggested alteration of refractory inclusions from the CM chondrite Mighei in the solar nebula, and not in the present or a previous generation of parent bodies.

Lithium isotopic ratios are of great interest due to their cosmological implications. In general, both lithium isotopes can be formed through three different processes: (1) galactic cosmic-ray spallation of heavier nuclides, mainly ^{12}C, ^{14}N and, ^{16}O, (2) $\alpha+\alpha$-fusion reactions, and (3) during primordial nucleosynthesis just after the big bang (Meneguzzi *et al.*, 1971; Reeves *et al.*, 1973; Olive and Schramm, 1992; Steigman and Walker, 1992; Thomas *et al.*, 1994a). While big bang nucleosynthesis produces almost pure ^{7}Li ($^{7}Li/^{6}Li$-ratio $\sim 10^{4}$), interactions of galactic cosmic ray spallation and fusion reactions lead to $^{7}Li/^{6}Li$-ratios of the order of one (Steigman and Walker, 1992). Therefore, the $^{7}Li/^{6}Li$-ratio in the solar system (~12) can only be explained by a mixture of lithium from different nucleosynthetic processes. Deviations from the CI-value in primitive solar system material would be of great interest, but have not been unambiguously found so far.

Since lithium has two stable isotopes, ^{6}Li and ^{7}Li with CI-abundances of 7.5 and 92.5 % (Anders and Grevesse, 1989), respectively, and no mass interferences occurs in the secondary ion spectra, it seemed to be predestined for isotope measurements with TOF-SIMS. Anyhow, within statistical error limits no evidence for deviations from the chondritic lithium isotope ratio other than caused by instrumental mass fractionation was observed with TOF-SIMS for the Li-rich phases in carbonaceous chondrites (Schirmeyer *et al.*, 1997). These results were also confirmed by DF-SIMS analysis (Schirmeyer *et al.*, 1997).

4.2. Organic molecules in Allan Hills 84001, Murchison, and Orgueil

Since the early 19th century, it is known that carbonaceous chondrites contain organic matter (Berzelius, 1834; "*Gibt dies möglicherweise einen Wink über die Gegenwart organischer Gebilde auf anderen Weltkörpern?*"). In the second half of the 20th century, due to new analytical techniques and a rising interest in space science, a lot of efforts were made to characterize these organic components (Hayes, 1967; Anders *et al.*, 1973; Cronin *et al.*, 1988). In the 1960s, amino acids were found in several carbonaceous chondrites, but contamination during handling and storage of the samples could not be unambiguously ruled out (Hayes, 1967). Reports of non-terrestrial fossil bacteria (Claus and Nagy, 1961) in those years were also soon compromised as terrestrial organisms (Hayes, 1967). In the early 1970s, analyses of the Murchison meteorite fallen in 1969 showed clear evidence for extraterrestrial amino acids, aliphatic and aromatic hydrocarbons in this CM chondrite (Kvenvolden *et al.*, 1970; Oró *et al.*, 1971; Pering and Ponnamperuma, 1971).

Although no connection of these organic compounds to extraterrestrial life can be drawn (Chyba and Sagan, 1987) – in contrary they have been linked to the interstellar medium (Allamandola *et al.*, 1987) – prebiotic organic matter from comets and asteroids delivered to Earth by meteorites and interplanetary dust might have been important for the origin of life on our planet (Anders, 1989; Chyba *et al.*, 1990; Chyba and McDonald, 1995).

For our neighboring planet, organic compounds known as polycyclic aromatic hydrocarbons (PAHs) in the Martian meteorite ALH 84001 (Thomas *et al.*, 1995) have been suggested as being indicative for the existence of past life on Mars (McKay *et al.*, 1996; Clemett *et al.*, 1998). Since then, the significance of PAHs as biomarkers in this case has

been questioned by many authors (Anders, 1996; Bell, 1996; Becker *et al.*, 1997, 1999; Stephan *et al.*, 1998a,b,c, 1999a; Zolotov and Shock, 1999).

Chemically, PAHs represent the transition state between aliphatic hydrocarbons and graphite. While the former are characterized by a H/C-ratio of ~2, this ratio becomes zero for the latter. For PAHs, H/C is below 0.8 and generally decreases with increasing mass. PAHs are omnipresent in our solar system and even beyond (Allamandola, 1996). In principle, they can derive from biogenic as well as non-biogenic sources. On Earth, PAHs derive mainly from anthropogenic emission caused by the combustion of fossil fuels and other natural biogenic sources (Laflamme and Hites, 1978; Wakeham *et al.*, 1980a,b). PAHs attributed to a non-biogenic origin can be found in ordinary and carbonaceous chondrites (Oró *et al.*, 1971; Pering and Ponnamperuma, 1971; Hahn *et al.*, 1988; Zenobi *et al.*, 1989; Wing and Bada, 1991; Clemett *et al.*, 1992; de Vries *et al.*, 1993). They have been detected in interplanetary dust particles (Clemett *et al.*, 1993), comet Halley (Moreels *et al.*, 1994), and also in circumstellar graphite grains extracted from primitive meteorites (Clemett *et al.*, 1996; Messenger *et al.*, 1998).

Therefore, the presence of PAHs in ALH 84001 is not indicative for past life on Mars. Nevertheless, is has been argued that their spatial association with other proposed biomarkers suggests a biogenic origin of PAHs in this Martian meteorite (McKay *et al.*, 1996). These biomarkers, most prominently the “nanofossils”, are all related to chemically zoned Ca-Mg-Fe-carbonates (Mittlefehldt, 1994; Scott *et al.*, 1998; Treiman and Romanek, 1998; Warren, 1998), which might have been deposited from hydrothermal fluids on Mars (McKay *et al.*, 1996). These distinct observations were made by use of entirely different techniques, which, simply from their spatial resolution, hampers a correlation of their results. Due to the small size of the supposed microfossils, 100 nm in longest dimension and 20–80 nm across, a scanning electron microscope with field emission gun (FEG-SEM) with a lateral resolution of about 2 nm was used (McKay *et al.*, 1996). On the other hand, PAHs were identified by μL^2MS analysis with a lateral resolution of about 40 µm (Thomas *et al.*, 1995). A meaningful mass spectrum was obtained by mapping a surface region of 750×750 μm^2 at a spatial resolution of 50×50 μm^2 (McKay *et al.*, 1996). Therefore, a correlation of PAHs even with carbonates, between 1 and ~250 µm in size (McKay *et al.*, 1996), could not be scrutinized by this technique.

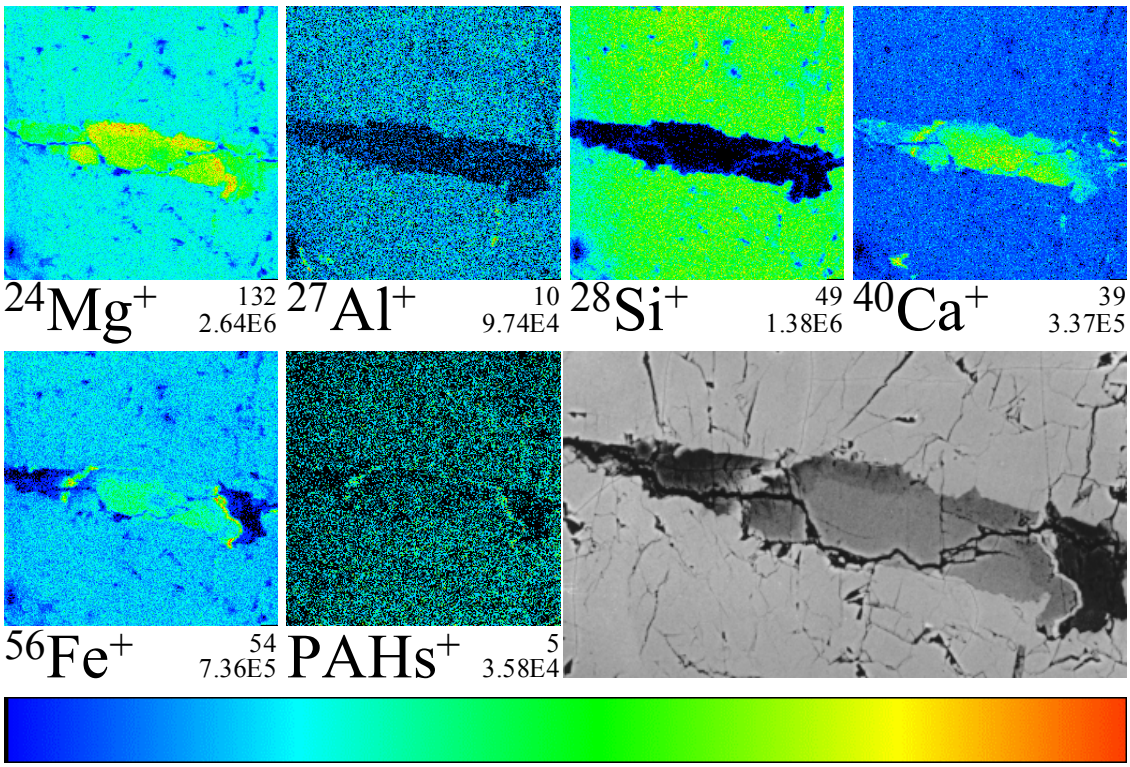

Fig. 26. Secondary ion and SEM-BSE images for an area of ALH 84001 dominated by a carbonate surrounded by orthopyroxene. The PAH image is obtained by summing up signals from characteristic PAH masses between 115 and 339 amu (cf. Fig. 28 and Fig. 29). Field of view is 100×100 μm^2, and 200 primary ion shots were applied to 256×256 pixels.

Here, TOF-SIMS has its advantages. The high lateral resolution in combination with parallel detection of atomic as well as molecular secondary ions should be predestined for an examination of the proposed spatial association. First TOF-SIMS studies of ALH 84001 were performed on polished thin sections of this meteorite (Stephan *et al.*, 1998a,b). Although a homogenization of the lateral PAH distribution by the polishing process was expected, PAHs were found to be distributed inhomogeneously, especially after removal of the uppermost monolayers through sputtering. However, a spatial association with carbonates could not be confirmed in this study. Although omnipresent in this Martian meteorite, in carbonates, compared to orthopyroxene and feldspathic glass, PAHs even seem to be slightly depleted. Spatial distributions of PAHs and major rock-forming elements are shown in Fig. 26 for one section of ALH 84001. The area is dominated by a carbonate, prevailing in the Ca^+-image, which is surrounded by orthopyroxene (dominant in the Si^+-image). In the meantime, the search for PAHs was extended to fractured surfaces. Preliminary results (Fig. 27) here also show no indication of PAH enrichments associated with carbonates. PAHs seem to be omnipresent on this surface. Nevertheless, no homogeneous

distribution of PAHs was observed in the corresponding image. The variability can at least in part be attributed to topographic effects, since here no flat surface was investigated.

A more detailed analysis of the TOF-SIMS spectra is helpful to elucidate the origin of the PAHs in ALH 84001. These mass spectra (Fig. 28) differ significantly from those obtained by μL^2MS (McKay *et al.*, 1996; Clemett *et al.*, 1998; Becker *et al.*, 1999). This can be explained by differences in ionization processes. Fragmentation of the PAHs occurs during primary ion bombardment, increasing the low-mass PAH signals.

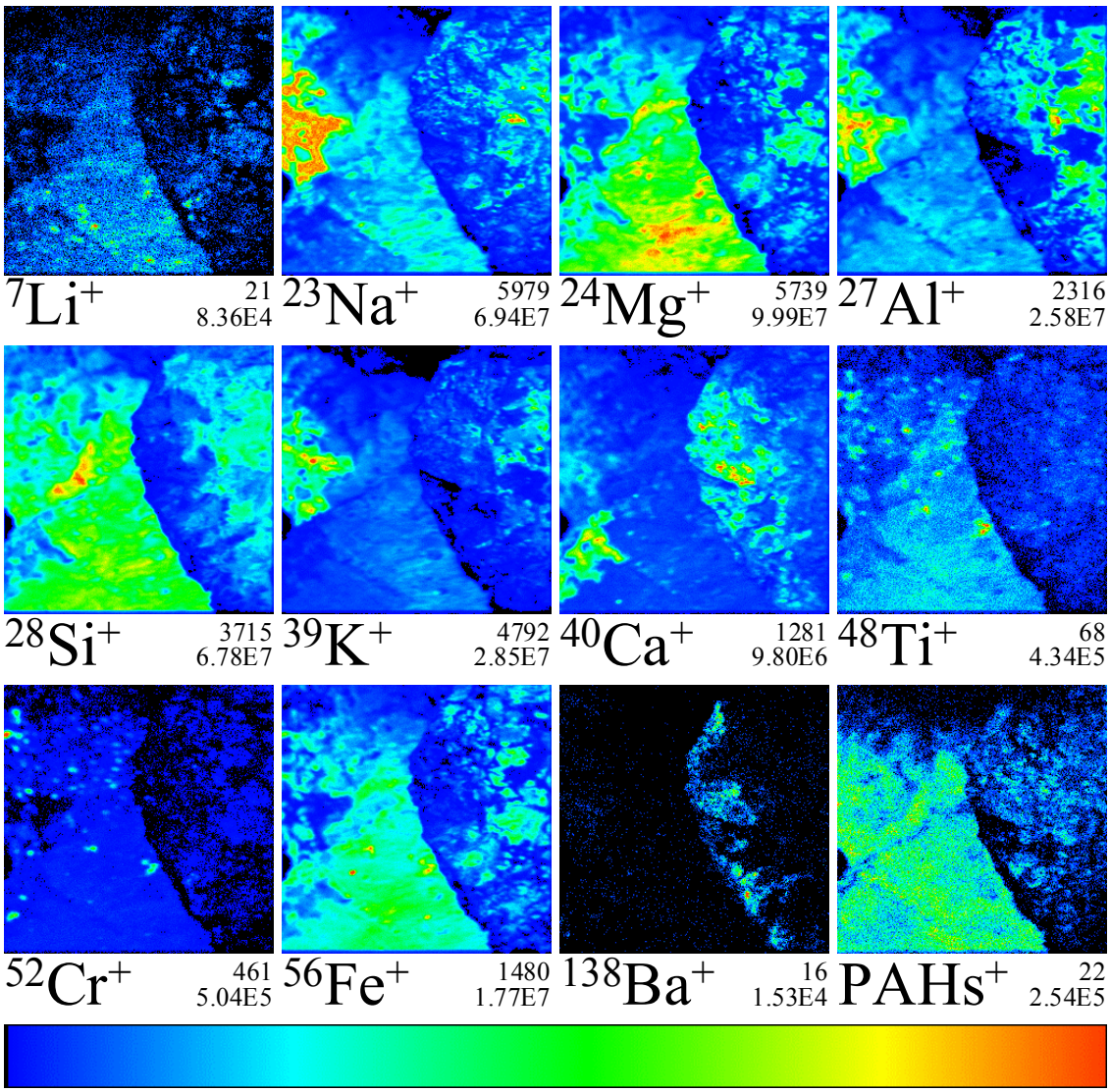

Fig. 27. Secondary ion images from a fracture surface of ALH 84001 (150×150 μm^2, 3200 shots/pixel, 256×256 pixels). Prevailing mineral phases are orthopyroxene (dominant in Mg^+-, Si^+-, and Fe^+-images), feldspathic glass (Na^+-, Al^+-, and K^+-images), and carbonate (Ca^+-image). One carbonate rich area is enriched in barium. Small chromite grains are apparent in the Cr^+-image and are rich in titanium. Lithium is also enriched in distinct spots, which show no clear correlation with any other element.

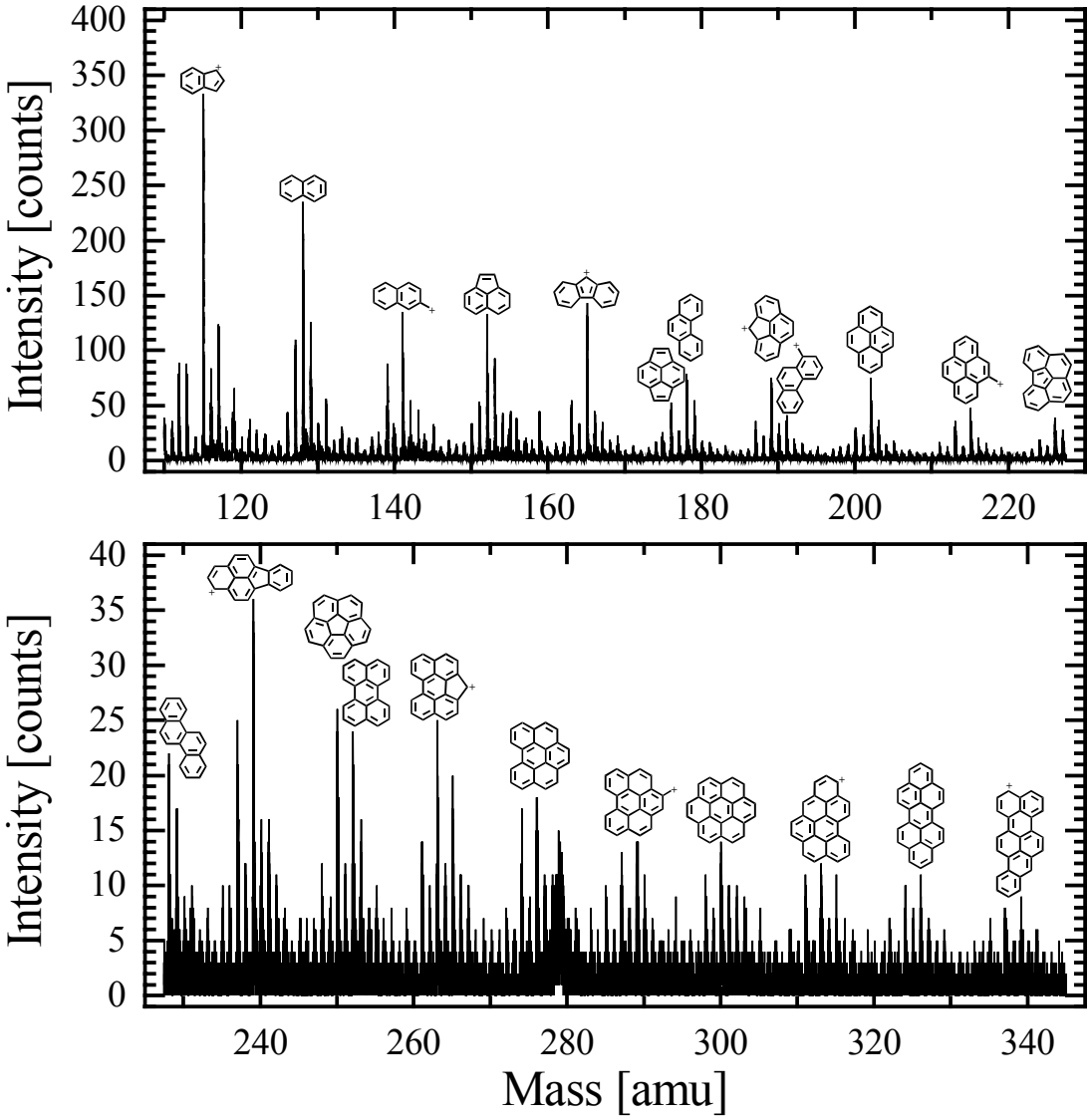

Fig. 28. Typical TOF-SIMS spectrum of mass range 110–345 amu for positive secondary ions obtained from a section of ALH 84001. Relative maxima are separated by mass differences of 11 or 13 amu, respectively. Often several maxima appear separated from each other by a mass difference corresponding to H_2. Since several structural isomers exist for all mass peaks, only examples for major peaks are given.

Pure PAH substances, pentacene ($C_{22}H_{14}$) and coronene ($C_{24}H_{12}$), as well as two carbonaceous chondrites containing PAHs, Murchison and Orgueil, were analyzed to investigate this fragmentation more thoroughly (Stephan *et al.*, 1998c, 1999a). Pentacene and coronene showed fractionation during primary ion bombardment, but to different extents (Fig. 29). The linear line-up of benzene rings in pentacene is more susceptible to fragmentation than their circular arrangement in coronene. However, for both substances the very same PAH fragments were observed as in ALH 84001 and the other two meteorites. From

these results, one can infer that PAHs similar to those observed by μL^2MS had produced the observed TOF-SIMS spectra upon sputtering.

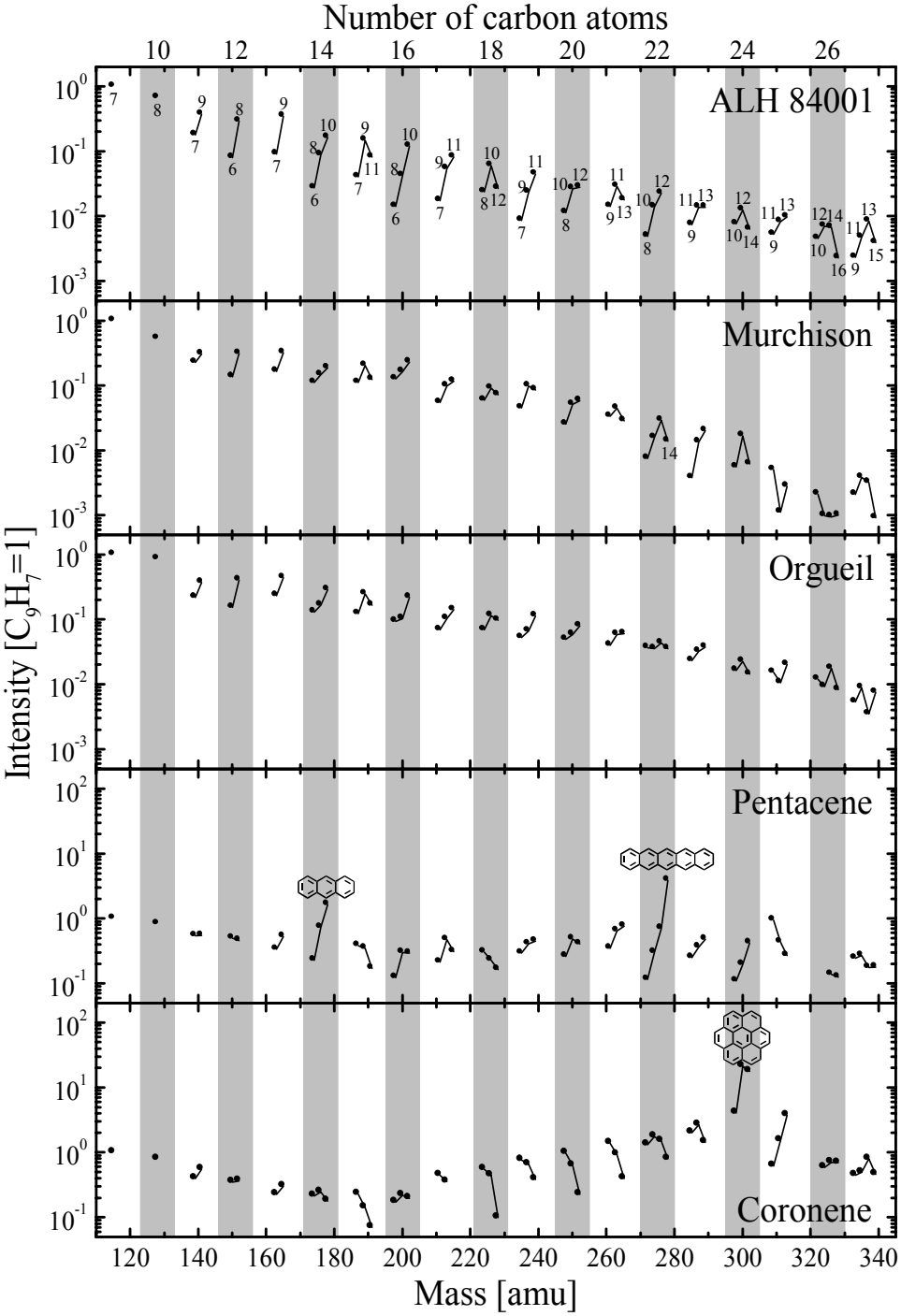

Fig. 29. Relative abundances of PAHs in TOF-SIMS spectra obtained from ALH 84001, Murchison, and Orgueil compared with those obtained from pure pentacene and coronene samples. Coronene and pentacene structures are shown as well as the structural formula of anthracene ($C_{14}H_{10}$) a major fragment of pentacene during sputtering. Besides the number of carbon atoms above the upper x-axis, numbers of hydrogen atoms are given for each major peak next to the ALH 84001 data points.

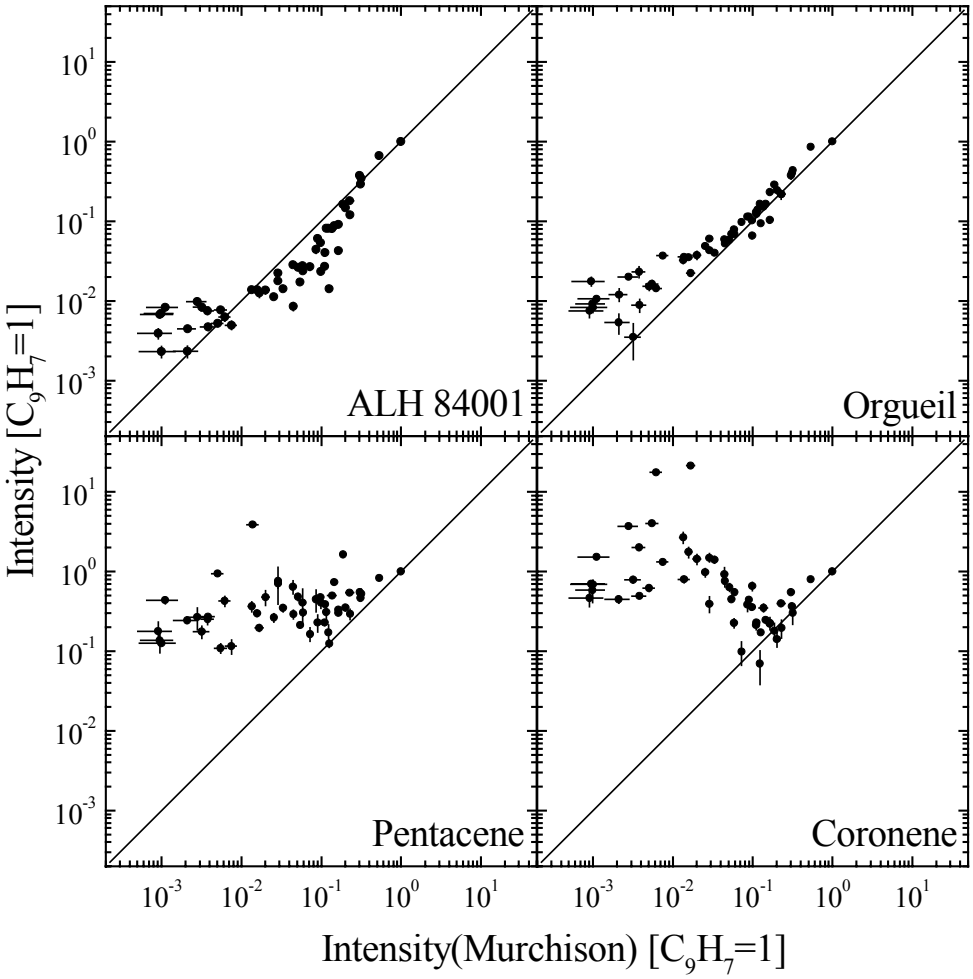

Fig. 30. Comparison of relative intensities of PAHs in ALH 84001 and Orgueil meteorites, as well as pentacene and coronene standards with PAH intensities in Murchison.

Since unambiguous proof for a connection between PAHs and indigenous features in ALH 84001 is missing, it has been suggested that PAHs as well as amino acids in ALH 84001 originate from the icy environment like observed in other Antarctic meteorites (Becker *et al.*, 1997; Bada *et al.*, 1998). Based on stable carbon isotope measurements, it was proposed that besides terrestrial contamination, a second organic carbon component exists, which might be extraterrestrial, probably Martian (Jull *et al.*, 1998; Becker *et al.*, 1999).

To investigate the origin of PAHs in ALH 84001 – terrestrial or Martian – extraterrestrial PAHs from the carbonaceous chondrites Murchison and Orgueil were analyzed with TOF-SIMS (Stephan *et al.*, 1999a). The mass spectra of PAHs from these two meteorites resemble remarkably well those obtained from ALH 84001 (Fig. 29). All three meteorites show essentially the same PAH fragmentation and, therefore, a similar, non-biogenic origin can be deduced. For biogenic PAHs we would expect higher degrees of

alkylation and the presence of aromatic heterocycles like observed in terrestrial samples (Wakeham *et al.*, 1980a,b). Heteroatoms would drastically increase the ionization yields of the PAHs. Because of this and since they would appear at different characteristic masses, they cannot be overlooked in the mass spectra.

So far, the comparison between the TOF-SIMS spectra of the three meteorites is not quantitative. To calculate the mean H/C-ratio for all observed PAH fragments, is a first attempt to overcome this deficiency. Here, the three meteorites yield similar values, 0.69 for ALH 84001 and 0.65 for both carbonaceous chondrites. These values differ significantly from those obtained for pentacene (0.58) and coronene (0.52). This difference and the similarities between all five PAH spectra are also emphasized in Fig. 30, where the data points from Fig. 29 for ALH 84001, Orgueil, and the two pure PAH substances are directly compared with those of Murchison. It is expected that future TOF-SIMS analyses of terrestrial biogenic PAHs will help to assess these results and to discover the true nature of PAHs in ALH 84001.

However, the present results, great similarities between PAHs in ALH 84001 and carbonaceous chondrites, supports the suggestion that these organic molecules derived from the exogenous delivery of meteoritic or cometary debris to the surface of Mars (Becker *et al.*, 1999), similar to those compounds delivered to the early Earth (Anders, 1989; Chyba *et al.*, 1990). Alternatively, an abiotic synthesis of PAHs on Mars is also conceivable, provided that this chemical process is similar to the formation process of PAHs in Murchison and Orgueil. This has also been proposed recently (Zolotov and Shock, 1999). Independent of the discussion about the significance of other suggested biomarkers in ALH 84001 (*e.g.*, Bradley *et al.*, 1996, 1997, 1998; Leshin *et al.*, 1998; Scott, 1999), TOF-SIMS studies revealed that no spatial association between PAHs and carbonates exists in this meteorite.

4.3. Further meteorite studies with TOF-SIMS

4.3.1. Orgueil

CI chondrites represent chemically the most pristine solar system material available for laboratory analysis. Except for the so-called CHON elements (carbon, hydrogen, oxygen, and nitrogen), lithium, and the noble gases, their composition is representative for the entire solar system (Anders and Grevesse, 1989).

Only little is known about the actual distribution of minor and trace elements in CI meteorites, despite their importance for the understanding of early solar system evolution. The knowledge of the actual distribution of trace elements in chondritic matter is of great interest also for the understanding of apparent enrichments of volatile trace elements in interplanetary dust (see below).

Imaging TOF-SIMS at high lateral resolution was therefore used to analyze the element distribution within the Orgueil CI meteorite (Stephan *et al.*, 1997a), which is generally used as *the* cosmic element abundance standard (Anders and Grevesse, 1989). The TOF-SIMS investigation revealed a rather homogeneous distribution for the major elements magnesium, aluminum, silicon, iron, and nickel. For sodium and potassium, enrichments throughout the entire section were observed in correlation with fluorine and chlorine. This might be explained by surface contamination, a general problem in TOF-SIMS studies (see above). Other elements are often concentrated in small, up to 100 µm sized regions. Calcium occurs in carbonates, as observed before in CI chondrites (Endreß and Bischoff, 1996). Chromium, typically together with iron, can be found in chromites. Iron and nickel enrichments are often correlated with sulfur, indicative for the presence of sulfides. Lithium, titanium, manganese, copper, bromine, and iodine showed enrichments in small regions, only a few micrometers in size. Further mineralogical studies are needed to elucidate the host phases of the enriched elements.

It should be mentioned that although Orgueil is *the* element standard in cosmochemistry, this meteorite is not suited as an element standard for TOF-SIMS, due to lack of homogeneity. Elements that are only present in distinctive mineral phases differ often drastically, up to orders of magnitude, in their secondary ion yield from elements in the bulk matrix.

4.3.2. Chassigny and Nakhla

A general interdisciplinary study on Martian meteorites has just been started recently. A central role in this investigation plays TOF-SIMS (Stephan *et al.*, 1999b). Besides the analysis of ALH 84001, two further Martian meteorites were investigated so far, namely Chassigny and Nakhla. In combination with SEM, electron microprobe, and TEM studies, so-called symplectic exsolutions in olivines were analyzed that set constraints on the formation of these Martian rocks, the oxidizing conditions and the cooling history (Greshake *et al.*, 1998). Figure 31 shows secondary ion images as well as an SEM-BSE

image from one of these objects found in Nakhla. A calcium-rich pyroxene (augite) can be seen as dark areas in the SEM image. Here calcium showed the highest secondary ion intensities. The bright phase in the SEM image is dominated by chromium-rich magnetite, prevailing in the Cr^+- and Fe^+-images with a slight enrichment in aluminum. Magnesium, silicon, and iron secondary ion images show the highest intensities outside the exsolution lamella in the olivine. Therefore, these images have been normalized to the most intense pixels inside the interesting region and not to the most intense pixels of the entire images. The fact that iron yield higher secondary ion intensities in olivine than in magnetite, although the iron concentration is higher in the latter, can be attributed to matrix effects.

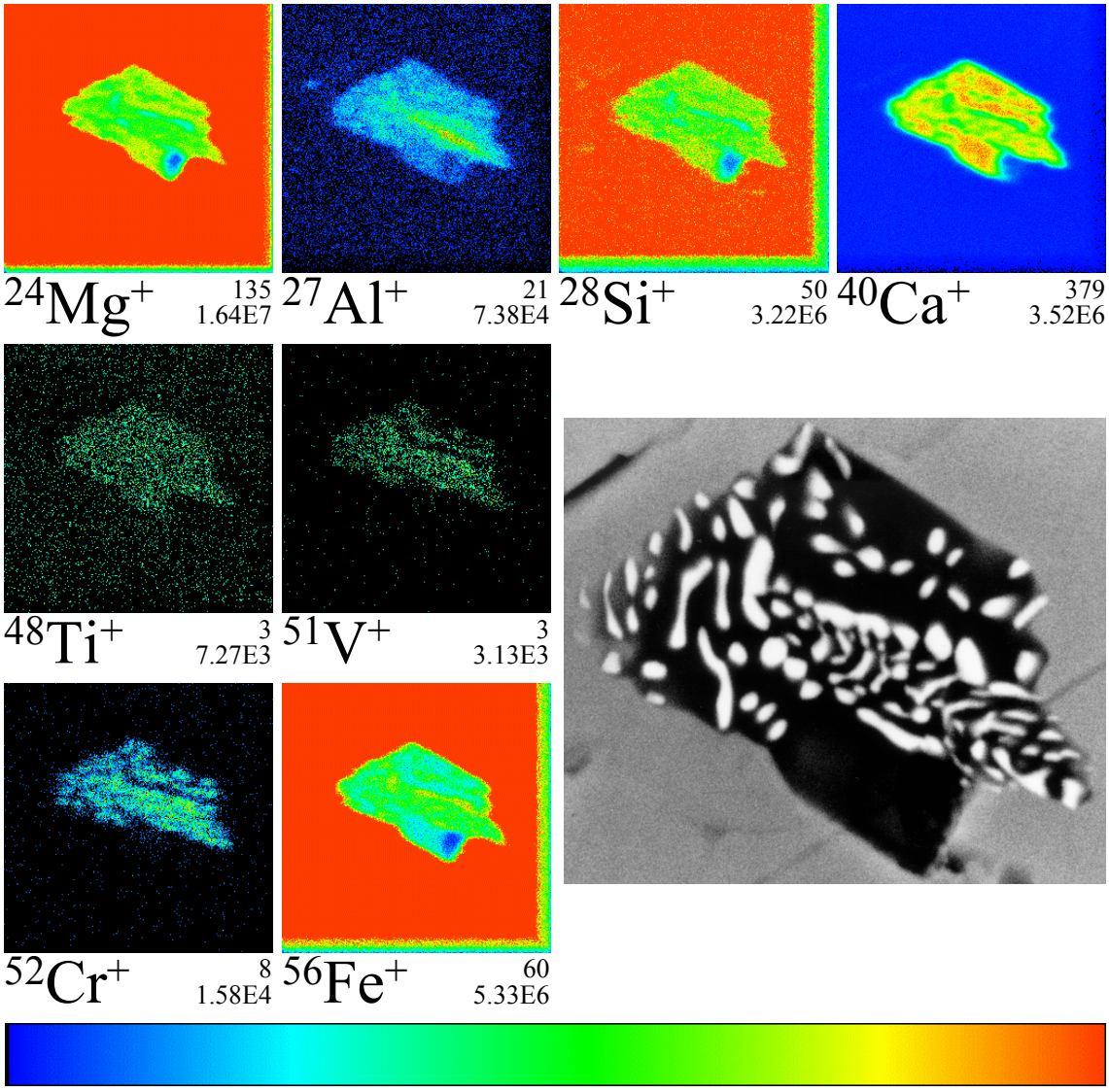

Fig. 31. Secondary ion images from a symplectic exsolution from the Nakhla Martian meteorite (20×20 µm^2, 1600 shots/pixel, 256×256 pixels). Lower intensities towards the very right and bottom of the images are an artifact, originating from adding up several scans of the ion beam, which have shifted during the analysis.

5. Interplanetary dust

In 1683, when the Italian-French astronomer G. D. Cassini first described the zodiacal light, he also gave the right explanation for this phenomenon (in Cassini, 1730): It is caused by sunlight scattered from dust particles concentrated in the ecliptic plane. Since 1981, interplanetary dust particles (IDPs) are collected routinely in the stratosphere using high-flying aircraft (Warren and Zolensky, 1994). They represent, besides meteorites and lunar rocks, the third class of extraterrestrial material available for laboratory investigation so far (Brownlee *et al.*, 1977). Due to their small size – typical IDPs have a size of ~10 μm – these samples require analytical techniques with high lateral resolution and high sensitivity.

IDPs are of high interest in planetary research since they potentially allow to investigate the most pristine solar system bodies, asteroids and comets (Brownlee, 1994; Dermott *et al.*, 1996). In particular for cometary material, they represent the only available source so far for an earthbound investigation. But also asteroidal IDPs should significantly differ from meteoritic material. While meteorites are generally accepted to derive primarily from the inner asteroid belt (Wetherill and Chapman, 1988), dust from all over the solar system, including the outer belt, should spiral towards the sun due to Poynting-Robertson-drag (Robertson, 1937; Klacka, 1994) and therefore contribute to the near-Earth dust population. Some of this dust eventually enters the Earth's atmosphere and can be collected in the stratosphere. IDPs still preserve information on their precursors, although several selection and alteration processes occur during their lifetime. For a general overview of IDPs refer to, *e.g.*, Zolensky *et al.* (1994), Brownlee (1996), Rietmeijer (1998), or Jessberger *et al.* (1999).

Major goals in IDP research are still to unambiguously differentiate cometary from asteroidal IDPs and to distinguish between features caused by atmospheric entry and collection in the stratosphere, and indigenous properties. Nevertheless, the "chondritic porous" subset of IDPs, anhydrous particles with highly porous microstructures, high carbon abundances, and often high atmospheric entry velocities are most promising candidates for

cometary dust. They consist mainly of Mg-rich, Fe-poor silicates, remarkably similar to those observed in dust around stars and from comets Halley and Hale-Bopp (Jessberger and Kissel, 1991; Bradley *et al.*, 1999a). Comets are probably the most primitive bodies in the solar system and therefore predestined as deep-freeze storehouses for presolar material. The search for interstellar matter in cometary IDPs has been one inspiring motivation for the analysis of these tiny grains (Bradley and Ireland, 1996). Recent observations link them – or at least parts of them known as GEMS (glass with embedded metal and sulfides) – to interstellar amorphous silicate grains (Bradley, 1994b; Bradley *et al.*, 1999b). Together with presolar grains extracted from primitive meteorites, constituents of cometary IDPs are the most primitive materials available for laboratory investigations and maybe the best analogue to present interstellar dust.

Due to its capabilities of analyzing small particles (Zehnpfenning *et al.*, 1994; Rost *et al.*, 1998a), TOF-SIMS was expected to be an appropriate technique for the investigation of IDPs.

5.1. Volatile elements

Many stratospheric IDPs are more rich in volatile elements than CI chondrites (Arndt *et al.*, 1996a), while major elements usually show chondritic abundances (Schramm *et al.*, 1989). Attempts to explain the enrichments range from postulating a new type of volatile-rich chondrite-like matter (Flynn and Sutton, 1992; Flynn *et al.*, 1996a) to invoking atmospheric contamination processes (Jessberger *et al.*, 1992). Before far reaching conclusions on nebular processes can be drawn, stratospheric processes, contamination during capture and handling, artifacts from various selection effects or from analytical techniques and even from data treatment have to be excluded (Stephan *et al.*, 1997b).

Due to their complex history, IDPs in the laboratory have already experienced several potential sources of contamination. For small particles, contamination in general is a more severe problem, because of the high surface-to-volume ratio, than for the comparably large “normal” meteorites. High porosity of IDPs also enhances the surface receptive to contamination (Stephan *et al.*, 1992a, 1994b). Furthermore, elements with very low abundances in chondritic matter are most susceptible to contamination because then even a small absolute amount added can yield high enrichments.

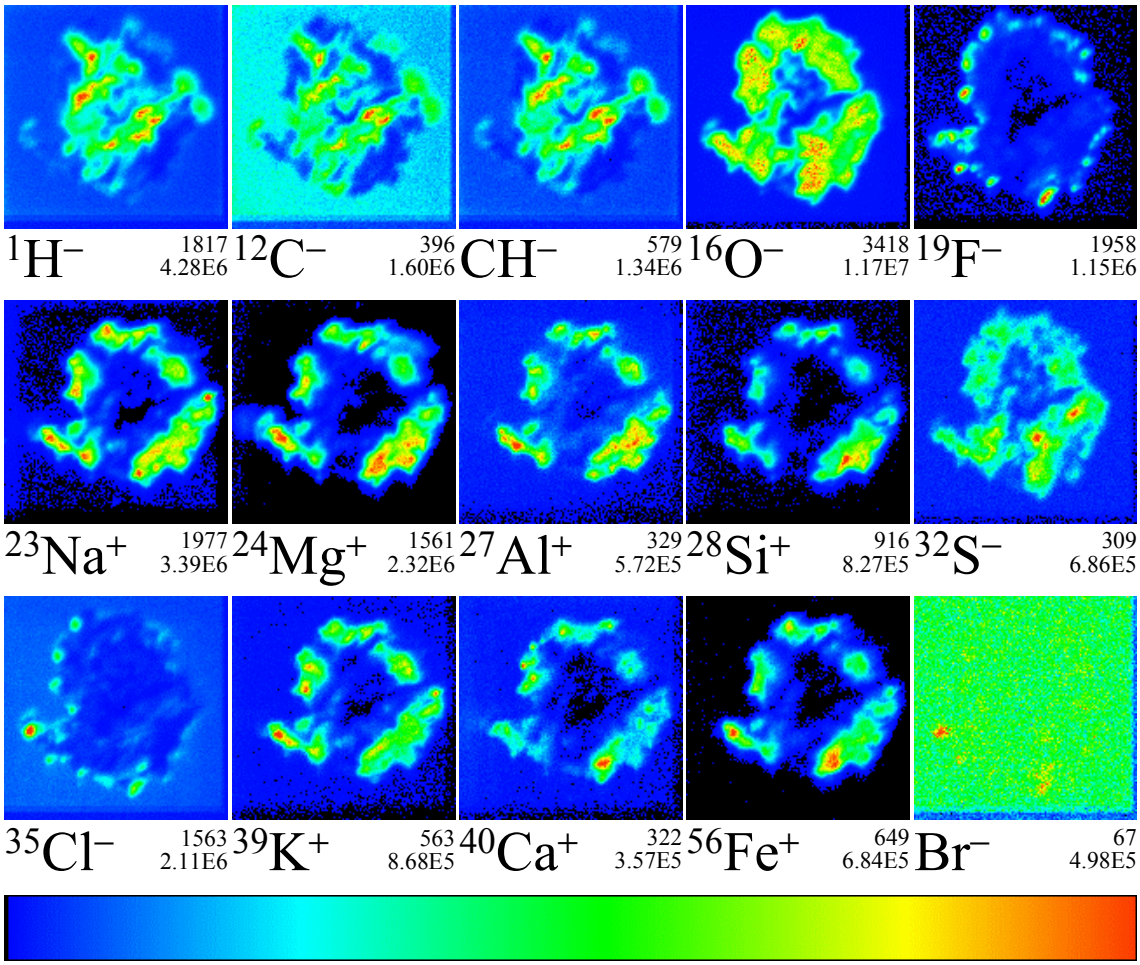

Fig. 32. Secondary ion images for positive as well as negative secondary ions from IDP L2006G1. The investigated area (30×30 µm^2, 128×128 pixels) was bombarded with Ga^+ primary ions (1000 shots/pixel and 800 shots/pixel for positive and negative secondary ions, respectively). Although the background for Br^--ions (here signals from both bromine isotopes ^{79}Br and ^{81}Br have been added up) is relatively high, a clear correlation with the other halogens fluorine and chlorine is obvious.

Bromine shows the highest enrichments in IDPs, with enrichment factors of up to 10^4×CI (Arndt *et al.*, 1996a). Since bromine, on the other hand, has only a CI-abundance of 3.56 ppm (Anders and Grevesse, 1989) and halogens are widespread in the stratosphere (Cicerone, 1981), contamination processes have to be considered as being responsible for high bromine concentrations in stratospheric particles. First direct experimental evidence for such a contamination were Br-salt nano-crystals attached to IDP W7029E5 (Rietmeijer, 1993) and a halogen rich exterior rim of IDP L2006G1 found with TOF-SIMS (Stephan *et al.*, 1994c). The distributions of secondary halogen ions from a section of this IDP reveal an outer ring structure for fluorine, chlorine, and also bromine, though the latter image is disturbed by rather high background (Fig. 32). Assuming a spherical particle, originally

20 µm in diameter, and a continuous 1 µm thick surface layer surrounding it, this layer represents ~25 vol.-% of the entire particle. Although only a rough estimate, these numbers illustrate the influence that surface contamination might have on bulk chemistry of small particles.

Other clear evidence for contamination as a major clue to halogen enrichments of stratospheric IDPs was found with test particles exposed to the stratosphere on a dust collector by Arndt *et al.* (1996b). Besides this, weakly bound bromine was observed in large IDPs (Flynn *et al.*, 1996b).

To test more directly for surface contamination with TOF-SIMS, the *original* surfaces of stratospheric particles were analyzed and compared with sections from the very same particles (Rost *et al.*, 1998b, 1999a,b). Here halogens were observed on several stratospheric particle surfaces although some analyses were obstructed by non-removable silicone oil residues. – Stratospheric dust collectors are coated with silicone oil, which is also used during particle handling. – A surface correlation of halogens on some particles was unequivocally proven by extensive sputtering, reducing and finally removing the halogens at least on certain particles (Rost *et al.*, 1999a). In addition, several dust particles in sections showed again outer rings of halogen contaminants (Rost *et al.*, 1998b, 1999b).

Another source of contamination, not in the stratosphere but from laboratory handling, was observed in TOF-SIMS studies in form of surface correlated beryllium. This results from the SEM-EDS analyses, which in case of these particles were performed on beryllium substrates (Rost *et al.*, 1999a). After such analyses, some particles tend to stick to the substrate and carry beryllium when they were removed.

For other elements, finally, no unambiguous evidence for or against contamination is available so far. For most volatiles an unequivocal enrichment cannot be claimed since the data set available in the literature typically is too incomplete for a clear statement (Arndt *et al.*, 1996a) and limitations of the applied analytical and mathematical techniques complicate the interpretation (Stephan *et al.*, 1997b). Trace element distributions are largely variable and reflect chemical inhomogeneity on a micron scale (Bohsung *et al.*, 1993; Stephan *et al.*, 1993a, 1994b; Arndt *et al.*, 1996a). Nevertheless, since most IDPs chemically are remarkably similar to CI chondrites, they represent an adequate sample of primitive solar system material.

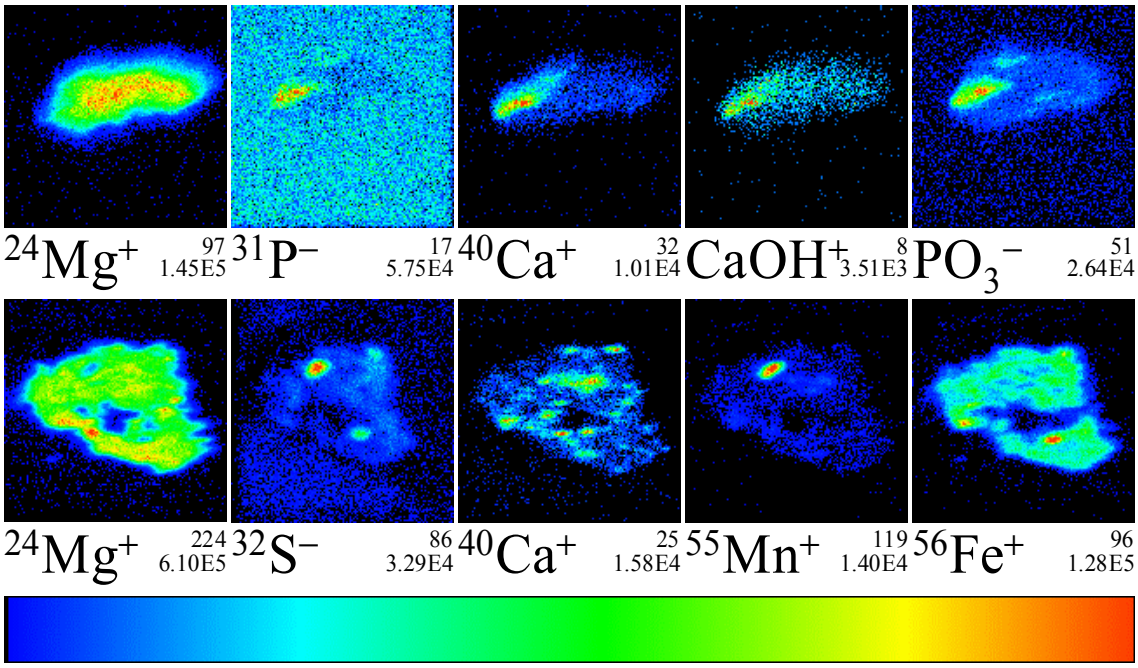

Fig. 33. Secondary ion images from IDPs L2006E10 (first row; Stephan *et al.*, 1994c) and U2071B6 (second row; Rost *et al.*, 1998b) show the first reported observations of calcium phosphate (presumably apatite) and manganese sulfide (most likely alabandite) in interplanetary dust. Fields of view are 25×25 μm^2 (L2006E10) and 30×30 μm^2 (U2071B6). Both samples were scanned with 128×128 pixels, and 1000 shots/pixel (L2006E10) and 2560/2400 shots/pixel (U2071B6, positive/negative secondary ions) were applied.

5.2. Mineral identification

TOF-SIMS has enabled the discovery of several unique mineral phases by secondary ion imaging, although the capabilities of quantification are limited for this technique. Calcium phosphate, probably apatite, was found for the first time to occur in an IDP (L2006E10, Fig. 33 top) by TOF-SIMS investigation (Stephan *et al.*, 1994c) and has meanwhile been reported in another IDP (Rost *et al.*, 1999b). For U2071B6 (Fig. 33 bottom), a manganese sulfide (most likely alabandite) was observed (Rost *et al.*, 1998b). While apatite is widespread in many different types of meteorites, alabandite usually is only found in meteorites that formed under highly reducing conditions, *e.g.*, enstatite chondrites or aubrites (Brearley and Jones, 1998; Mittlefehldt *et al.*, 1998). However, no further connection between these meteorite classes and this specific IDP can be drawn from TEM studies so far (W. Klöck, pers. comm.).

Although an unambiguous identification of the actual mineral phase is not possible through TOF-SIMS analysis alone, indicative elemental correlations can help to recognize interesting regions within a sample, which can be analyzed later by appropriate techniques like TEM for an unequivocal mineral assignment.

5.3. The collector project

As long as no interplanetary dust particle has been captured gently in outer space (cf. Brownlee *et al.*, 1996, 1997), retrieved to Earth, and recovered successfully from the capture medium (probably aerogel; Tsou, 1996), IDPs collected in the stratosphere are the first-choice samples of interplanetary dust. Therefore, a comprehensive consortium study was initiated to investigate all particles from one collection surface (U2071) with as many different techniques as possible (Stephan *et al.*, 1994d). This suite of analytical methods (cf. Table 3) includes TOF-SIMS for surface studies (Stephan *et al.*, 1995a; Rost *et al.*, 1996, 1999a,b) as well as for the investigation of interior element distributions (Rost *et al.*, 1998b, 1999b) in sections within the same particles. Not only the investigation of contamination processes as mentioned above is the aim of this ongoing study, but to investigate the mineralogical and chemical properties of an unbiased sample of stratospheric dust particles as thoroughly as possible. By studying all particles from one collector, one avoids human selection effects prevailing in most studies. Only "chondritic looking" (black and fluffy) particles are picked from the collector flags in most cases (J. L. Warren, pers. comm.) and only particles pre-classified as "cosmic" due to their chondritic major element composition are further investigated. Therefore, one major objective of this study is to track down non-chondritic interplanetary dust particles.

Table 3 gives an overview of the present status of this consortium study. All 326 particles with diameters ≥10 µm on collection surface U2071 were investigated under an optical microscope, and 90 of them were selected for the first round of investigations. After SEM imaging and EDS analysis of major element concentrations including carbon (Thomas *et al.*, 1993, 1994b), these particles were pre-classified as cosmic particles (C), terrestrial contamination, natural (TCN) and artificial (TCA), aluminum oxide spheres (AOS; solid fuel rocket exhaust), and non-classified particles. The classification scheme was used according to the *Cosmic Dust Catalogs* (Warren and Zolensky, 1994).

TABLE 3. Analytical sequence and present status of the consortium study on particles from stratospheric collector U2071.

Analytical technique	Particles from collector U2071
Optical microscope	326 particles ≥10 µm
SEM (images)	90 particles
SEM-EDS	90 particles
TOF-SIMS (surface)	B3, B6, B7a, C3, D1, D4, D8, E6, E8, F3, G8, H1a, H9, I9, J9a, L1, L2
PIXE (bulk)	B3, B6, C3, D1, D8, E6, F3, G8, H1a, H9, I9, L2
STIM (bulk)	B3, B6, C3, D1, D8, E6, F3, G8, H1a, H9, I9, L2
TEM (section)	B6, C3, D1, D4, E6, E8, F3, G8, H9, I9, L1
TOF-SIMS (section)	B6, C3, D1, D4, E6, E8, H9, I9, L1
PIXE (section)	*in preparation*

Underlined names represent particles pre-classified as cosmic (type C) IDPs. Other types are terrestrial contamination, natural (TCN: E6) and artificial (TCA: I9), aluminum oxide spheres (AOS: B3, D8, G8, L2), as well as non-classified particles (type ?: D1). The TEM studies are presently in progress.

Surface analysis with TOF-SIMS followed to study contamination effects (see above). Subsequently, the particles were investigated with PIXE (proton induced X-ray emission) analysis including STIM (scanning transmission ion microprobe). PIXE allows trace element studies with high sensitivity down to ppm levels for elements with atomic numbers >11 (Traxel *et al.*, 1995; Bohsung *et al.*, 1995). STIM yield particle densities and masses (Maetz *et al.*, 1994; Arndt *et al.*, 1996c, 1997). This first PIXE investigation was done at limited proton current and dose to avoid destruction of hydrous minerals (Maetz *et al.*, 1996). The information depth in PIXE is of the order of 30 µm, the typical dimension of the dust particles. The information in SEM-EDS comes from the upper 1–2 µm, and TOF-SIMS only investigates the surface. Consequently, even for elements that are detectable with all three analytical techniques, the results are not straightforward to compare (Stephan *et al.*, 1995b).

After these analyses, the particles are imbedded in epoxy and cut with an ultramicrotome. The microtome sections were prepared for TEM studies and the particle residues in the epoxy were analyzed again with TOF-SIMS. This allows a direct comparison of mineralogical results (TEM) and element distribution images (TOF-SIMS) of adjacent sections.

It is further planned to produce sections several micrometers thick from the remaining epoxy stubs for further PIXE studies. As the last analytical step for these particles, PIXE can now be performed at high proton current, dose, and therefore increased sensitivity. Since the final stage in the sequence of analytical steps is now reached, precautions concerning mineral destruction have not to be considered any longer.

The general principle for this sequence of analytical techniques is to go from non-destructive via less destructive to the most destructive techniques. The analysis of contamination effects in the stratosphere has to be made as early as possible to minimize the risk of additional contamination in the laboratory. It is expected that the great variety of analytical techniques applied to individual IDPs in this ongoing study will finally be instrumental in a comprehensive understanding of the origin and history of interplanetary dust.

5.4. Particle impact residues from space probes

Each surface exposed in space is subject to dust particle bombardment. Within the Earth's orbit, this dust consists of interplanetary dust as well as man-made space debris. To discern between these populations and to reveal their respective frequencies were major objectives of the capture cell experiment A0187-2 on the LDEF (long duration exposure facility) satellite (Amari *et al.*, 1991, 1993; Bernhard *et al.*, 1993a,b; Hörz *et al.*, 1995).

At typical relative velocities of several kilometers per second, an impinging dust particle evaporates almost entirely. Nevertheless, some material may be deposited in or around the impact crater. These impact residues provide information on the chemical composition of the precursor particles, although tremendous elemental fractionation processes occurring during particle impact have to be considered (Lange *et al.*, 1986). The typical amount of sample material deposited by high-velocity impact is confined to 1–5 atomic layers. TOF-SIMS with its high surface sensitivity here seems to be ideally suited for the analysis of these impact residues. Due to parallel detection of all secondary ions with one polarity, TOF-SIMS allows to investigate numerous elements even within these extreme thin layers. This might help to elucidate the origin of the respective impacting particle.

TOF-SIMS studies were performed on two impact residues from the above mentioned LDEF capture cell experiment A0187-2 (Stephan *et al.*, 1992b) as well as on several impact craters from the Hubble space telescope solar cell array (unpublished data) to reveal the origin of the impacting particles.

Prior to the TOF-SIMS analysis of the LDEF impacts, both samples were investigated with DF-SIMS (Amari *et al.*, 1991). From these analyses, the two projectiles that had produced the impact features were classified as probably chondritic, based on relative abundances of magnesium, aluminum, calcium, titanium, and iron. However, an unambiguous identification of the true nature of the impacting particle is hampered by the huge elemental fractionation.

With TOF-SIMS, high secondary ion intensities for copper were found in both LDEF residues (Stephan *et al.*, 1992b). Although a proper quantification is not possible, copper was identified as the dominating element. These findings seem to exclude an extraterrestrial origin of the respective particles, since high abundances of elements with extreme low cosmic abundances like copper are indicative for space debris. Copper has a mean chondritic abundance of only 126 ppm (Anders and Grevesse, 1989) and should not be present as major element in interplanetary dust. These results clearly demonstrate the advantages of TOF-SIMS especially when sample material is limited. DF-SIMS only allowed to analyze a limited number of elements within the thin layers. This is often not sufficient for a proper classification of impact residues. The parallel detection in TOF-SIMS led to the discovery of the copper enrichment. Beforehand, such enrichments were not expected and therefore copper was not selected for DF-SIMS analysis.

5.5. Further TOF-SIMS studies

As mentioned before, to decipher the origin of an interplanetary dust particle, its connection to asteroids or comets is a major aim of IDP research. The TOF-SIMS study of an anhydrous particle supported the idea of a relation between chondritic porous IDPs and comets (Stephan *et al.*, 1993b; Jessberger *et al.*, 1999). The element abundances of this particle, L2006B21, are similar to the element abundances observed in comet Halley's dust (Jessberger *et al.*, 1988).

Besides interplanetary dust collected in the stratosphere and impact residues from surfaces exposed in Earth's orbit, also micrometeorites extracted from Antarctic ice have been investigated by TOF-SIMS (Stephan *et al.*, 1995b). So-called COPS phases, iron oxide rich in carbon, phosphorous, and sulfur (Engrand *et al.*, 1993), were found on the surface and in voids of the micrometeorites. The lateral distribution supported the idea that COPS phases grew on the surface of micrometeorites, possibly by modification of indigenous material, and by incorporation of material during atmospheric passage and Antarctic

residence (Maurette *et al.*, 1994; Kurat *et al.*, 1994; Stephan *et al.*, 1995b; Jessberger *et al.*, 1999).

First attempts to study organic molecules or fullerenes in IDPs using TOF-SIMS have been made in the past (Radicati di Brozolo and Fleming, 1992; Stephan *et al.*, 1996), but no systematic investigation has been performed so far. Here the general contamination problem complicates the analyses. Residual silicone oil as well as carbon-containing embedding materials obstruct a proper examination.

Oxygen isotopic imaging with TOF-SIMS has been performed for four IDPs in order to search for sub-micrometer sized stardust (Messenger, 1999). The comparison with DF-SIMS results of the same particles (Messenger, 1998) showed no significant differences in $^{18}O/^{16}O$ isotopic ratios. Nevertheless, within the large statistical error limits (30–90 per mill in $\delta^{18}O$), the values obtained by TOF-SIMS are also not discernable from solar ratios.

6. Presolar grains

The year 1987 became a major turning point in cosmochemistry through the first discovery and isolation of individual pristine presolar dust grains (for reviews on presolar dust cf. Anders and Zinner, 1993; Ott, 1993; Zinner, 1998). This discovery was the reward for more than 20 years of efforts to locate the carriers of several highly anomalous noble gas components in meteorites (Tang *et al.*, 1988; Tang and Anders, 1988a,b). Major types of presolar dust found so far are diamond (Lewis *et al.*, 1987), silicon carbide (Bernatowicz *et al.*, 1987; Zinner *et al.*, 1987), graphite (Amari *et al.*, 1990), corundum (Huss *et al.*, 1992; Hutcheon *et al.*, 1994; Nittler *et al.*, 1994), and silicon nitride (Nittler *et al.*, 1995). Titanium carbide was found inside graphite and silicon carbide grains (Bernatowicz *et al.*, 1991, 1992). Aluminum within silicon carbide and graphite grains showed a correlation with nitrogen, an indication for the presence of aluminum nitride (Zinner *et al.*, 1991a; Virag *et al.*, 1992; Stephan *et al.*, 1997c).

6.1. Isotope measurements

Conventional DF-SIMS has played the major role in the study of presolar grains, because this technique allows to measure isotopic compositions of individual grains down to ~1 μm in size (Zinner, 1998). These isotopic compositions, often different from mean solar system values by several orders of magnitude, clearly prove the extrasolar origin of these grains. Due to the tremendous magnitude of the anomalies, the required precision for this kind of analysis is rather low.

TOF-SIMS seemed to be a promising technique for the analysis of individual presolar grains. Especially the high lateral resolution together with the simultaneous detection of the entire mass range were expected to allow new insights into the properties of individual presolar grains. Isotopic studies should be possible but were not the major purpose of these investigations.

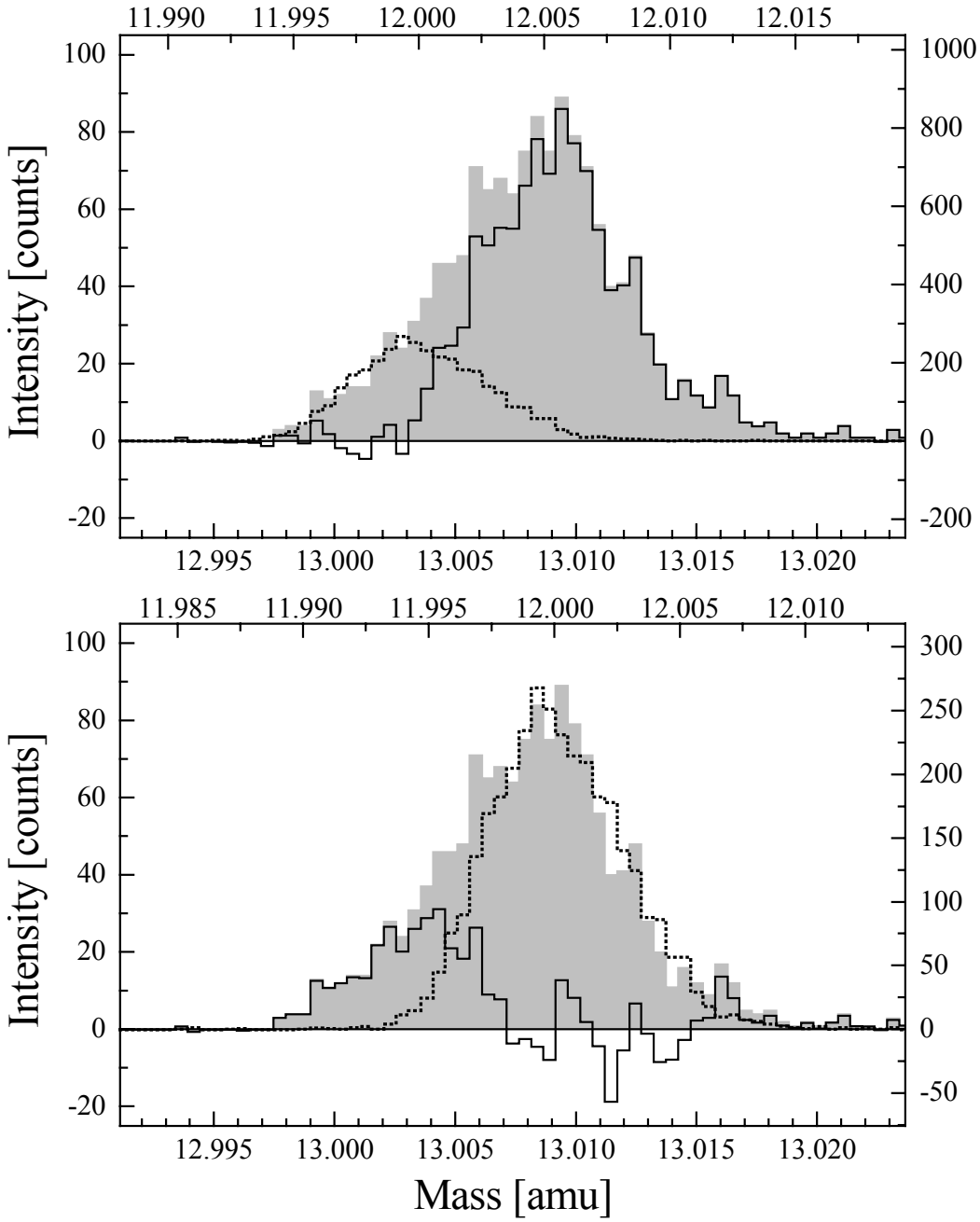

Fig. 34. Negative secondary ion mass spectrum at 13 amu obtained from a presolar SiC grain (KJG2-1412). The mass peaks can be separated in two different ways. In the upper spectrum, the ^{12}C-peak (dotted line, top x- and right y-axes) was used to fit the left edge of the spectrum at 13 amu (shaded area, bottom x- and left y-axes). Here, the scaling factor 9.9±0.9 gives directly the ^{12}C/^{13}C isotopic ratio. The difference between the two spectra (solid line) represents the ^{12}C^{1}H-peak. In the lower spectrum, the ^{12}C-peak was compared with the right edge of the shaded area resulting from the ^{12}C^{1}H-peak. Here the ^{13}C-peak can be retrieved from the difference of both spectra (solid line). In this case, the ^{12}C/^{13}C-ratio becomes 10.9±2.1. Both results agree well within their error limits with the DF-SIMS result, ^{12}C/^{13}C=9.795.

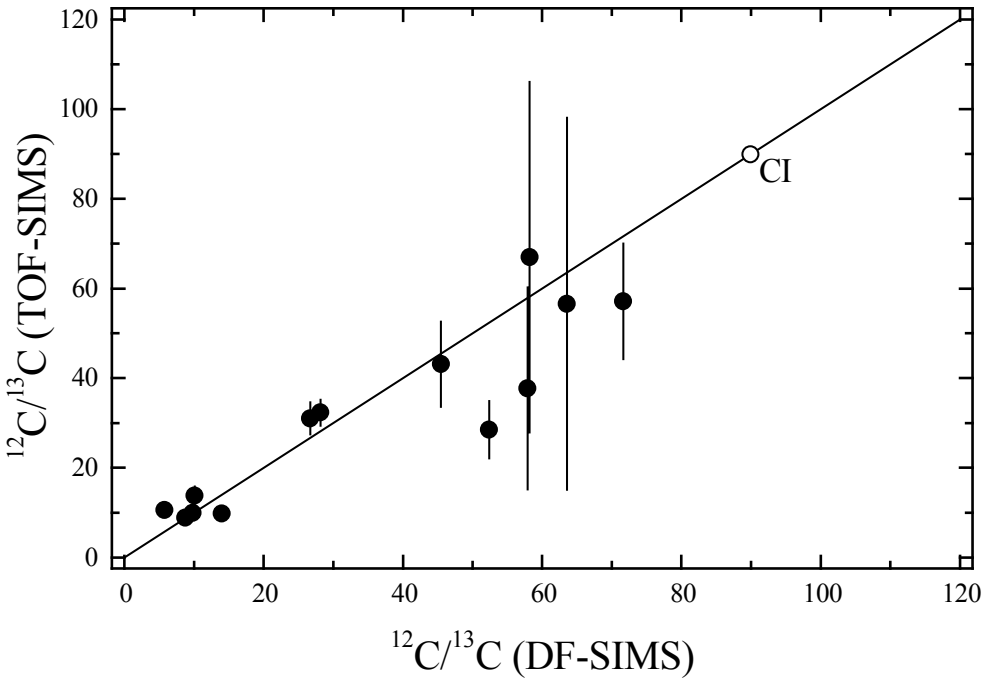

Fig. 35. Comparison between $^{12}C/^{13}C$ isotopic ratios obtained with TOF-SIMS and those from DF-SIMS analyses for 13 different SiC grains from the Murchison KJG fraction (Amari *et al.*, 1994). All analyses were performed on grains with $^{12}C/^{13}C$-ratios below the chondritic (CI) value.

However, in the first TOF-SIMS study of presolar grains (Stephan and Jessberger, 1996; Stephan *et al.*, 1997c) it was tried to reproduce already known carbon isotopic ratios for silicon carbide (SiC) grains from the Murchison meteorite, previously investigated by DF-SIMS (Hoppe *et al.*, 1994). As discussed before, the major problem for carbon isotope analysis at high lateral resolution (necessary for small presolar grains) is the separation of ^{13}C from $^{12}C^{1}H$. Since this is typically not possible satisfactorily with TOF-SIMS, mathematical peak deconvolution techniques have to be applied. In principle, similar to the technique described above (Fig. 23), two peak fitting routines are possible (Fig. 34): The ^{12}C-peak can be used (1) as a prototype for the ^{13}C-peak or (2) to fit the $^{12}C^{1}H$-peak. Although the first approach (Fig. 34 top) seems to be more promising – both carbon isotopes should indeed have the same peak shapes – the second method (Fig. 34 bottom) is often more appropriate. The latter allows using more actual channels of the spectrum for the fitting routine and is therefore less susceptible to statistical variations.

TOF-SIMS allowed a proper analysis of the carbon isotopic ratio for 13 different SiC grains so far (Fig. 35). In most cases, these results agree well with those obtained by DF-

SIMS (Hoppe *et al.*, 1994). Nevertheless, the limited mass resolution only allows the analysis of grains significantly enriched in ^{13}C compared to chondritic isotope ratios. A significant increase in mass resolution is impeded by the required high lateral resolution.

The analysis of nitrogen isotopic ratios was unsatisfactory due to the limitation in mass resolution. Since $^{12}C^{15}N^-$ cannot be resolved from $^{13}C^{14}N^-$, the relatively high statistical error in the ^{13}C analysis prevents an appropriate determination of ^{15}N.

Silicon and magnesium isotopic measurements were recently performed successfully with TOF-SIMS on presolar SiC grains from Murchison and Semarkona meteorites by Fahey and Messenger (1999). The burst mode (see above) was used in the investigation to increase the secondary ion data rates. From ^{26}Mg secondary ion imaging, it was possible to identify several so-called X-grains (Zinner *et al.*, 1991b; Amari *et al.*, 1992; Hoppe *et al.*, 1996) among silicon carbides from Murchison (Fahey and Messenger, 1999).

6.2. Element mapping with TOF-SIMS

However, the imaging capabilities of TOF-SIMS are much more impressive than its abilities in isotope analysis. *Interstellar grains within interstellar grains* (Bernatowicz *et al.*, 1991) have been identified with the TEM as titanium carbide (TiC) grains inside graphite and SiC grains (Bernatowicz *et al.*, 1991, 1992). Although a general correlation of aluminum and nitrogen was found for SiC grains (Zinner *et al.*, 1991a; Virag *et al.*, 1992), no separate Al-bearing phase like aluminum nitride (AlN) has been detected with the TEM (Bernatowicz *et al.*, 1992). Therefore, imaging TOF-SIMS has been used to search for possible subunits within SiC grains (Stephan *et al.*, 1997c).

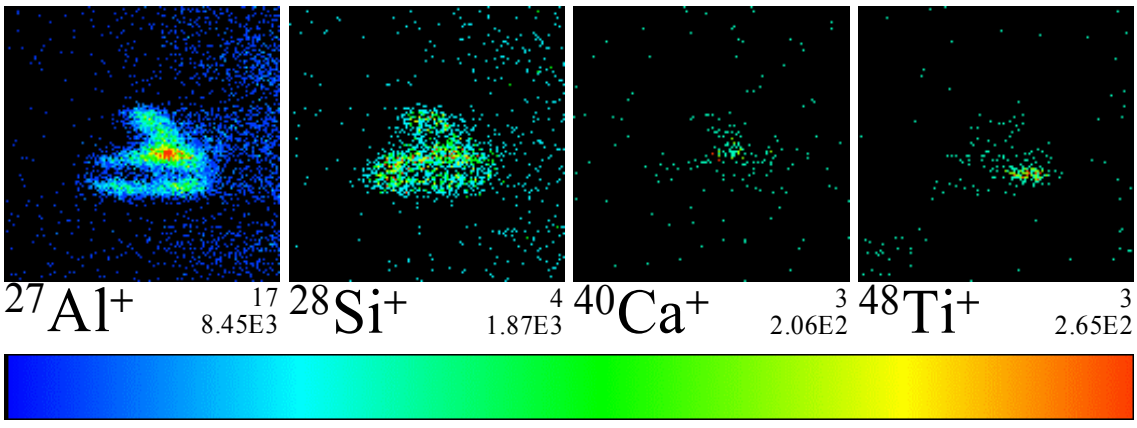

Fig. 36. TOF-SIMS images for SiC grain KJG2-0411 show a rather inhomogeneous distribution for aluminum, calcium, and titanium. Field of view is 12×12 μm^2. The sample was scanned with 128×128 pixels and 800 shots/pixel were applied.

TOF-SIMS studies of presolar SiC grain KJG2-0411 revealed an inhomogeneous distribution for several elements (Stephan *et al.*, 1997c). Secondary ion images of aluminum, silicon, calcium, and titanium are shown in Fig. 36. Silicon is distributed homogeneously, whereas aluminum is enriched in a distinct area, which appeared after sputtering. Consecutive analyses of the grain showed that Al-rich material is concentrated in the center of this presolar grain. A correlation between Al/Si- and CN/Si-ratios (Fig. 37) indicates again the presence of aluminum nitride (Stephan *et al.*, 1997c). Whether AlN is present as distinct phase or in solid solution with the SiC as suggested before (Bernatowicz *et al.*, 1992), cannot be clarified with TOF-SIMS. The increase of the Al/Si-ratio towards the center of the grain might be due to destruction of AlN on or near the surface during chemical processing when the grains were extracted from the meteorite (Stephan *et al.*, 1997c). Although signal intensities are rather low, calcium showed also a correlation with aluminum and nitrogen (Fig. 36). Titanium, on the other hand, is enriched in a different region of the same grain, maybe indicative for the presence of TiC.

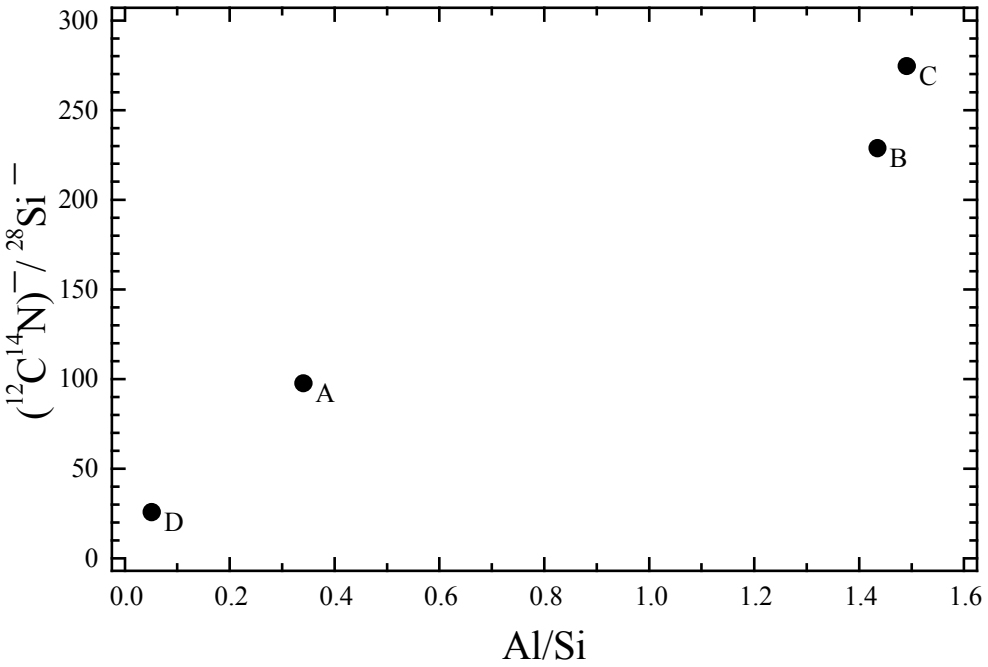

Fig. 37. Al/Si and CN^-/Si^- show a linear correlation, indicating AlN as the dominating aluminum bearing phase in KJG2-0411. Data point (A) corresponds to the Si-rich, Al-poor area in the lower left of the particle in Fig. 36. (B) is the Al-rich area to the right. (C) is the titanium hot spot. (D) comes from an earlier measurement of the entire particle before sputtering.

These analyses clearly demonstrate the potential of TOF-SIMS for the investigation of presolar grains. High lateral resolution in combination with parallel detection of all secondary ion species is ideally suited to localize and identify interesting grains or subgrains, even if the ability to measure isotopes is limited. Although no presolar grain has been found *in situ* with TOF-SIMS so far, this technique should be in principle suited for this kind of search. *In situ* localization would also allow investigating the real link between SiC and AlN, because chemical processing during isolation of the grains may selectively destroy AlN. The major advantage of *in situ* analysis is, however, that information about the petrographic environment of the presolar grains could be obtained. This would help to clarify possible connections of presolar grains with other constituents of the respective meteorites, *e.g.*, CAIs, chondrules, or matrix.

7. TOF-SIMS in space

To apply analytical methods in space, rugged and simplified techniques are required. Limitations mainly arise from size, mass, energy, and data transmission constraints. Compared to other types of mass spectrometers, the time-of-flight principle should be advantageous. Since no magnet or other heavy components are needed, the mass of the instrument can be kept comparatively low. Power consumption can also be low for this kind of mass spectrometer. Time-of-flight mass spectrometers were therefore used and are still used aboard several space probes. Three missions to comet 1p/Halley applied TOF mass spectrometry after impact ionization of dust particles with high relative velocities (Kissel and Krueger, 1987a; Hornung and Kissel, 1994). The PIA (particle impact analyzer) instrument on Giotto and the PUMA (пыле-ударный масс анализатор, *pyle-udarnyi mass analizator*, Russian for *dust impact mass analyzer*) instruments on both Vega missions to comet Halley (Kissel *et al.*, 1986a,b) delivered a wealth of information on the elemental and isotopic composition of Halley's dust (Jessberger *et al.*, 1988, 1989; Jessberger and Kissel, 1991). A modern variant of these instruments, CIDA (cometary and interstellar dust analyzer), was launched in February 1999 aboard the Stardust space vehicle to comet 81p/Wild 2 (Brownlee *et al.*, 1996, 1997).

The first SIMS instrument envisioned for space flight was an astronaut operated DF-SIMS instrument for on-site analysis of the lunar surface in the framework of the Apollo missions (Rüdenauer, 1994), which never flew. The DION system on both Soviet space probes to the Martian satellite Phobos was the "largest" SIMS instrument ever built. Secondary ions sputtered from the surface were to be analyzed in a quadrupole mass spectrometer at a cruising altitude of 50 m above Phobos (Balebanov *et al.*, 1986; Hamelin *et al.*, 1990; Rüdenauer, 1994). A time-of-flight instrument was also on board both Phobos missions, the LIMA-D experiment (Sagdeev *et al.*, 1986; Pellinen *et al.*, 1990). The plan was to use the cruising altitude of 50 m as flight path for ions generated by high-energy laser pulses. Unfortunately, both spacecraft were lost prior to arrival at Phobos.

A new era in TOF-SIMS will hopefully commence in 2011, when the first instrument of this type is planned to reach comet 46p/Wirtanen on ESA's Rosetta spacecraft. After reaching its target, it is planned to collect cometary dust intact at low relative speed. The dust particles then will be analyzed in a TOF-SIMS instrument named CoSIMA (cometary secondary ion mass analyzer) with a specially designed liquid metal primary ion source, operated with indium (Kissel *et al.*, 1988). An earlier version of this instrument (CoMA = cometary matter analyzer) was designed for NASA's cometary rendezvous and asteroid flyby mission (CRAF) that was cancelled in 1992 (Zscheeg *et al.*, 1992; Beck, 1994; Beck and Kissel, 1994). With the CoSIMA instrument, a lateral resolution of 5 µm with 100 ns primary ion pulse width can be obtained. In a second mode, with 3 ns pulse width, 20 µm spatial resolution is possible. The mass resolution, up to $m/\Delta m$=2000, is sufficient for the separation of most hydrocarbon interferences from elemental peaks. The CoSIMA results will certainly not reach the same quality as laboratory TOF-SIMS analyses, but this cannot be expected from an instrument with mass less than 20 kg and primary power between 8.2 and 19.5 W (technical data J. Kissel, pers. comm.). However, it is expected, that profound information on the composition of cometary matter can be obtained with CoSIMA. The experience with TOF-SIMS analysis of extraterrestrial matter, gathered here on Earth and reported in the present study, will definitely help to interpret the results that will be acquired in space. Especially the surface analysis of IDPs has to deal with similar problems as expected for the space experiment, *e.g.*, rough surfaces. Since complex mixtures of organic material and silicates are expected for cometary dust (Kissel and Krueger, 1987b), laboratory TOF-SIMS investigation of organic compounds in analogous material, *e.g.*, chondrites and IDPs is essential (Heiss *et al.*, 1998).

8. Summary

Time-of-flight secondary ion mass spectrometry has been successfully introduced into cosmochemistry during the past decade and has demonstrated its special abilities. Its major advantage results from the simultaneous detection of all secondary ions with one polarity. In combination with high lateral resolution, this technique is therefore especially qualified for the analysis of small samples, becoming more and more important in the investigation of extraterrestrial matter.

Although mass resolution and quantification capabilities are limited in TOF-SIMS compared to conventional ion microprobes, its advantages open a specific field of applications, not or less accessible with DF-SIMS. Consequently, these two SIMS techniques are more complementary than in competition with each other. Parallel detection of all ions expressly does not require a pre-selection of masses to be analyzed. Therefore, TOF-SIMS is predestined to make unexpected discoveries. On the other hand, for a better quantification of these findings, subsequent investigations with other techniques including DF-SIMS are often required.

Further technical developments in TOF-SIMS will help to overcome some of its limitations: A new generation of liquid metal ion guns allows to increase the primary ion current and therefore the secondary ion intensity even at relatively high lateral resolution. Decreasing primary beam sizes below 100 nm will extend the applications to very small entities. Especially laser post-ionization is expected to expand the possibilities of quantification. Nevertheless, even today, TOF-SIMS is a powerful tool for the investigation of natural terrestrial and extraterrestrial samples. Applications near the borderline between life sciences and cosmochemistry, studying the origin of life in our solar system, might be one promising field for TOF-SIMS. First results, although negative for ALH 84001, were encouraging concerning the applicability of this technique.

Particle analysis is already one of the strong points of TOF-SIMS. To obtain a maximum of information on single grains without completely destroying the sample is one of the requirements in this field. Here, a wealth of new discoveries from TOF-SIMS studies can be expected in the future.

9. Acknowledgements

The author is indebted to many people who made this work possible. E. K. Jessberger accompanied me as a superior, colleague, and friend through the ups and downs of 10 years of TOF-SIMS research. I would like to thank him for his tremendous support and encouragement, countless discussions, and that he always was open-minded.

A special thank goes to A. Benninghoven who welcomed me in his working group, where I was able to learn the basics of TOF-SIMS. Without the support by D. Stöffler, especially in the beginning when funding was a major problem, this study would have been impossible. J. Kissel as principal investigator of the CoSIMA experiment on ESA's Rosetta space mission made the laboratory TOF-SIMS instrument available for numerous studies.

Many colleagues and friends supported me throughout the past decade and contributed with their work to this study. I only can name here a few of them. My thank goes to P. Arndt, P. Beck, A. Bischoff, M. Commer, A. Deutsch, A. Greshake, B. Hagenhoff, C. H. Heiss, T. Henkel, U. Jürgens, W. Klöck, F. Kötter, M. Maetz, K. Meyer, H. Rulle, S. Schirmeyer, J. Urbainczyk, L. Weisser, and J. Zehnpfenning. Especially I would like to thank D. Rost who always was a reliable colleague and friend. He contributed during the past five years with a lot of commitment to the success of our TOF-SIMS studies.

Help with numerous minor and major technical and organizational problems was essential for this work. I would like to thank F. Bartschat, R. Budell, M. Flucks, T. Grund, U. Heitmann, G. McCormack, D. Pitzler, R. Thewes, and the members of the technical departments of the Max-Planck-Institut für Kernphysik in Heidelberg and the University of Münster.

I am grateful to S. Amari, P. Hoppe, F. J. Stadermann, and E. K. Zinner for not only providing samples, but also for making their DF-SIMS data available, and for offering insider information on the ion microprobe technique.

I thank K. P. Jochum for providing the glass standards used in this study.

This work was supported by the *Deutsche Forschungsgemeinschaft* through grants Je96/6 and Je96/10. A special grant from the *Ministerium für Schule und Weiterbildung, Wissenschaft und Forschung des Landes Nordrhein-Westfalen* is gratefully acknowledged.

This research has made use of NASA's Astrophysics Data System Abstract Service.

I would like to thank my wife Petra and our son Alexander, who encouraged me in a lot of ways during this work.

10. References

ALLAMANDOLA L. J. (1996) PAHs, they're everywhere! In *The Cosmic Dust Connection* (ed. J. M. Greenberg), pp. 81–102. Kluwer Academic Publishers, Dordrecht.

ALLAMANDOLA L. J., SANDFORD S. A. AND WOPENKA B. (1987) Interstellar polycyclic aromatic hydrocarbons and carbons in interplanetary dust particles and meteorites. *Science* **237,** 56–59.

AMARI S., ANDERS E., VIRAG A. AND ZINNER E. (1990) Interstellar graphite in meteorites. *Nature* **345,** 238–240.

AMARI S., FOOTE J., SIMON C., SWAN P., WALKER R. M., ZINNER E. K., JESSBERGER E. K., LANGE G. AND STADERMANN F. (1991) SIMS chemical analysis of extended impact features from the trailing edge portion of experiment A0187-2. *Proc. First LDEF Post-Retrieval Symposium*, 503–516.

AMARI S., HOPPE P., ZINNER E. AND LEWIS R. S. (1992) Interstellar SiC with unusual isotopic compositions: Grains from a supernova? *Astrophys. J.* **394,** L43–L46.

AMARI S., FOOTE J., SWAN P., WALKER R. M., ZINNER E. K. AND LANGE G. (1993) SIMS chemical analysis of extended impacts on the leading and trailing edges of LDEF experiment A0187-2. *Proc. Second LDEF Post-Retrieval Symposium*, 513–528.

AMARI S., LEWIS R. S. AND ANDERS E. (1994) Interstellar grains in meteorites: I. Isolation of SiC, graphite, and diamond; size distributions of SiC and graphite. *Geochim. Cosmochim. Acta* **58,** 459–470.

ANDERS E. (1989) Pre-biotic organic matter from comets and asteroids. *Nature* **342,** 255–257.

ANDERS E. (1996) Evaluating the evidence for past life on Mars. *Science* **274,** 2119–2121.

ANDERS E. AND GREVESSE N. (1989) Abundances of the elements: Meteoritic and solar. *Geochim. Cosmochim. Acta* **53,** 197–214.

ANDERS E. AND ZINNER E. (1993) Interstellar grains in primitive meteorites: Diamond, silicon carbide, and graphite. *Meteoritics* **28,** 490–514.

ANDERS E., HAYATSU R. AND STUDIER M. H. (1973) Organic compounds in meteorites. *Science* **182,** 781–790.

ARLINGHAUS H. F. AND GUO X. Q. (1998) Depth profiling and imaging with laser postionization SNMS. *Secondary Ion Mass Spectrometry, Proc. SIMS XI* (eds. G. Gillen, R. Lareau, J. Bennett and F. Stevie), pp. 677–680. Wiley, Chichester.

ARLINGHAUS H. F., WHITAKER T. J., JOYNER C. F., KWOKA P., JACOBSON B. AND TOWER J. (1997) Present status of laser postionization analyses. *Secondary Ion Mass Spectrometry, Proc.*

SIMS X (eds. A. Benninghoven, B. Hagenhoff and H. W. Werner), pp. 123–130. Wiley, Chichester.

ARNDT P., BOHSUNG J., MAETZ M. AND JESSBERGER E. K. (1996a) The elemental abundances in interplanetary dust particles. *Meteorit. Planet. Sci.* **31,** 817–833.

ARNDT P., JESSBERGER E. K., WARREN J. AND ZOLENSKY M. (1996b) Bromine contamination of IDPs during collection (abstract). *Meteorit. Planet. Sci.* **31,** A8.

ARNDT P., MAETZ M., REIMOLD D., WALLIANOS A. AND JESSBERGER E. K. (1996c) Mass and multielement analyses of interplanetary dust particles with PIXE and STIM at the Heidelberg proton microprobe (abstract). *Meteorit. Planet. Sci.* **31,** A8–A9.

ARNDT P., JESSBERGER E. K., MAETZ M., REIMOLD D. AND TRAXEL K. (1997) On the accuracy of element concentrations and masses of micron sized samples determined with the Heidelberg proton microprobe. *Nucl. Instr. and Meth. B* **130,** 192–198.

BADA J. L., GLAVIN D. P., MCDONALD G. D. AND BECKER L. (1998) A search for endogenous amino acids in Martian meteorite ALH84001. *Science* **279,** 362–365.

BALEBANOV B. M., BEGHIN C., BELOUSOV K. G., BUJOR M., EVLANOV E. N., HAMELIN M., INAL-IPA A., KHROMOV V. I., KOHNEV V. A., LANGEVIN Y., LESPAGNOL J., MANAGADZE G. G., MARTINSON A. A., MICHAU J. L., MINKALA J. L., PELINEN R., PODKOLZIN S. N., POMATHIOD L., RIEDLER W., SAGDEEV R. Z., SCHWINGENSCHUH K., STELLER M., THOMAS R. AND ZUBKOV B. V. (1986) Presentation of the DION experiment: Preliminary results of SIMS method on mineralogical samples. *Scientific and Methodological Aspects of the PHOBOS Study, Proc. Int. Workshop*, pp. 245–260. Space Research Institute, USSR Academy of Science, Moscow, USSR.

BECK P. (1994) CoMA: A high resolution time of flight secondary ion mass spectrometer for in situ analysis of cometary matter. *Secondary Ion Mass Spectrometry, Proc. SIMS IX* (eds. A. Benninghoven, Y. Nihei, R. Shimizu and H. W. Werner), pp. 923–926. Wiley, Chichester.

BECK P. AND KISSEL J. (1994) CoMA: A cometary matter analyzer for in situ analysis with high mass resolution (abstract). *Lunar Planet. Sci.* **25,** 75–76.

BECKER L., GLAVIN D. P. AND BADA J. L. (1997) Polycyclic aromatic hydrocarbons (PAHs) in Antarctic Martian meteorites, carbonaceous chondrites, and polar ice. *Geochim. Cosmochim. Acta* **61,** 475–481.

BECKER L., POPP B., RUST T. AND BADA J. L. (1999) The origin of organic matter in the Martian meteorite ALH84001. *Earth Planet. Sci. Lett.* **167,** 71–79.

BELL J. F. (1996) Evaluating the evidence for past life on Mars. *Science* **274,** 2121–2122.

BENNINGHOVEN A. (1973) Surface investigation of solids by the statical method of secondary ion mass spectroscopy (SIMS). *Surface Sci.* **35,** 427–457.

BENNINGHOVEN A. (1975) Developments in secondary ion mass spectroscopy and applications to surface studies. *Surface Sci.* **53,** 596–625.

BENNINGHOVEN A. (1985) Static SIMS applications – From silicon single crystal oxidation to DNA sequencing. *J. Vac. Sci. Technol. A* **3,** 451–460.

BENNINGHOVEN A. (1994) Surface analysis by secondary ion mass spectroscopy (SIMS). *Surface Sci.* **299/300,** 246–260.

BERNATOWICZ T., FRAUNDORF G., TANG M., ANDERS E., WOPENKA B., ZINNER E. AND FRAUNDORF P. (1987) Evidence for interstellar SiC in the Murray carbonaceous meteorite. *Nature* **330,** 728–730.

BERNATOWICZ T. J., AMARI S., ZINNER E. K. AND LEWIS R. S. (1991) Interstellar grains within interstellar grains. *Astrophys. J.* **373,** L73–L76.

BERNATOWICZ T. J., AMARI S. AND LEWIS R. S. (1992) TEM studies of a circumstellar rock (abstract). *Lunar Planet. Sci.* **23,** 91–92.

BERNHARD R. P., HÖRZ F., ZOLENSKY M. E., SEE T. H. AND BARRETT R. A. (1993a) Composition and frequency of impact residues detected on LDEF surfaces. *Proc. First European Conference on Space Debris*, 189–194.

BERNHARD R. P., SEE T. H. AND HÖRZ F. (1993b) Projectile compositions and modal frequencies on the "chemistry of micrometeoroids" LDEF experiment. *Proc. Second LDEF Post-Retrieval Symposium*, 551–573.

BERZELIUS J. J. (1834) Ueber Meteorsteine. *Ann. Phys. Chem.* **33,** 113–148.

BISCHOFF A. (1998) Aqueous alteration of carbonaceous chondrites: Evidence for preaccretionary alteration – A review. *Meteorit. Planet. Sci.* **33,** 1113–1122.

BLAISE G. (1994) New description of the charge mechanism of insulators. *Secondary Ion Mass Spectrometry, Proc. SIMS IX* (eds. A. Benninghoven, Y. Nihei, R. Shimizu and H. W. Werner), pp. 45–48. Wiley, Chichester.

BOHSUNG J., JESSBERGER E. K. AND TRAXEL K. (1993) PIXE analyses of interplanetary dust particles using the new Heidelberg proton microprobe (abstract). *Meteoritics* **28,** 326–327.

BOHSUNG J., ARNDT P., JESSBERGER E. K., MAETZ M., TRAXEL K. AND WALLIANOS A. (1995) High resolution PIXE analyses of interplanetary dust particles with the new Heidelberg proton microprobe. *Planet. Space Sci.* **43,** 411–428.

BOTTAZZI P., OTTOLINI L., VANNUCCI R. AND ZANETTI A. (1994) An accurate procedure for the quantification of rare earth elements in silicates. *Secondary Ion Mass Spectrometry, Proc. SIMS IX* (eds. A. Benninghoven, Y. Nihei, R. Shimizu and H. W. Werner), pp. 927–930. Wiley, Chichester.

BRADLEY J. P. (1994a) Nanometer-scale mineralogy and petrography of fine-grained aggregates in anhydrous interplanetary dust particles. *Geochim. Cosmochim. Acta* **58,** 2123–2134.

BRADLEY J. P. (1994b) Chemically anomalous, preaccretionally irradiated grains in interplanetary dust from comets. *Science* **265,** 925–929.

BRADLEY J. AND IRELAND T. (1996) The search for interstellar components in interplanetary dust particles. In *Physics, Chemistry, and Dynamics of Interplanetary Dust, ASP Conf. Series 104* (eds. B. Å. S. Gustafson and M. S. Hanner), pp. 275–282. ASP, San Francisco.

BRADLEY J. P., HARVEY R. P. AND MCSWEEN H. Y., JR. (1996) Magnetite whiskers and platelets in the ALH84001 Martian meteorite: Evidence of vapor phase growth. *Geochim. Cosmochim. Acta* **60,** 5149–5155.

BRADLEY J. P., HARVEY R. P. AND MCSWEEN H. Y., JR. (1997) No 'nanofossils' in martian meteorites. *Science* **390,** 454–456.

BRADLEY J. P., MCSWEEN H. Y., JR. AND HARVEY R. P. (1998) Epitaxial growth of nanophase magnetite in Martian meteorite Allan Hills 84001: Implications for biogenic mineralization. *Meteorit. Planet. Sci.* **33,** 765–773.

BRADLEY J. P., SNOW T. P., BROWNLEE D. E. AND HANNER M. S. (1999a) Mg-rich olivine and pyroxene grains in primitive meteoritic materials: Comparison with crystalline silicate data from ISO. In *Solid Interstellar Matter: The ISO Revolution* (eds. L. d'Hendecourt, C. Joblin and A. Jones), pp. 297–315. Springer-Verlag, Berlin, Heidelberg.

BRADLEY J. P., KELLER L. P., SNOW T. P., HANNER M. S., FLYNN G. J., GEZO J. C., CLEMETT S. J., BROWNLEE D. E. AND BOWEY J. E. (1999b) An infrared spectral match between GEMS and interstellar grains. *Science* **285,** 1716–1718.

BREARLEY A. J. AND JONES R. H. (1998) Chondritic meteorites. In *Planetary Materials* (ed. J. J. Papike), pp. (3)1–(3)398. Reviews in Mineralogy, Mineralogical Society of America, Washington, D. C.

BROWNING L. B. AND KEIL K. (1997) Were CM chondrites aqueously altered in the quiescent interior of their parent body? (abstract). *Lunar Planet. Sci.* **28,** 163–164.

BROWNING L. B., MCSWEEN H. Y., JR. AND ZOLENSKY M. E. (1996) Correlated alteration effects in CM carbonaceous chondrites. *Geochim. Cosmochim. Acta* **60,** 2621–2633.

BROWNLEE D. (1994) The origin and role of dust in the early solar system. In *Analysis of Interplanetary Dust, AIP Conference Proc. 310* (eds. M. E. Zolensky, T. L. Wilson, F. J. M. Rietmeijer and G. J. Flynn), pp. 5–8. AIP, New York.

BROWNLEE D. E. (1996) The elemental composition of interplanetary dust. In *Physics, Chemistry, and Dynamics of Interplanetary Dust, ASP Conf. Series 104* (eds. B. Å. S. Gustafson and M. S. Hanner), pp. 261–273. ASP, San Francisco.

BROWNLEE D. E., TOMANDL D. A. AND OLSZEWSKI E. (1977) Interplanetary dust; A new source of extraterrestrial material for laboratory studies. *Proc. Lunar Sci. Conf.* **8th,** 149–160.

BROWNLEE D. E., BURNETT D., CLARK B., HANNER M. S., HÖRZ F., KISSEL J., NEWBURN R., SANDFORD S., SEKANINA Z., TSOU P. AND ZOLENSKY M. (1996) Stardust: Comet and interstellar dust sample return mission. In *Physics, Chemistry, and Dynamics of Interplanetary Dust, ASP Conf. Series 104* (eds. B. Å. S. Gustafson and M. S. Hanner), pp. 223–226. ASP, San Francisco.

BROWNLEE D. E., TSOU P., BURNETT D., CLARK B., HANNER M. S., HÖRZ F., KISSEL J., MCDONNELL J. A. M., NEWBURN R. L., SANDFORD S., SEKANINA Z., TUZZOLINO A. J. AND ZOLENSKY M. (1997) The Stardust mission: Returning comet samples to Earth (abstract). *Meteorit. Planet. Sci.* **32,** A22.

BUSECK P. R., DEVOUARD B. AND HUA X. (1997) Comparison of the mineralogy of fine-grained rims and adjacent matrix in CM2 chondrites (abstract). *Meteorit. Planet. Sci.* **32,** A24–A25.

CASSINI G. D. (1730) Découverte de la lumière celeste qui paroist dans le zodiaque. *Mem. Acad. Roy. Sci. Paris VIII (1666–1699*), 119–209.

CHAUSSIDON M. AND LIBOUREL G. (1993) Boron partitioning in the upper mantle: An experimental and ion probe study. *Geochim. Cosmochim. Acta* **57,** 5053–5062.

CHAUSSIDON M., ROBERT F., MANGIN D., HANON P. AND ROSE E. (1998) Microscale boron isotope analysis in meteoritic matter. *Secondary Ion Mass Spectrometry, Proc. SIMS XI* (eds. G. Gillen, R. Lareau, J. Bennett and F. Stevie), pp. 43–46. Wiley, Chichester.

CHYBA C. F. AND MCDONALD G. D. (1995) The origin of life in the solar system: Current issues. *Annu. Rev. Earth Planet. Sci.* **23,** 215–249.

CHYBA C. F. AND SAGAN C. (1987) Cometary organics but no evidence for bacteria. *Nature* **329,** 208.

CHYBA C. F., THOMAS P. J., BROOKSHAW L. AND SAGAN C. (1990) Cometary delivery of organic molecules to the early Earth. *Science* **249,** 366–373.

CICERONE R. J. (1981) Halogens in the atmosphere. *Rev. Geophys. Space Phys.* **19,** 123–139.

CLAUS G. AND NAGY B. (1961) A microbiological examination of some carbonaceous chondrites. *Nature* **192,** 594–596.

CLEMETT S. J., MAECHLING C. R., ZARE R. N. AND ALEXANDER C. M. O. (1992) Analysis of polycyclic aromatic hydrocarbons in seventeen ordinary and carbonaceous chondrites (abstract). *Lunar Planet. Sci.* **23,** 233–234.

CLEMETT S. J., MAECHLING C. R., ZARE R. N., SWAN P. D. AND WALKER R. M. (1993) Identification of complex aromatic molecules in individual interplanetary dust particles. *Science* **262,** 721–725.

CLEMETT S. J., MESSENGER S., CHILLIER X. D. F., GAO X., WALKER R. M. AND ZARE R. N. (1996) Indigenous polycyclic aromatic hydrocarbon molecules in circumstellar graphite grains (abstract). *Lunar Planet. Sci.* **27,** 229–230.

CLEMETT S. J., DULAY M. T., GILLETTE J. S., CHILLIER X. D. F., MAHAJAN T. B. AND ZARE R. N. (1998) Evidence for the extraterrestrial origin of polycyclic aromatic hydrocarbons (PAHs) in the Martian meteorite ALH84001. *Faraday Disc. Chem. Soc.* **109,** 417–436.

COMPSTON W., WILLIAMS I. S. AND MEYER C. (1984) U-Pb geochronology of zircons from lunar breccia 73217 using a sensitive high mass-resolution ion microprobe. *Proc. Lunar Planet. Sci. Conf.* **14th,** *J. Geophys. Res.* **89,** B525–B534.

CRONIN J. R., PIZZARELLO S. AND CRUIKSHANK D. P. (1988) Organic matter in carbonaceous chondrites, planetary satellites, asteroids and comets. In *Meteorites and the Early Solar System* (eds. J. F. Kerridge and M. S. Matthews), pp. 819–857. Univ. Arizona Press, Tucson.

CROZAZ G. AND ZINNER E. (1985) Ion probe determinations of the rare earth concentrations of individual meteoritic phosphate grains. *Earth Planet. Sci. Lett.* **73,** 41–52.

DE CHAMBOST E., HILLION F., RASSER B. AND MIGEON H. N. (1992) The CAMECA IMS 1270: A description of the secondary ion optical system. *Secondary Ion Mass Spectrometry, Proc. SIMS VIII* (eds. A. Benninghoven, T. F. Janssen, J. Tümpner and H. W. Werner), pp. 207–210. Wiley, Chichester.

DE CHAMBOST E., SCHUHMACHER M., LÖVESTAM G. AND CLAESSON S. (1997) Achieving high transmission with the Cameca IMS1270. *Secondary Ion Mass Spectrometry, Proc. SIMS X* (eds. A. Benninghoven, B. Hagenhoff and H. W. Werner), pp. 1003–1006. Wiley, Chichester.

DE VRIES M. S., REIHS K., WENDT H. R., GOLDEN W. G., HUNZIKER H. E., FLEMING R., PETERSON E. AND CHANG S. (1993) A search for C_{60} in carbonaceous chondrites. *Geochim. Cosmochim. Acta* **57,** 933–938.

DERMOTT S. F., GROGAN K., GUSTAFSON B. Å. S., JAYARAMAN S., KORTENKAMP S. J. AND XU Y. L. (1996) Sources of interplanetary dust. In *Physics, Chemistry, and Dynamics of Interplanetary Dust, ASP Conf. Series 104* (eds. B. Å. S. Gustafson and M. S. Hanner), pp. 143–153. ASP, San Francisco.

DIDENKO P. I. AND KOVAL V. B. (1994) SIMS measurement of metal isotope-ratios in geological samples. *Secondary Ion Mass Spectrometry, Proc. SIMS IX* (eds. A. Benninghoven, Y. Nihei, R. Shimizu and H. W. Werner), pp. 931–933. Wiley, Chichester.

EILER J. M., VALLEY J. W. AND GRAHAM C. M. (1998) Oxygen and carbon isotope analysis by SIMS: A case study of the Martian meteorite ALH84001. *Secondary Ion Mass Spectrometry, Proc. SIMS XI* (eds. G. Gillen, R. Lareau, J. Bennett and F. Stevie), pp. 47–50. Wiley, Chichester.

ENDRESS M. AND BISCHOFF A. (1996) Carbonates in CI chondrites: Clues to parent body evolution. *Geochim. Cosmochim. Acta* **60,** 489–507.

ENGRAND C., MAURETTE M., KURAT G., BRANDSTÄTTER F. AND PERREAU M. (1993) A new carbon-rich phase ("COPS") in Antarctic micrometeorites (abstract). *Lunar Planet. Sci.* **24,** 441–442.

ESPOSITO F., SPINELLI N., VELOTTA R. AND BERARDI V. (1991) Dead time correction of time distribution measurements. *Rev. Sci. Instrum.* **62,** 2822–2827.

EUGSTER O., ARMSTRONG J. T. AND WASSERBURG G. J. (1985) Identification of isobaric interferences. A computer program for ion microprobe mass spectral data. *Int. J. Mass Spectrom. Ion Process.* **66,** 291–312.

FAHEY A. J. (1998) Measurements of REE abundances in NIST SRM-600 series glasses and direct measurements of REE oxide to REE ion signals. *Secondary Ion Mass Spectrometry, Proc. SIMS XI* (eds. G. Gillen, R. Lareau, J. Bennett and F. Stevie), pp. 789–792. Wiley, Chichester.

FAHEY A. J. AND MESSENGER S. (1999) Isotopic measurements of Murchison and Semarkona residues by TOF-SIMS (abstract). *Lunar Planet. Sci.* **30,** #1101.

FLOSS C. AND JOLLIFF B. (1998) Rare earth element sensitivity factors in calcic plagioclase (anorthite). *Secondary Ion Mass Spectrometry, Proc. SIMS XI* (eds. G. Gillen, R. Lareau, J. Bennett and F. Stevie), pp. 785–788. Wiley, Chichester.

FLYNN G. J. AND SUTTON S. R. (1992) Element abundances in stratospheric cosmic dust: Indications for a new chemical type of chondritic material (abstract). *Lunar Planet. Sci.* **23,** 373–374.

FLYNN G. J., BAJT S., SUTTON S. R., ZOLENSKY M. E., THOMAS K. L. AND KELLER L. P. (1996a) The abundance pattern of elements having low nebular condensation temperatures in interplanetary dust particles: Evidence for a new chemical type of chondritic material. In *Physics, Chemistry, and Dynamics of Interplanetary Dust, ASP Conf. Series 104* (eds. B. Å. S. Gustafson and M. S. Hanner), pp. 291–294. ASP, San Francisco.

FLYNN G. J., BAJT S. AND SUTTON S. R. (1996b) Evidence for weakly bound bromine in large interplanetary dust particles collected from the stratosphere (abstract). *Lunar Planet. Sci.* **27,** 367–368.

FROUDE D. O., IRELAND T. R., KINNY P. D., WILLIAMS I. S., COMPSTON W., WILLIAMS I. R. AND MYERS J. S. (1983) Ion microprobe identification of 4,100–4,200 Myr-old terrestrial zircons. *Nature* **304,** 616–618.

GRESHAKE A., STEPHAN T. AND ROST D. (1998) Symplectic exsolutions in olivine from the Martian meteorite Chassigny: Evidence for slow cooling under highly oxidizing conditions (abstract). *Lunar Planet. Sci.* **29,** #1069.

HAGENHOFF B. (1997) Quantification in molecular SIMS. *Secondary Ion Mass Spectrometry, Proc. SIMS X* (eds. A. Benninghoven, B. Hagenhoff and H. W. Werner), pp. 81–88. Wiley, Chichester.

HAGENHOFF B., VAN LEYEN D., NIEHUIS E. AND BENNINGHOVEN A. (1989) Time-of-flight secondary ion mass spectrometry of insulators with pulsed charge compensation by low-energy electrons. *J. Vac. Sci. Technol. A* **7,** 3056–3064.

HAGENHOFF B., KOCK R., DEIMEL M., BENNINGHOVEN A. AND BAUCH H.-J. (1992) Quantification of molecular SIMS by internal standards. *Secondary Ion Mass Spectrometry, Proc. SIMS VIII* (eds. A. Benninghoven, T. F. Janssen, J. Tümpner and H. W. Werner), pp. 831–834. Wiley, Chichester.

HAHN J. H., ZENOBI R., BADA J. L. AND ZARE R. N. (1988) Application of two-step laser mass spectrometry to cosmogeochemistry: Direct analysis of meteorites. *Science* **239,** 1523–1525.

HAMELIN M., BALEBANOV V. M., BÉGHIN C., EVLANOV E. N., GRARD R., INAL-IPA A., KHROMOV V. N., KOTCHNEV V. A., LANGEVIN Y., LIEDE I., MANAGADZE G. G., MICHAU J. L.,

PELLINEN R., PIIRONEN J., POMATHOID L., RAITALA J., RIEDLER W., ROUX A., SAGDEEV R. Z., SCHWINGENSCHUH K., THOMAS R., TROTIGNON J. G. AND ZUBKOV B. V. (1990) SIMS remote analysis of the Phobos surface: The DION experiment. *Adv. Space Res.* **10,** (3)49–(3)52.

HAYES J. M. (1967) Organic constituents of meteorites – a review. *Geochim. Cosmochim. Acta* **31,** 1395–1440.

HEISS C. H., STEPHAN T., JESSBERGER E. K., WANCZEK K. P. AND KISSEL J. (1998) Analysis of organic cometary compounds with TOF-SIMS (abstract). *1st European Workshop on Secondary Ion Mass Spectrometry*, 32.

HILLION F., DAIGNE B., GIRARD F., SLODZIAN G. AND SCHUHMACHER M. (1994) A new high performance instrument the Cameca "Nanosims 50". *Secondary Ion Mass Spectrometry, Proc. SIMS IX* (eds. A. Benninghoven, Y. Nihei, R. Shimizu and H. W. Werner), pp. 254–257. Wiley, Chichester.

HILLION F., DAIGNE B., GIRARD F. AND SLODZIAN G. (1997) The Cameca "Nanosims 50" experimental results. *Secondary Ion Mass Spectrometry, Proc. SIMS X* (eds. A. Benninghoven, B. Hagenhoff and H. W. Werner), pp. 979–982. Wiley, Chichester.

HOPPE P., AMARI S., ZINNER E., IRELAND T. AND LEWIS R. S. (1994) Carbon, nitrogen, magnesium, silicon, and titanium isotopic compositions of single interstellar silicon carbide grains from the Murchison carbonaceous chondrite. *Astrophys. J.* **430,** 870–890.

HOPPE P., STREBEL R., EBERHARDT P., AMARI S. AND LEWIS R. S. (1996) Type II supernova matter in a silicon carbide grain from the Murchison meteorite. *Science* **272,** 1314–1316.

HORNUNG K. AND KISSEL J. (1994) On shock wave impact ionization of dust particles. *Astron. Astrophys.* **291,** 324–336.

HÖRZ F., SEE T. H., BERNHARD R. P. AND BROWNLEE D. E. (1995) Natural and orbital debris particles on LDEF's trailing and forward-facing surfaces. *Proc. Third LDEF Post-Retrieval Symposium*, 415–430.

HURST G. S., PAYNE M. G., KRAMER S. D. AND YOUNG J. P. (1979) Resonance ionization spectroscopy and one-atom detection. *Rev. Mod. Phys.* **51,** 767–819.

HUSS G. R., HUTCHEON I. D., WASSERBURG G. J. AND STONE J. (1992) Presolar (?) corundum in the Orgueil meteorite (abstract). *Lunar Planet. Sci.* **23,** 563–564.

HUTCHEON I. D., HUSS G. R., FAHEY A. J. AND WASSERBURG G. J. (1994) Extreme ^{26}Mg and ^{17}O enrichments in an Orgueil corundum: Identification of a presolar oxide grain. *Astrophys. J.* **425,** L97–L100.

JESSBERGER E. K. AND KISSEL J. (1991) Chemical properties of cometary dust and a note on carbon isotopes. In *Comets in the Post-Halley Era* (eds. R. L. Newburn, M. Neugebauer and J. Rahe), pp. 1075–1092. Kluwer Academic Publishers, Dordrecht.

JESSBERGER E. K., CHRISTOFORIDIS A. AND KISSEL J. (1988) Aspects of the major element composition of Halley's dust. *Nature* **332,** 691–695.

JESSBERGER E. K., KISSEL J. AND RAHE J. (1989) The composition of comets. In *Origin and Evolution of Planetary and Satellite Atmospheres* (eds. S. K. Atreya, J. B. Pollack and M. S. Matthews), pp. 167–191. Univ. Arizona Press, Tucson.

JESSBERGER E. K., BOHSUNG J., CHAKAVEH S. AND TRAXEL K. (1992) The volatile element enrichment of chondritic interplanetary dust particles. *Earth Planet. Sci. Lett.* **112,** 91–99.

JESSBERGER E. K., STEPHAN T., ROST D., ARNDT P., MAETZ M., STADERMANN F. J., BROWNLEE D. E., BRADLEY J. P. AND KURAT G. (1999) Properties of interplanetary dust: Information from collected samples. In *Interplanetary Dust* (eds. S. F. Dermott, H. Fechtig, E. Grün and B. Å. S. Gustafson), in press. Univ. of Arizona Press, Tucson.

JOCHUM K. P., DINGWELL D. B., HOFMANN A. W., STOLL B., RACZEK I., ROCHOLL A., BECKER S., BESMEHN A., BESSETTE D., DIETZE H.-J., DULSKI P., ERZINGER J., HELLEBRAND E., HOPPE P., HORN I., JANSSENS K., JENNER G., KLEIN M., MCDONOUGH W. M., MAETZ M., NIKOGOSIAN I. K., PICKHARDT C., SEUFERT H. M., SIMAKIN S. G., SOBOLEV A. V., SPETTEL B., STRAUB S., VINCZE L., WALLIANOS A., WECKWERTH G., WOLF D. AND ZIMMER M. (1999) New geological standard reference glasses for in-situ microanalysis. *Geostandards Newsletter*, submitted.

JULL A. J. T., COURTNEY C., JEFFREY D. A. AND BECK J. W. (1998) Isotopic evidence for a terrestrial source of organic compounds found in Martian meteorites Allan Hills 84001 and Elephant Moraine 79001. *Science* **279,** 366–369.

JÜRGENS U. (1993) Oberflächenanlyse von Si-Wafern mit der Flugzeit-SIMS. Dissertation, Westfälische Wilhelms-Universität Münster. 120 pp.

JÜRGENS U., CRAMER H.-G., HELLER T., NIEHUIS E., ZHANG Z. AND BENNINGHOVEN A. (1992) Ultra trace detection of metal contamination on wafer surfaces. *Secondary Ion Mass Spectrometry, Proc. SIMS VIII* (eds. A. Benninghoven, T. F. Janssen, J. Tümpner and H. W. Werner), 277–280. Wiley, Chichester.

KAMPWERTH G., TERHORST M., HELLER T., NIEHUIS E. AND BENNINGHOVEN A. (1990) TOF-SNMS by nonresonant laser-postionization. *Secondary Ion Mass Spectrometry, Proc. SIMS VII* (eds. A. Benninghoven, C. A. Evans, Jr., K. D. McKeegan, H. A. Storms and H. W. Werner), pp. 203–206. Wiley, Chichester.

KISSEL J. AND KRUEGER F. R. (1987a) Ion formation by impact of fast dust particles and comparison with related techniques. *Appl. Phys. A* **42,** 69–85.

KISSEL J. AND KRUEGER F. R. (1987b) The organic component in dust from comet Halley as measured by the PUMA mass spectrometer on board Vega 1. *Nature* **326,** 755–760.

KISSEL J., BROWNLEE D. E., BÜCHLER K., CLARK B. C., FECHTIG H., GRÜN E., HORNUNG K., IGENBERGS E. B., JESSBERGER E. K., KRUEGER F. R., KUCZERA H., MCDONNELL J. A. M., MORFILL G. M., RAHE J., SCHWEHM G. H., SEKANINA Z., UTTERBACK N. G., VÖLK H. J. AND ZOOK H. A. (1986a) Composition of comet Halley dust particles from Giotto observations. *Nature* **321,** 336–337.

KISSEL J., SAGDEEV R. Z., BERTAUX J. L., ANGAROV V. N., AUDOUZE J., BLAMONT J. E., BÜCHLER K., EVLANOV E. N., FECHTIG H., FOMENKOVA M. N., VON HOERNER H., INOGAMOV N. A., KHROMOV V. N., KNABE W., KRUEGER F. R., LANGEVIN Y., LEONAS V. B., LAVASSEUR-REGOURD A. C., MANAGADZE G. G., PODKOLZIN S. N., SHAPIRO V. D., TABALDYEV S. R. AND ZUBKOV B. V. (1986b) Composition of comet Halley dust particles from Vega observations. *Nature* **321,** 280–282.

KISSEL J., ZSCHEEG H. AND RÜDENAUER F. G. (1988) Pulsed operation of a liquid metal ion source. *Appl. Phys. A* **47,** 167–169.

KLACKA J. (1994) Dust particle in the solar gravitational and electromagnetic fields. *Earth, Moon, and Planets* **64,** 55–58.

KOVALENKO L. J., PHILIPPOZ J.-M., BUCENELL J. R., ZENOBI R. AND ZARE R. N. (1991) Organic chemical analysis on a microscopic scale using two-step laser desorption/laser ionization mass spectrometry. *Space Sci. Rev.* **56,** 191–195.

KOVALENKO L. J., MAECHLING C. R., CLEMETT S. J., PHILIPPOZ J.-M., ZARE R. N. AND ALEXANDER C. M. O. (1992) Microscopic organic analysis using two-step laser mass spectrometry: Application to meteoritic acid residues. *Anal. Chem.* **64,** 682–690.

KÖTTER F. AND BENNINGHOVEN A. (1997) Time-of-flight mass spectrometry of sputtered neutrals after electron beam postionization. *Secondary Ion Mass Spectrometry, Proc. SIMS X* (eds. A. Benninghoven, B. Hagenhoff and H. W. Werner), pp. 1011–1014. Wiley, Chichester.

KURAT G., KOEBERL C., PRESPER T., BRANDSTÄTTER F. AND MAURETTE M. (1994) Petrology and geochemistry of Antarctic micrometeorites. *Geochim. Cosmochim. Acta* **58,** 3879–3904.

KVENVOLDEN K., LAWLESS J., PERING K., PETERSON E., FLORES J., PONNAMPERUMA C., KAPLAN I. R. AND MOORE C. (1970) Evidence for extraterrestrial amino-acids and hydrocarbons in the Murchison meteorite. *Nature* **228,** 923–926.

LAFLAMME R. E. AND HITES R. A. (1978) The global distribution of polycyclic aromatic hydrocarbons in recent sediments. *Geochim. Cosmochim. Acta* **42,** 289–303.

LANGE G., EIGNER S., IGENBERGS E., JESSBERGER E. K., KUCZERA H., MAAS D., SUTTON S., WEISHAUPT U. AND ZINNER E. (1986) Ion microprobe sensitivities and their application to multielement analysis of LDEF impact residues (abstract). *Lunar Planet. Sci.* **17,** 456–457.

LESHIN L. A., MCKEEGAN K. D., CARPENTER P. K. AND HARVEY R. P. (1998) Oxygen isotopic constraints on the genesis of carbonates from Martian meteorite ALH84001. *Geochim. Cosmochim. Acta* **62,** 3–13.

LEWIS R. S., TANG M., WACKER J. F., ANDERS E. AND STEEL E. (1987) Interstellar diamonds in meteorites. *Nature* **326,** 160–162.

MA Z., THOMPSON R. N., LYKKE K. R., PELLIN M. J. AND DAVIS A. M. (1995) New instrument for microbeam analysis incorporating submicron imaging and resonance ionization mass spectrometry. *Rev. Sci. Instrum.* **66,** 3168–3176.

MACPHERSON G. J. AND DAVIS A. M. (1994) Refractory inclusions in the prototypical CM chondrite, Mighei. *Geochim. Cosmochim. Acta* **58,** 5599–5625.

MACPHERSON G. J., WARK D. A. AND ARMSTRONG J. T. (1988) Primitive material surviving in chondrites: Refractory inclusions. In *Meteorites and the Early Solar System* (eds. J. F. Kerridge and M. S. Matthews), pp. 746–807. Univ. Arizona Press, Tucson.

MAETZ M., ARNDT P., BOHSUNG J., JESSBERGER E. K. AND TRAXEL K. (1994) Comprehensive analysis of six IDPs with the Heidelberg proton microprobe (abstract). *Meteoritics* **29,** 494–495.

MAETZ M., ARNDT P., GRESHAKE A., JESSBERGER E. K., KLÖCK W. AND TRAXEL K. (1996) Structural and chemical modifications of microsamples induced during PIXE analysis. *Nucl. Instr. and Meth. B* **109/110,** 192–196.

MAMYRIN B. A., KRATAEV V. I., SHMIKK D. V. AND ZAGULIN V. A. (1973) The mass-reflectron, a new nonmagnetic time-of-flight mass spectrometer with high resolution. *Sov. Phys. JETP* **37,** 45–48.

MAURETTE M., IMMEL G., HAMMER C., HARVEY R., KURAT G. AND TAYLOR S. (1994) Collection and curation of IDPs from the Greenland and Antarctic ice sheets. In *Analysis of Interplanetary Dust, AIP Conference Proc. 310* (eds. M. E. Zolensky, T. L. Wilson, F. J. M. Rietmeijer and G. J. Flynn), pp. 277–289. AIP, New York.

MCKAY D. S., GIBSON E. K., JR., THOMAS-KEPRTA K. L., VALI H., ROMANEK C. S., CLEMETT S. J., CHILLIER X. D. F., MAECHLING C. R. AND ZARE R. N. (1996) Search for past life on Mars: Possible relic biogenic activity in Martian meteorite ALH84001. *Science* **273,** 491–504.

MCKEEGAN K. D., WALKER R. M. AND ZINNER E. (1985) Ion microprobe isotopic measurements of individual interplanetary dust particles. *Geochim. Cosmochim. Acta* **49,** 1971–1987.

MCKEEGAN K. D., LESHIN L. A., RUSSEL S. S. AND MACPHERSON G. J. (1998) Oxygen isotopic abundances in calcium-aluminum-rich inclusions from ordinary chondrites: Implications for nebular heterogeneity. *Science* **280,** 414–418.

MENEGUZZI M., AUDOUZE J. AND REEVES H. (1971) The production of the elements Li, Be, B by galactic cosmic rays in space and its relation with stellar observations. *Astron. Astrophys.* **15,** 337–359.

MESSENGER S. (1998) Oxygen isotopic imaging of interplanetary dust (abstract). *Meteorit. Planet. Sci.* **33,** A106–A107.

MESSENGER S. (1999) Oxygen isotopic imaging of interplanetary dust by TOF-SIMS (abstract). *Lunar Planet. Sci.* **30,** #1600.

MESSENGER S., AMARI S., GAO X., WALKER R. M., CLEMETT S. J., CHILLIER X. D. F., ZARE R. N. AND LEWIS R. S. (1998) Indigenous polycyclic aromatic hydrocarbons in circumstellar graphite grains from primitive meteorites. *Astrophys. J.* **502,** 284–295.

METZLER K., BISCHOFF A. AND STÖFFLER D. (1992) Accretionary dust mantles in CM chondrites: Evidence for solar nebular processes. *Geochim. Cosmochim. Acta* **56,** 2873–2897.

MEYER C., JR. (1979) Trace element analysis of silicates by ion microprobe. *Secondary Ion Mass Spectrometry, Proc. SIMS II* (eds. A. Benninghoven, C. A. Evans, Jr., R. A. Powell, R. Shimizu and H. A. Storms), pp. 67–69. Springer, New York.

MITTLEFEHLDT D. W. (1994) ALH84001, a cumulate orthopyroxenite member of the martian meteorite clan. *Meteoritics* **29,** 214–221.

MITTLEFEHLDT D. W., MCCOY T. J., GOODRICH C. A. AND KRACHER A. (1998) Non-chondritic meteorites from asteroidal bodies. In *Planetary Materials* (ed. J. J. Papike), pp. (4)1–(4)195. Reviews in Mineralogy, Mineralogical Society of America, Washington, D. C.

MOREELS G., CLAIREMIDI J., HERMINE P., BRECHIGNAC P. AND ROUSSELOT P. (1994) Detection of a polycyclic aromatic molecule in comet P/Halley. *Astron. Astrophys.* **282,** 643–656.

NICOLUSSI G. K., PELLIN M. J., LYKKE K. R., TREVOR J. L., MENCER D. E. AND DAVIS A. M. (1996) Surface analysis by SNMS: Femtosecond laser postionization of sputtered and laser desorbed atoms. *Surf. Interface Anal.* **24,** 363–370.

NICOLUSSI G. K., DAVIS A. M., PELLIN M. J., LEWIS R. S., CLAYTON R. N. AND AMARI S. (1997a) The isotopic composition of molybdenum in single presolar silicon carbide grains (abstract). *Lunar Planet. Sci.* **28,** 1021–1022.

NICOLUSSI G. K., DAVIS A. M., PELLIN M. J., LEWIS R. S., CLAYTON R. N. AND AMARI S. (1997b) S-process zirconium in individual presolar silicon carbide grains (abstract). *Lunar Planet. Sci.* **28,** 1023–1024.

NICOLUSSI G. K., PELLIN M. J., LEWIS R. S., DAVIS A. M., AMARI S. AND CLAYTON R. N. (1998a) Molybdenum isotopic composition of individual presolar silicon carbide grains from the Murchison meteorite. *Geochim. Cosmochim. Acta* **62,** 1093–1104.

NICOLUSSI G. K., PELLIN M. J., DAVIS A. M., LEWIS R. S. AND CLAYTON R. N. (1998b) Zr and Mo isotopes in single presolar graphite grains: A record of stellar nucleosynthesis (abstract). *Lunar Planet. Sci.* **29,** #1415.

NIEHUIS E. (1990) Exact mass determination using TOF-SIMS. *Secondary Ion Mass Spectrometry, Proc. SIMS VII* (eds. A. Benninghoven, C. A. Evans, Jr., K. D. McKeegan, H. A. Storms and H. W. Werner), pp. 299–304. Wiley, Chichester.

NIEHUIS E. (1994) Surface analysis by nonresonant multiphoton ionization of sputtered neutrals. *Secondary Ion Mass Spectrometry, Proc. SIMS IX* (eds. A. Benninghoven, Y. Nihei, R. Shimizu and H. W. Werner), pp. 429–433. Wiley, Chichester.

NIEHUIS E. (1997) Microanalysis with gallium liquid metal ion guns. *Secondary Ion Mass Spectrometry, Proc. SIMS X* (eds. A. Benninghoven, B. Hagenhoff and H. W. Werner), pp. 47–54. Wiley, Chichester.

NIEHUIS E., HELLER T., FELD H. AND BENNINGHOVEN A. (1987) Design and performance of a reflectron based time-of-flight secondary ion mass spectrometer with electrodynamic primary ion mass separation. *J. Vac. Sci. Technol. A* **5,** 1243–1246.

NITTLER L. R., ALEXANDER C. M. O., GAO X., WALKER R. M. AND ZINNER E. K. (1994) Interstellar oxide grains from the Tieschitz meteorite. *Nature* **370,** 443–446.

NITTLER L. R., HOPPE P., ALEXANDER C. M. O., AMARI S., EBERHARDT P., GAO X., LEWIS R. S., STREBEL R., WALKER R. M. AND ZINNER E. (1995) Silicon nitride from supernovae. *Astrophys. J.* **453,** L25–L28.

OECHSNER H. (1994) Secondary neutral microprobes. *Secondary Ion Mass Spectrometry, Proc. SIMS IX* (eds. A. Benninghoven, Y. Nihei, R. Shimizu and H. W. Werner), pp. 316–322. Wiley, Chichester.

OLIVE K. A. AND SCHRAMM D. N. (1992) Astrophysical ^{7}Li as a product of Big Bang nucleosynthesis and galactic cosmic-ray spallation. *Nature* **360,** 439–442.

ORÓ J., GIBERT J., LICHTENSTEIN H., WIRKSTROM S. AND FLORY D. A. (1971) Amino-acids, aliphatic and aromatic hydrocarbons in the Murchison meteorite. *Nature* **230,** 105–106.

OTT U. (1993) Interstellar grains in meteorites. *Nature* **364,** 25–33.

PELLIN M. J., YOUNG C. E., CALWAY W. F., BURNETT J. W., JØRGENSEN B., SCHWEITZER E. L. AND GRUEN D. M. (1987) Sensitive, low damage surface analysis using resonance ionization of sputtered atoms. *Nucl. Instr. and Meth. B* **18,** 446–451.

PELLINEN R., PIIRONEN J., SILÉN J., SAGDEEV R. Z., MANAGADZE G. G., SHUTYAEV I., TIMOFEEV P., BONDARENKO A. AND TER-MIKAELIYAN V. (1990) Laser-ionization studies with the technical models of the LIMA-D/PHOBOS experiment. *Adv. Space Res.* **10,** (3)57–(3)61.

PERING K. L. AND PONNAMPERUMA C. (1971) Aromatic hydrocarbons in the Murchison meteorite. *Science* **173,** 237–239.

RADICATI DI BROZOLO F., HARRIS D. W., CHAKEL J. A., FLEMING R. H. AND BUNCH T. E. (1991) Imaging analysis of LDEF craters (abstract). *Meteoritics* **26,** 387.

RADICATI DI BROZOLO F. AND FLEMING R. H. (1992) Mass spectrometric observation of organic species in a single IDP thin section (abstract). *Lunar Planet. Sci.* **23,** 1123–1124.

REEVES H., AUDOUZE J., FOWLER W. A. AND SCHRAMM D. N. (1973) On the origin of light elements. *Astrophys. J.* **179,** 909–930.

RIETMEIJER F. J. M. (1993) The bromine content of micrometeorites: Arguments for stratospheric contamination. *J. Geophys. Res.* **98,** E7409–E7414.

RIETMEIJER F. J. M. (1998) Interplanetary dust particles. In *Planetary Materials* (ed. J. J. Papike), pp. (2)1–(2)95. Reviews in Mineralogy, Mineralogical Society of America, Washington, D. C.

ROBERTSON H. P. (1937) Dynamical effects of radiation in the solar system. *Mon. Not. Roy. Astron. Soc.* **97,** 423–438.

ROST D., STEPHAN T. AND JESSBERGER E. K. (1996) Surface analysis of stratospheric dust particles with TOF-SIMS: New results (abstract). *Meteorit. Planet. Sci.* **31,** A118–A119.

ROST D., STEPHAN T. AND JESSBERGER E. K. (1998a) Imaging of small particles with TOF-SIMS (abstract). *1st European Workshop on Secondary Ion Mass Spectrometry*, 31.

ROST D., STEPHAN T., JESSBERGER E. K., NAKAMURA K. AND KLÖCK W. (1998b) New TOF-SIMS analyses of sections from stratospheric dust particles (abstract). *Lunar Planet. Sci.* **29,** #1637.

ROST D., STEPHAN T. AND JESSBERGER E. K. (1999a) Surface analysis of stratospheric dust particles. *Meteorit. Planet. Sci.* **34,** 637–646.

ROST D., STEPHAN T., WIES C. AND JESSBERGER E. K. (1999b) Analysis of sections and surfaces of interplanetary dust particles (abstract). *Meteorit. Planet. Sci.* **34,** A99.

RÜDENAUER F. G. (1994) SIMS in space. *Secondary Ion Mass Spectrometry, Proc. SIMS IX* (eds. A. Benninghoven, Y. Nihei, R. Shimizu and H. W. Werner), pp. 901–905. Wiley, Chichester.

SAGDEEV R. Z., PROKHOROV A. M., MANAGADZE G. G., KISSEL J., PELLINEN R., BALEBANOV V. M., TABALDYEV S. R., SHUTYAEV I. YU., BONDARENKO A. L., TIMOFEEV P. P., TER-MIKAELYAN V. M., TERENT'EV V. I., NATENZON M. JA., VON HOERNER H., RIEDLER B., BERG R., ZLATEV S., KYNCHEV A., BELYAKOV P., SIMEONOV L., SILEN J., PHIRONEN J., LEHTO A., SALMU CH., PELTONEN P., DUL'NEV G. N., PASHENIN P. P., MALYUTIN A. A., IL'ICHEV N. N., ARUMOV G. P. AND PERSHIN S. M. (1986) LIMA-D experiment: Methodology laboratory tests. *Scientific and Methodological Aspects of the PHOBOS Study, Proc. Int. Workshop*, pp. 220–230. Space Research Institute, USSR Academy of Science, Moscow, USSR.

SCHIFF L. I. (1936) Statistical analysis of counter data. *Phys. Rev.* **50,** 88–96.

SCHIRMEYER S., BISCHOFF A., STEPHAN T. AND JESSBERGER E. K. (1996a) Lithium-bearing phases in Ca,Al-rich inclusions from CM-chondrites: Indication of nebular alteration processes (abstract). *Lunar Planet. Sci.* **27,** 1141–1142.

SCHIRMEYER S., BISCHOFF A., STEPHAN T. AND JESSBERGER E. K. (1996b) Lithium distribution within the carbonaceous chondrites Lancé (CO3) and Allende (CV3): Preliminary results (abstract). *Meteorit. Planet. Sci.* **31,** A123–A124.

SCHIRMEYER S., HOPPE P., STEPHAN T., BISCHOFF A. AND JESSBERGER E. K. (1997) A lithium-bearing Ca,Al-rich inclusion from the CM-chondrite Cold Bokkeveld studied by TOF-SIMS and conventional SIMS (abstract). *Lunar Planet. Sci.* **28,** 1253–1254.

SCHNIEDERS A. (1999) Quantitative surface analysis by laser postionization of sputtered neutrals. Dissertation, Westfälische Wilhelms-Universität Münster. 141 pp.

SCHNIEDERS A., MÖLLERS R., TERHORST M., CRAMER H.-G. AND NIEHUIS E. (1996) Quantification of metal trace contaminants on Si wafer surfaces by laser SNMS and TOF-SIMS using sputter deposited submonolayer standards. *J. Vac. Sci. Technol. B* **14,** 2712–2724.

SCHNIEDERS A., KOLLMER F. AND BENNINGHOVEN A. (1998) Fundamental investigations with imaging laser-SNMS. *Secondary Ion Mass Spectrometry, Proc. SIMS XI* (eds. G. Gillen, R. Lareau, J. Bennett and F. Stevie), pp. 661–664. Wiley, Chichester.

SCHRAMM L. S., BROWNLEE D. E. AND WHEELOCK M. M. (1989) Major elemental composition of stratospheric micrometeorites. *Meteoritics* **24,** 99–112.

SCHUELER B. W. (1992) Microscope imaging by time-of-flight secondary ion mass spectrometry. *Microsc. Microanal. Microstruct.* **3,** 119–139.

SCHUELER B. W., SANDER P. AND REED D. A. (1990) A time-of-flight secondary ion microscope. *Vacuum* **41,** 1661–1664.

SCHUHMACHER M., DE CHAMBOST E., MCKEEGAN K. D., HARRISON T. M. AND MIGEON H. N. (1994) In situ U/Pb dating of zircon with the CAMECA ims 1270. *Secondary Ion Mass Spectrometry, Proc. SIMS IX* (eds. A. Benninghoven, Y. Nihei, R. Shimizu and H. W. Werner), pp. 919–922. Wiley, Chichester.

SCHWIETERS J., CRAMER H.-G., HELLER T., JÜRGENS U., NIEHUIS E., ZEHNPFENNING J. AND BENNINGHOVEN A. (1991) High mass resolution surface imaging with a time-of-flight secondary ion mass spectroscopy scanning microprobe. *J. Vac. Sci. Technol. A* **9,** 2864–2871.

SCHWIETERS J., CRAMER H.-G., JÜRGENS U., NIEHUIS E., RULLE H., HELLER T., ZEHNPFENNING J. AND BENNINGHOVEN A. (1992) TOF-SIMS scanning microprobe for high mass resolution surface imaging. *Secondary Ion Mass Spectrometry, Proc. SIMS VIII* (eds. A. Benninghoven, T. F. Janssen, J. Tümpner and H. W. Werner), pp. 497–500. Wiley, Chichester.

SCOTT E. R. D. (1999) Origin of carbonate-magnetite-sulfide assemblages in Martian meteorite ALH84001. *J. Geophys. Res.* **104,** E3803–E3813.

SCOTT E. R. D., KROT A. N. AND YAMAGUCHI A. (1998) Carbonates in fractures of Martian meteorite Allan Hills 84001: Petrologic evidence for impact origin. *Meteorit. Planet. Sci.* **33,** 709–719.

SIGMUND P. (1969) Theory of sputtering. I. Sputtering yield of amorphous and polycrystalline targets. *Phys. Rev.* **184,** 383–416.

SLODZIAN G., LORIN J. C. AND HAVETTE A. (1980) Isotopic effect on the ionization probabilities in secondary ion emission. *J. Physique Lett.* **41,** L555–L558.

SLODZIAN G., CHAINTREAU M., DENNEBOUY R. AND RASSER B. (1998) Isotope ratio measurements over micro-areas. The challenge of high precision repeatability. *Secondary Ion Mass Spectrometry, Proc. SIMS XI* (eds. G. Gillen, R. Lareau, J. Bennett and F. Stevie), pp. 29–34. Wiley, Chichester.

STADERMANN F. J., WALKER R. M. AND ZINNER E. (1999a) Sub-micron isotopic measurements with the CAMECA NanoSIMS (abstract). *Lunar Planet. Sci.* **30,** #1407.

STADERMANN F. J., WALKER R. M. AND ZINNER E. (1999b) NanoSIMS: The next generation ion probe for the microanalysis of extraterrestrial material (abstract). *Meteorit. Planet. Sci.* **34,** A111–A112.

STEIGMAN G. AND WALKER T. P. (1992) Production of Li, Be, and B in the early galaxy. *Astrophys. J.* **385,** L13–L16.

STEPHAN T. (1992) Statistical analysis of single-ion-counting data and isotopic measurements with TOF-SIMS. *Secondary Ion Mass Spectrometry, Proc. SIMS VIII* (eds. A. Benninghoven, T. F. Janssen, J. Tümpner and H. W. Werner), pp. 115–118. Wiley, Chichester.

STEPHAN T. AND JESSBERGER E. K. (1996) TOF-SIMS analysis of interstellar SiC grains (abstract). *Lunar Planet. Sci.* **27,** 1267–1268.

STEPHAN T., BISCHOFF A., CRAMER H.-G. AND ZEHNPFENNING J. (1991) TOF-SIMS, applications in meteorite research, first results (abstract). *Meteoritics* **26,** 397.

STEPHAN T., KLÖCK W., JESSBERGER E. K. AND ZEHNPFENNING J. (1992a) Analysis of stratospheric interplanetary dust particles with TOF-SIMS, SEM, and TEM (abstract). *Meteoritics* **27,** 292.

STEPHAN T., STADERMANN F., CRAMER H.-G. AND ZEHNPFENNING J. (1992b) TOF-SIMS analysis of LDEF impact residues (abstract). *Lunar Planet. Sci.* **23,** 1357–1358.

STEPHAN T., KLÖCK W., JESSBERGER E. K., RULLE H. AND ZEHNPFENNING J. (1993a) Multielement analysis of interplanetary dust particles using TOF-SIMS (abstract). *Lunar Planet. Sci.* **24,** 1349–1350.

STEPHAN T., KLÖCK W., JESSBERGER E. K., THOMAS K. L., KELLER L. P. AND BEHLA F. (1993b) Multielement analysis of carbon-rich interplanetary dust particles with TOF-SIMS (abstract). *Meteoritics* **28,** 443–444.

STEPHAN T., ZEHNPFENNING J. AND BENNINGHOVEN A. (1994a) Correction of dead time effects in time-of-flight mass spectrometry. *J. Vac. Sci. Technol. A* **12,** 405–410.

STEPHAN T., JESSBERGER E. K., KLÖCK W., RULLE H. AND ZEHNPFENNING J. (1994b) TOF-SIMS analysis of interplanetary dust. *Earth Planet. Sci. Lett.* **128,** 453–467.

STEPHAN T., JESSBERGER E. K., RULLE H., THOMAS K. L. AND KLÖCK W. (1994c) New TOF-SIMS results on hydrated interplanetary dust particles (abstract). *Lunar Planet. Sci.* **25,** 1341–1342.

STEPHAN T., THOMAS K. L. AND WARREN J. L. (1994d) Comprehensive consortium study of stratospheric particles from one collector (abstract). *Meteoritics* **29,** 536–537.

STEPHAN T., ROST D. AND JESSBERGER E. K. (1995a) Surface analysis of stratospheric particles with TOF-SIMS – bromine enrichments due to contamination (abstract). *Meteoritics* **30,** 583.

STEPHAN T., ARNDT P., JESSBERGER E. K., MAETZ M., REIMOLD D. AND WALTER J. (1995b) Multielement analysis of Antarctic micrometeorites using SEM, EDXA, EMPA, TOF-SIMS, and PIXE (abstract). *Lunar Planet. Sci.* **26,** 1353–1354.

STEPHAN T., JESSBERGER E. K., KELLER L. P., FLYNN G. J., BAJT S. AND CHAPMAN H. N. (1996) Fullerenes in interplanetary dust? (abstract). *Meteorit. Planet. Sci.* **31,** A134.

STEPHAN T., ROST D., JESSBERGER E. K. AND KLÖCK W. (1997a) Time-of-flight secondary ion mass spectrometry (TOF-SIMS) analysis of the Orgueil CI meteorite at high lateral resolution (abstract). *Meteorit. Planet. Sci.* **32,** A124–A125.

STEPHAN T., ROST D. AND JESSBERGER E. K. (1997b) Volatile-element enrichments in interplanetary dust due to nebular processes? In *Workshop on Parent-Body and Nebular Modification of Chondritic Materials* (eds. M. E. Zolensky, A. N. Krot and E. R. D. Scott), pp. 59–60. LPI Tech. Rpt. 97–02, Part 1, Lunar and Planetary Institute, Houston.

STEPHAN T., ROST D., JESSBERGER E. K., BUDELL R., GRESHAKE A., ZINNER E. K., AMARI S., HOPPE P. AND LEWIS R. S. (1997c) TOF-SIMS analysis of SiC grains with high lateral resolution (abstract). *Lunar Planet. Sci.* **28,** 1371–1372.

STEPHAN T., ROST D., JESSBERGER E. K. AND GRESHAKE A. (1998a) Polycyclic aromatic hydrocarbons in ALH84001 analyzed with time-of-flight secondary ion mass spectrometry (abstract). *Lunar Planet. Sci.* **29,** #1263.

STEPHAN T., ROST D., JESSBERGER E. K. AND GRESHAKE A. (1998b) Polycyclic aromatic hydrocarbons are everywhere in Allan Hills 84001 (abstract). *Meteorit. Planet. Sci.* **33,** A149–A150.

STEPHAN T., ROST D., HEISS C. H., JESSBERGER E. K. AND GRESHAKE A. (1998c) The lateral distribution of polycyclic aromatic hydrocarbons in Allan Hills 84001 – implications for their origin. In *Workshop on the Issue Martian Meteorites: Where Do We Stand and Where Are We Going?* pp. 50–51. LPI Contribution No.956, Lunar and Planetary Institute, Houston.

STEPHAN T., HEISS C. H., ROST D. AND JESSBERGER E. K. (1999a) Polycyclic aromatic hydrocarbons in meteorites: Allan Hills 84001, Murchison, and Orgueil (abstract). *Lunar Planet. Sci.* **30,** #1569.

STEPHAN T., JESSBERGER E. K., ROST D. AND HEISS C. H. (1999b) TOF-SIMS analysis of Martian rocks. *International Symposium: Mars Exploration Program & Sample Return Missions*, #O9/S4(32). CNES, Paris.

STORMS H. A. AND PETERSON C. L. (1994) Contributions of deadtime and mass bias uncertanties to isotopic composition measurement error. *Secondary Ion Mass Spectrometry, Proc. SIMS IX* (eds. A. Benninghoven, Y. Nihei, R. Shimizu and H. W. Werner), pp. 39–44. Wiley, Chichester.

TANG M. AND ANDERS E. (1988a) Isotopic anomalies of Ne, Xe, and C in meteorites. II. Interstellar diamond and SiC: Carriers of exotic noble gases. *Geochim. Cosmochim. Acta* **52,** 1235–1244.

TANG M. AND ANDERS E. (1988b) Isotopic anomalies of Ne, Xe, and C in meteorites. III. Local and exotic noble gas components and their interrelations. *Geochim. Cosmochim. Acta* **52,** 1245–1254.

TANG M., LEWIS R. S., ANDERS E., GRADY M. M., WRIGHT I. P. AND PILLINGER C. T. (1988) Isotopic anomalies of Ne, Xe, and C in meteorites. I. Separation of carriers by density and chemical resistance. *Geochim. Cosmochim. Acta* **52,** 1221–1234.

TERHORST M., KAMPWERTH G., NIEHUIS E. AND BENNINGHOVEN A. (1992) Sputtered neutrals mass spectrometry of organic molecules using multiphoton postionization. *J. Vac. Sci. Technol. A* **10,** 3210–3215.

TERHORST M., MÖLLERS R., NIEHUIS E. AND BENNINGHOVEN A. (1994) Time-of-flight mass spectrometry of laser postionized sputtered molecules. *Secondary Ion Mass Spectrometry, Proc. SIMS IX* (eds. A. Benninghoven, Y. Nihei, R. Shimizu and H. W. Werner), pp. 355–358. Wiley, Chichester.

TERHORST M., CRAMER H.-G. AND NIEHUIS E. (1997) Dual source ion column for depth profiling by TOF-SIMS. *Secondary Ion Mass Spectrometry, Proc. SIMS X* (eds. A. Benninghoven, B. Hagenhoff and H. W. Werner), pp. 427–430. Wiley, Chichester.

THOMAS D., SCHRAMM D. N., OLIVE K. A., MATHEWS G. J., MEYER B. S. AND FIELDS B. D. (1994a) Production of lithium, beryllium, and boron from baryon inhomogeneous primordial nucleosynthesis. *Astrophys. J.* **430,** 291–299.

THOMAS K. L., BLANFORD G. E., KELLER L. P., KLÖCK W. AND MCKAY D. S. (1993) Carbon abundance and silicate mineralogy of anhydrous interplanetary dust particles. *Geochim. Cosmochim. Acta* **57,** 1551–1566.

THOMAS K. L., KELLER L. P., BLANFORD G. E. AND MCKAY D. S. (1994b) Quantitative analyses of carbon in anhydrous and hydrated interplanetary dust particles. In *Analysis of Interplanetary Dust, AIP Conference Proc. 310* (eds. M. E. Zolensky, T. L. Wilson, F. J. M. Rietmeijer and G. J. Flynn), pp. 165–172. AIP, New York.

THOMAS K. L., ROMANEK C. S., CLEMETT S. J., GIBSON E. K. AND MCKAY D. S. (1995) Preliminary analysis of polycyclic aromatic hydrocarbons in the Martian (SNC) meteorite ALH 84001 (abstract). *Lunar Planet. Sci.* **26,** 1409–1410.

TOMEOKA K. AND BUSECK P. R. (1984) Transmission electron microscopy of the "LOW-CA" hydrated interplanetary dust particle. *Earth Planet. Sci. Lett.* **69,** 243–254.

TOMEOKA K. AND BUSECK P. R. (1985) Indicators of aqueous alteration in CM carbonaceous chondrites: Microtextures of a layered mineral containing Fe, S, O and Ni. *Geochim. Cosmochim. Acta* **49,** 2149–2163.

TOMEOKA K. AND BUSECK P. R. (1988) Matrix mineralogy of the Orgueil CI carbonaceous chondrite. *Geochim. Cosmochim. Acta* **52,** 1627–1640.

TRAXEL K., ARNDT P., BOHSUNG J., BRAUN-DULLAEUS K. U., MAETZ M., REIMOLD D., SCHIEBLER H. AND WALLIANOS A. (1995) The new Heidelberg proton microprobe: The success of a minimal concept. *Nucl. Instr. and Meth. B* **104,** 19–25.

TREIMAN A. H. AND ROMANEK C. S. (1998) Bulk and stable isotopic compositions of carbonate minerals in Martian meteorite Allan Hills 84001: No proof of high formation temperature. *Meteorit. Planet. Sci.* **33,** 737–742.

TSOU P. (1996) Hypervelocity capture of meteoroids in aerogel. In *Physics, Chemistry, and Dynamics of Interplanetary Dust, ASP Conf. Series 104* (eds. B. Å. S. Gustafson and M. S. Hanner), pp. 237–242. ASP, San Francisco.

VIRAG A., WOPENKA B., AMARI S., ZINNER E., ANDERS E. AND LEWIS R. S. (1992) Isotopic, optical, and trace element properties of large single SiC grains from the Murchison meteorite. *Geochim. Cosmochim. Acta* **56,** 1715–1733.

WAKEHAM S. G., SCHAFFNER C. AND GIGER W. (1980a) Polycyclic aromatic hydrocarbons in recent lake sediments – I. Compounds having anthropogenic origins. *Geochim. Cosmochim. Acta* **44,** 403–413.

WAKEHAM S. G., SCHAFFNER C. AND GIGER W. (1980b) Polycyclic aromatic hydrocarbons in recent lake sediments – II. Compounds derived from biogenic precursors during early diagenesis. *Geochim. Cosmochim. Acta* **44,** 415–429.

WARREN J. L. AND ZOLENSKY M. E. (1994) Collection and curation of interplanetary dust particles recovered from the stratosphere by NASA. In *Analysis of Interplanetary Dust, AIP Conference Proc. 310* (eds. M. E. Zolensky, T. L. Wilson, F. J. M. Rietmeijer and G. J. Flynn), pp. 245–254. AIP, New York.

WARREN P. H. (1998) Petrologic evidence for low-temperature, possibly flood evaporitic origin of carbonates in the ALH84001 meteorite. *J. Geophys. Res.* **103,** E16759–E16773.

WERNER H. W. AND MORGAN A. E. (1976) Charging of insulators by ion bombardment and its minimization for secondary ion mass spectrometry (SIMS) measurements. *J. Appl. Phys.* **47,** 1232–1242.

WERNER H. W. AND WARMOLTZ N. (1984) Beam techniques for the analysis of poorly conducting materials. *J. Vac. Sci. Technol. A* **2,** 726–731.

WETHERILL G. W. AND CHAPMAN C. R. (1988) Asteroids and Meteorites. In *Meteorites and the Early Solar System* (eds. J. F. Kerridge and M. S. Matthews), pp. 35–67. Univ. Arizona Press, Tucson.

WILLIAMS P. (1998) Sputtering artifacts in SIMS depth profiles. *Secondary Ion Mass Spectrometry, Proc. SIMS XI* (eds. G. Gillen, R. Lareau, J. Bennett and F. Stevie), pp. 3–10. Wiley, Chichester.

WING M. R. AND BADA J. L. (1991) Geochromatography on the parent body of the carbonaceous chondrite Ivuna. *Geochim. Cosmochim. Acta* **55,** 2937–2942.

WITTMAACK K. (1994) Electron impact postionization of sputtered neutrals: Basic aspects and recent progress. *Secondary Ion Mass Spectrometry, Proc. SIMS IX* (eds. A. Benninghoven, Y. Nihei, R. Shimizu and H. W. Werner), pp. 309–315. Wiley, Chichester.

WITTMAACK K. (1998) Physical and chemical parameters determining ion yields in SIMS analyses: A closer look at the oxygen-induced yield enhancement effect. *Secondary Ion Mass Spectrometry, Proc. SIMS XI* (eds. G. Gillen, R. Lareau, J. Bennett and F. Stevie), pp. 11–18. Wiley, Chichester.

ZEHNPFENNING J., CRAMER H. G., HELLER T., NIEHUIS E., RULLE H., STEPHAN T. AND BENNINGHOVEN A. (1994) Particle analysis by imaging TOF-SIMS. *Secondary Ion Mass Spec-*

trometry, Proc. SIMS IX (eds. A. Benninghoven, Y. Nihei, R. Shimizu and H. W. Werner), pp. 453–456. Wiley, Chichester.

ZENOBI R., PHILIPPOZ J.-M., BUSECK P. R. AND ZARE R. N. (1989) spatially resolved organic analysis of the Allende meteorite. *Science* **246,** 1026–1029.

ZINNER E. (1989) Isotopic measurements with the ion microprobe. *Proc. Workshop on New Frontiers in Stable Isotope Research, USGS Bulletin* **1890,** 145–162.

ZINNER E. (1991) Cometary and interstellar dust grains: Analysis by ion microprobe mass spectrometry and other techniques. *Space Sci. Rev.* **56,** 147–156.

ZINNER E. (1998) Trends in the study of presolar dust grains from primitive meteorites. *Meteorit. Planet. Sci.* **33,** 549–564.

ZINNER E. AND CROZAZ G. (1986) A method for the quantitative measurement of rare earth elements in the ion microprobe. *Int. J. Mass Spectrom. Ion Process.* **69,** 17–38.

ZINNER E., TANG M. AND ANDERS E. (1987) Large isotopic anomalies of Si, C, N and noble gases in interstellar silicon carbide from the Murray meteorite. *Nature* **330,** 730–732.

ZINNER E., TANG M. AND ANDERS E. (1989) Interstellar SiC in the Murchison and Murray meteorites: Isotopic composition of Ne, Xe, Si, C, and N. *Geochim. Cosmochim. Acta* **53,** 3273–3290.

ZINNER E., AMARI S., ANDERS E. AND LEWIS R. (1991a) Large amounts of extinct ^{26}Al in interstellar grains from the Murchison meteorite. *Nature* **349,** 51–54.

ZINNER E., AMARI S. AND LEWIS R. S. (1991b) Silicon carbide from a supernova? (abstract). *Meteoritics* **26,** 413.

ZOLENSKY M. E. (1997) Aqueous alteration of carbonaceous chondrites: Evidence for asteroidal alteration. In *Workshop on Parent-Body and Nebular Modification of Chondritic Materials* (eds. M. E. Zolensky, A. N. Krot and E. R. D. Scott), pp. 70–71. LPI Tech. Rpt. 97–02, Part 1, Lunar and Planetary Institute, Houston.

ZOLENSKY M. E., WILSON T. L., RIETMEIJER F. J. M. AND FLYNN G. J. (eds.) (1994) *Analysis of interplanetary dust. AIP Conference Proc. 310*. AIP, New York. 357 pp.

ZOLOTOV M. AND SHOCK E. (1999) Abiotic synthesis of polycyclic aromatic hydrocarbons on Mars. *J. Geophys. Res.* **104,** E14033–E14049.

ZSCHEEG H., KISSEL J. AND NATOUR GH. (1992) CoMA – a high resolution time-of-flight secondary ion mass spectrometer (TOF-SIMS) for in situ analysis of cometary matter. *Asteroids, Comets, Meteors 1991,* pp. 683–686. Lunar and Planetary Institute, Houston.

11. Appendix

A suite of eight different glass standards was used throughout this study. These glasses were prepared by fusing samples of basalt, andesite, komatiite, peridotite, tonalite, and rhyolite. They have been analyzed by different bulk and microanalytical techniques in various laboratories to determine their composition of major, minor, and trace element. An exact description of the samples, their preparation and analytical results is given by Jochum *et al.* (1999).

Secondary ion sensitivities relative to silicon are comprised in the following tables for all eight glass standards. Data are given for positive as well as negative secondary ions, with simultaneous argon sputtering and after sputtering, respectively. All glass standards were analyzed with the gallium source at ~600 ps primary pulse width, except for StHs6/80-G, which was measured at ~5 ns pulse width. Errors from the uncertainties in compositional data or TOF-SIMS counting statistics are not given. These errors are typically much smaller than the difference between values from individual standards.

Abundances in the tables are given according to Jochum *et al.* (1999) in weight-% for major elements and ppm (µg/g) for trace elements. Most chlorine sensitivities are increased probably due to surface adsorption and given in parentheses. For the chlorine sensitivity in Fig. 22, the minimum value obtained from standard ATHO-G during sputtering (Table A4) was used.

TABLE A1. Secondary ion sensitivities for glass KL2-G prepared from a basalt from the Kilauea volcano of Hawaii.

Element	Abundance	Positive with Ar-sputtering	Positive after Ar-sputtering	Negative with Ar-sputtering	Negative after Ar-sputtering
Li	5.4	6.3	6.5		
Be	0.88	1.4	1.1		
B	2.6	1.3	0.77		
O [%]	45.2	0.00086	0.00079	30	45
Na [%]	1.68	21	20		
Mg [%]	4.37	5.8	6.5		
Al [%]	6.93	7.6	7.4		
Si [%]	23.4	1	1	1	1
P	1080	0.030	0.026	1.9	1.6
Cl	30			(340)	(4900)
K	3900	34	33		
Ca [%]	7.79	12	12		
Sc	32.3	7.9	4.1		
Ti [%]	1.53	4.7	4.3		
V	370	3.6	3.6		
Cr	306	2.7	2.6		
Mn	1270	3.6	3.9		
Fe [%]	8.24	1.9	1.9		
Co	41.6	1.3	1.3		
Ni	117		0.85		
Cu	95	0.90	1.2		
Rb	8.9	59	60		
Sr	364	12	11		
Ba	123	9.0	8.7		

TABLE A2. Secondary ion sensitivities for glass ML3B-G prepared from a basalt from the Mauna Loa volcano of Hawaii.

Element	Abundance	Positive with Ar-sputtering	Positive after Ar-sputtering	Negative with Ar-sputtering	Negative after Ar-sputtering
Li	4.2	13	23		
Be	0.75	1.1	2.4		
B	2.2	0.84	1.0		
O [%]	45.8	0.0010	0.00089	32	53
Na [%]	1.74	18	29		
Mg [%]	3.94	8.1	10		
Al [%]	7.04	7.3	7.5		
Si [%]	23.7	1	1	1	1
P	960		0.025	3.4	2.6
K	3200	37	56		
Ca [%]	7.43	15	15		
Sc	31.4	7.7	5.1		
Ti [%]	1.26	7.5	6.1		
V	260	5.7	6.3		
Cr	170	7.6	10.6		
Mn	1370	3.8	4.8		
Fe [%]	8.39	1.8	2.6		
Co	41.4	0.79	2.0		
Cu	115	0.33	0.47		
Rb	5.78	49	93		
Sr	315	14	14		
Cs	0.142	65	59		
Ba	80.1	10	18		

TABLE A3. Secondary ion sensitivities for glass StHs6/80-G prepared from an andesite from the St. Helens (USA) eruption.

Element	Abundance	Positive with Ar-sputtering	Positive after Ar-sputtering	Negative with Ar-sputtering	Negative after Ar-sputtering
Li	19	11	14		
Be	1.4	1.8	1.5		
B	13	0.52	0.71		
O [%]	47.4	0.00091	0.00063	23	57
Na [%]	3.39	22	22		
Mg [%]	1.19	7.0	8.1		
Al [%]	9.33	6.6	7.1		
Si [%]	29.8	1	1	1	1
P	700				1.4
Cl	260				(720)
K	10700	35.5	26		
Ca [%]	3.76	13.6	15		
Ti [%]	0.42	6.4	6.1		
V	96	4.0			
Mn	590	5.8	3.4		
Fe [%]	3.39	3.1	3.4		
Rb	29.5	58	37		
Sr	486	16	15		
Cs	1.89	47			
Ba	302	14	14		

TABLE A4. Secondary ion sensitivities for glass GOR128-G prepared from a komatiite from the Gorgona Island, Colombia.

Element	Abundance	Positive with Ar-sputtering	Positive after Ar-sputtering	Negative with Ar-sputtering	Negative after Ar-sputtering
Li	7.3	22	25		
Be	0.04		3.8		
B	22	0.58	0.63		
O [%]	44.6	0.0012	0.0010	24	40
Na [%]	0.417	31	32		
Mg [%]	15.6	9.0	9.6		
Al [%]	5.2	8.7	8.3		
Si [%]	21.5	1	1	1	1
P	120	0.023		2.1	
K	300	50	53		
Ca [%]	4.39	19	16		
Sc	31.1	11	5.5		
Ti [%]	0.168	7.5	6.0		
V	170	5.9	5.1		
Cr	2150	5.8	5.6		
Mn	1390	4.2	4.3		
Fe [%]	7.58	2.1	2.1		
Co	79.5	1.4	1.8		
Ni	1070	1.2	0.74		
Cu	63	0.90	2.0		

TABLE A5. Secondary ion sensitivities for glass GOR132-G prepared from a komatiite from the Gorgona Island, Colombia.

Element	Abundance	Positive with Ar-sputtering	Positive after Ar-sputtering	Negative with Ar-sputtering	Negative after Ar-sputtering
Li	7.9	15	23		
B	18	0.44	0.62		
O [%]	44.1	0.0011	0.0010	26	40
Na [%]	0.592	25	29		
Mg [%]	13.5	8.5	10		
Al [%]	5.77	8.0	8.4		
Si [%]	21.3	1	1	1	1
P	170			1.7	
K	270	37	45		
Ca [%]	6.07	17	15		
Sc	34.6		7.2		
Ti [%]	0.18	6.4	5.8		
V	189	5.4	5.7		
Cr	2410	5.5	6.2		
Mn	1180	4.4	5.1		
Fe [%]	7.93	1.8	2.6		
Co	88.2	1.1	2.1		
Ni	1170	0.67	1.3		
Cu	180		1.5		
Rb	2.14		78		
Sr	15.6		13		
Cs	8.08	47	56		

TABLE A6. Secondary ion sensitivities for glass BM90/21-G prepared from a peridotite from the Ivrea Zone, Italy.

Element	Abundance	Positive with Ar-sputtering	Positive after Ar-sputtering	Negative with Ar-sputtering	Negative after Ar-sputtering
Li	1.4	20	15		
B	2.8	0.93	1.4		
O [%]	45.9	0.00097	0.00092	23	35
Na [%]	0.0838	24	19		
Mg [%]	20.6	8.1	8.3		
Al [%]	1.23	7.6	6.9		
Si [%]	24.9	1	1	1	1
K	31	65	59		
Ca [%]	1.5	16	11		
Sc	11.3	7.5	7.1		
Ti [%]	0.037	6.5	4.9		
V	40	8.1	6.2		
Cr	2100	5.6	5.1		
Mn	829	4.5	4.4		
Fe [%]	5.24	2.3	2.6		
Co	88.5	1.5	1.9		
Ni	1880	0.83	1.2		
Cs	1.2	45			

TABLE A7. Secondary ion sensitivities for glass T1-G prepared from a tonalite from the Italian Alps.

Element	Abundance	Positive with Ar-sputtering	Positive after Ar-sputtering	Negative with Ar-sputtering	Negative after Ar-sputtering
Li	19.8	8.5	9.8		
Be	2.4	1.3	1.7		
B	4.6	0.88	0.79		
O [%]	46.6	0.00083	0.00078	33	56
Na [%]	2.32	18	16		
Mg [%]	2.25	7.1	7.8		
Al [%]	9.05	7.6	6.6		
Si [%]	27.3	1	1	1	1
P	772	0.043	0.039	3.0	1.6
Cl	86			(860)	(3000)
K	15900	34	27		
Ca [%]	5.05	14	11		
Sc	26.7	8.6	4.2		
Ti [%]	0.445	6.7	5.2		
V	190	5.6	4.8		
Cr	20	6.5	6.2		
Mn	1020	4.1	4.3		
Fe [%]	5.02	2.2	2.4		
Co	18.9	1.3	1.8		
Cu	21	0.90			
Rb	79.3	40	30		
Sr	282	15	11		
Cs	2.85	44	37		
Ba	393	17	10		

TABLE A8. Secondary ion sensitivities for glass ATHO-G prepared from a rhyolite from Iceland.

Element	Abundance	Positive with Ar-sputtering	Positive after Ar-sputtering	Negative with Ar-sputtering	Negative after Ar-sputtering
Li	27.6	5.9	7.7		
Be	3.7	0.78	1.5		
B	5.8	0.46	0.75		
O [%]	49.0	0.00073	0.00071	30	53
Na [%]	3	11	24		
Mg [%]	0.068	4.5	6.9		
Al [%]	6.16	5.4	5.5		
Si [%]	35.5	1	1	1	1
P	110	0.066	0.040	2.9	
Cl	400			140	(450)
K	22100	14	24		
Ca [%]	1.18	9.5	12		
Sc	5.03	6.5	4.1		
Ti [%]	0.145	5.6	4.6		
V	4.4	3.2	5.1		
Cr	5.3	3.6	4.2		
Mn	790	3.6	5.3		
Fe [%]	2.42	2.5	3.6		
Co	2.2		2.0		
Rb	63.8	14	25		
Sr	95.8	9.7	9.8		
Cs	1.31		57		
Ba	549	10	8.8		